University of "Roma Tre"
Faculty of Computer Science Engineering
Engineering Department

Ph.D. School in Engineering - Computer Science and Automation Section

Doctor of Phylosophy Dissertation

XXV Cycle

Swarming Algorithms for Multi-Robot Systems

by

Attilio Priolo

Tutor

Prof. Giovanni Ulivi

Ph.D. School Coordinator

Prof. Stefano Panzieri

Reviewer
Prof. **Carlos Sagues**
Universidad de Zaragoza

Reviewer
Prof. **Alan Winfield**
University of the West of England, Bristol

Rome, 2013

Non est quod timeas ne operam perdideris, si tibi didicisti.
(Seneca)

Acknowledgments

I wish to thank all the people that, directly or indirectly, have influenced my "Ph.D. experience". I know that it is impossible to cite them all... so I apologize ahead to whom I am going to forget. First of all, I feel grateful to prof. Giovanni Ulivi for being my tutor. His advice and suggestions were dramatically useful during my studies. Apart from the academic-related stuff, I want to thank him for the sincere and direct way he was used to talk to me. Thank you! I wish to thank my friend prof. Andrea Gasparri for all the help he provided me with. He is a constant source of new ideas and his support was necessary to achieve this result. I really appreciated his maniacal precision and I thank him for instilling me with this skill. I feel grateful and I wish to thank two people who I met in the ending part of this experience: prof. Carlos Sagüés Blázquiz and prof. Eduardo Montijano Muñoz. Visiting them in Zaragoza was one of the most valuable experiences of my life. Their brilliant minds inspired me and deeply modified the way I was conceiving research. Thank you again. I wish to thank my family: my father Antonio my mother Annarita my sister Serena my nephew Annachiara my brother-in-law Andrea, my cousins Matteo Sara Andrea and Roberto, my aunts Stella and Sandra, my uncles Marco e Giacomo my grandmothers and grandfathers Chiara, Bianca, Attilio and Ennio and all the other people in the family who I cannot cite here but are in my mind. I hope that you are proud of me because I am proud of being a member of this family. I want to thank also Claudio and Graziella for accepting me as a part of their family. I want to thank all the guys and girls, all the young researchers or young engineers, all the friends I met: prof. Federica, prof. Stefano, Sandro, Alessandro Longhi (dato un Alessandro A_L da un insieme di Alessandri $\mathcal{A}$), Carletto, Flavio, Alessandro Milano, Giovanni, Chiara, Daniela (e Giulia!), Giusj, Roberto, Dorian, Estibaliz, Diego, Daniel, Carlos Franco, Luis, Beniamino, Antonello, Claudio... All of you! Thank you!!!

Eventually, I feel deeply grateful to my love Chiara. My words cannot give you back all the moments I took away from us, but I hope that now I made you proud of me and believe me when I say that I feel lucky of having a woman like you beside me. I love you.

With deep gratitude,
Attilio.

Abstract

A large effort has been devoted by the scientific community to the field of multi-robot systems. The main reason relies on the fact that they exhibit better fault-tolerance, flexibility and performance than a single robot unit. In this thesis, novel contributions to this field are given. Novel decentralized swarming algorithms integrated with obstacle avoidance techniques where the interaction is assumed to be limited by a range of view are presented. Furthermore, to better comply with the hardware/software limitations of mobile robotic platforms, the actuators of the robots are assumed to be saturated.

Due to technological advances in the field of electronic devices, the robots are able to share data in a fast and reliable manner among themselves. This capability is used within this thesis to carry out a distributed estimation of system wide quantities to adjust the interactions of each individual with its neighbors. In particular, the average consensus problem over digraphs is addressed and a distributed strategy to solve it is presented. Moreover, a finite time condition to check if the communication digraph is strongly connected or it is not is detailed. It can be verified in a distributed fashion by the robots and can be employed to avoid useless steps in the estimation process reviewed within this work.

A theoretical characterization of the properties of the presented approaches is provided. Moreover, experiments in real scenarios using a team of low-cost mobile robots SAETTA (built in our laboratory) to demonstrate the effectiveness of the proposed algorithms have been carried out. Finally, a relative distance and a relative localization system are introduced to provide the indispensable input for the swarming algorithms.

Contents

List of Figures

CHAPTER 1

Introduction

The coordination problem of multi-robot systems has been an active research field in the last decades [1, 2, 3, 4, 5, 6, 7]. The interest in this research field is motivated by the large number of possible applications ranging from environmental exploration [8] and monitoring [9, 10], search and rescue operations [11, 12], to agricultural foraging [13, 14] or de-mining tasks[15, 16]. However, the inherently distributed nature of these systems makes the design of effective algorithms very challenging as the overall performance depends significantly on the issues arising from the complex interactions among the robots.

Swarm robotics represents an approach focusing on the coordination of a large number of a relatively simple robots [17]. Since recent times it has been considered as a well-developed field belonging to the multi-robot coordination front. The key idea behind swarm robotics relies on substituting a complex and expensive single robot unit with a more affordable and flexible set of robots. It takes inspiration from the suggestive world of social insects like bees, termites and ants in which the cooperation of several individuals produces remarkably complex behaviors. In the literature, works implementing these behaviors like social foraging [18, 19], formation control [20], swarm aggregation (see [21], [22] and the references therein), hole-avoidance [23] and self-assembly [24] appeared in the last decades. The objective of swarm robotics is to design simple local control laws for each individual to let the whole multi-robot system perform a complex task. The behavior of the whole system is called *emergent*, because it emerges from the interactions among the robots and between each robot and the environment. In this thesis, one peculiar behavior of robots swarms has been

investigated, i.e., *swarm aggregation*. In this case, the interactions among the individuals are constituted by (see [25, 26]):

- *attractive forces*,
- *repulsive forces*.

In order to show the presence of attractive and repulsive forces in the nature, let us consider the schooling behavior of the fishes. It has been observed that:

- Attraction is generally based on vision and has a long range.
- Repulsion is based on the pressure on the side of the fish and has a short range (but it is stronger than attraction).
- Both attraction and repulsion are always on.
- The resulting behavior is due to the interplay between these two forces.
- There is a distance (called the "equilibrium distance" in biology) at which attraction and repulsion between two individuals balance.

From recent studies, it turns out that in swarms or flocks of animals, there are no central units coordinating the motion of the individuals. In other terms, a single point of failure able to compromise the whole task performed by the swarm does not exist. Instead, the swarm or flock behavior is generated by several parameters as the wing span of the birds or the position within the flock itself [27]. The absence of a central coordination unit may lead to an improvement of several characteristics [28] as:

- Robustness.
- Flexibility.
- Scalability.

The robustness of a system is its ability of performing the assigned task also in presence of failures of any individual. It is affected by several factors such as the large number of individuals belonging to the swarm. In fact, even if a subset of individuals suddenly fail, the rest of the swarm may keep performing the assigned task. Another important factor is the distributed nature of the system. The absence of a central coordination unit avoids that its failure could jeopardize the accomplishment of the mission. The flexibility is the ability of the swarm to adapt its behavior to different assigned tasks.

For example, let us take into account the collaborative pushing task as the one in [29]. If the force exerted by a single robot is not enough to push the object, the collaboration with other robots is necessary to accomplish the task. Therefore, the same swarm can adapt itself to another task, for example, it can pursue an environmental coverage mission as the one in [30]. The scalability property allows the system to keep performing the tasks despite of the changes occurring to the number of individuals. This characteristic is strictly related with the local nature of the interactions because each individual is not required to be aware of the state of the whole swarm, e.g., the number of members within the swarm, but only of its neighbors. The main drawback in the use of fully distributed control laws relies on the growing complexity in the design of this kind of algorithms. In fact, the designer has to take into account the limited information possessed by each individual and the limited communication and computation capabilities.

By nature, swarm systems are able to operate in a parallel fashion. This peculiar ability allows the swarm to perform an assigned task more efficiently w.r.t. a single complex robot.

For a comprehensive overview of swarm robotic systems, the reader is referred to [22, 21, 31]. Instead, for works dealing with the robustness of swarming algorithms, the reader is referred to [32, 33] and to [34] for a very recent discussion on the implications of swarm approaches on fault tolerance.

In this thesis, control laws for robot swarms aggregation are proposed. Two of them explicitly take into account the limited capabilities of the actuators of the simple robotic units belonging to the swarm. Moreover, all the control laws cope with the problem of a limited range of sensing, i.e., each robot interacts only with the other robots within a visibility range. A graph theoretic approach has been used to model the interaction among the robots where robots are represented by nodes and the interactions by edges. The existence of an edge in the graph is dictated by the limited range of visibility of common the sensor devices. Therefore, limiting the range of visibility is of extreme importance when dealing with real hardware. It becomes of mandatory considering indoor scenarios where the GPS system can not be employed by the robots. Finally, an obstacle avoidance technique is integrated within the control laws.

Swarm aggregation algorithms are based on the sensing capabilities of each member of the swarm. Due to technological advances in the field of electronics and the miniaturization of the devices, nowadays the robots are capable of exchanging data among themselves in a fast and reliable manner [35, 36]. Therefore, it is possible to exploit communication in order to adjust the interactions among the robots. For example, consensus

based algorithms exploiting inter-robots communication can be employed to solve the rendezvous problem [37]. However, within several works related to this topic, the communication among the robots is modeled using an undirected communication graph (see [38, 39] and the references therein). This is founded on the assumptions that the communication is isotropic, i.e., the employed antenna radiates its power uniformly in all directions and that the transmitter and receiver gains are the same. Therefore, if a robot can communicate with another one, the opposite is possible as well. However, these assumptions are not realistic in real world scenarios due, for example, to environmental effects or the radiation pattern of the robots [40].

In this thesis, a novel contribution in the field of multi-robot systems where the communication is modeled using digraphs with nodes modeling the robots and the edges the inter-robot communications is given. In particular, by assuming the digraph to be strongly connected, a technique to estimate the left eigenvector associated to the zero eigenvalue of the Laplacian matrix encoding the communication digraph originally proposed in [41] is reviewed. This technique paves the way for developing communication based algorithms under the assumption of unidirectional data exchange, for example, consensus based algorithms for robots rendezvous. Furthermore, a necessary and sufficient condition to check the strong connectivity of a weighted digraph in finite-time is proposed. The latter represents a practical stopping condition for the left eigenvector estimation algorithm to avoid useless data exchanges.

Summarizing, the main contributions within this thesis are the following:

- Control laws solving the swarm aggregation problem taking into account both input saturations and local interactions.
- Two effective obstacle avoidance techniques integrated within the control laws.
- A necessary and sufficient condition to check in a finite-time and in a distributed fashion the strongly connectedness of the communication digraph.
- A purely broadcast modified average consensus algorithm to be executed concurrently with the left eigenvector estimation.
- A complete theoretical analysis of the proposed approaches.
- A distance and a relative position measurement techniques for robot swarms.

- Simulations and experiments to corroborate the theoretical findings.

It is worthy to note that the contributions in this thesis are driven by real problems arising from hardware related issues. The proposed control laws copes with the problems arising from the physical limitations of actuators and sensing devices. The same hold for the techniques arising from the left eigenvector estimation algorithm. In fact, note that in this thesis the first technique suitable for an implementation based on a pure broadcast communication scheme is described. Indeed, this represents a significant novelty compared to the works available in the literature for which the communication is required to be point-to-point or the knowledge of the out-degree is necessary. Publications (published and submitted) related with the topics in this thesis are [42, 43, 44, 45, 46, 47, 48, 49, 50, 51, 52, 53].

CHAPTER 2

Literature Review

There is a very large literature regarding robotic swarms. One of the pioneeristic works on this topic is [54]. In this paper, the author proposes a model for the motion of flocks of birds where the behavior of each bird is considered independently. The following three basic rules governing the interactions among the birds are identified:

- **Collision avoidance**: each member of the flock has to avoid collisions with its neighbors.
- **Velocity matching**: each member of the flock has to match its speed with the ones of its neighbors.
- **Flock centering**: each member of the flock has to remain close to its neighbors.

In [55], a large scale multi-robot system is controlled through the application of the social potential field method. Basically, this method consists in designing the interaction forces among the robots incorporating attractive and repulsive terms. Such forces can be viewed as the relationship governing the behaviors of the robots. Note that, these social potential fields agree with the rules proposed by Reynolds in [54]; in particular, the repulsive term matches with the collision avoidance rule, while the attractive term with the flock centering one. An important aspect is represented by the distributed nature of this control law and its asynchronism, i.e., no central clock is required to the robots in order to apply the control input. One of the first theoretical analysis regarding the stability of robot swarms is carried out in [56]. In this work, the authors propose a linear asynchronous model for the

swarm and analyze its convergence. In particular, a sufficient condition is given to let the swarm converge to the synchronous configuration, i.e., to the configuration that the swarm would achieve if the the communication within the swarm would be synchronous. A probabilistic modeling of robot swarms is proposed in [57] where Probabilistic Finite State Machines are used to model both the behavior of a single unit belonging to the swarm and the one of the swarm itself using a decentralized manipulation task as case of study. This work attempts to link the microscopic properties of individual robots to the emergent macroscopic behaviors of the overall swarm. In [58] two macroscopic model for robot swarms are proposed, namely, the Stock & Flow model and a spatially resolved model based on diffusion processes. Both offer high prediction quality of the swarm behavior and experimental results are shown to corroborate the authors findings. The reader is referred to [59] for a review of the works dealing with macroscopic probabilistic models for robot swarms.

In the last decade, several swarm aggregation algorithms were proposed [60, 5, 19, 61, 62, 63, 64, 65, 7, 66, 67]. In [60] a decentralized continuous-time model for finite-time swarm aggregation is proposed. An interaction function based on a linear and an exponential term is analyzed. A bound of the convergence area along with the time required by the swarm to reach it is given. An extension of this work is given in [5], where a generalized interaction function is proposed. In particular, classes of attractive and repulsive functions are used and a theoretical analysis on the ultimate boundedness of the trajectory of the swarm is presented along with the finite time convergence. This approach is further extended considering the case of social foraging swarms [19]. The robots are provided with a potential function modeling the attractive or repelling areas. Its gradient is used in the control law to provide a navigation objective to the swarm. In [61], the assumption of isotropic sensing/communication among the robots is released and the model in [60] is generalized. The circular area where the swarm converges into is detailed in terms of its radius and the stability of the swarm is proven. In [62], a robust control strategy based on artificial potential functions and sliding mode control is designed. The proposed swarm algorithm is applied to robot systems with vehicles dynamics, i.e., to the dynamical model of a mobile robot. An adaptive velocity swarm model which extends the well-known Vicsek model is proposed in [63]. To control the swarm formation, a computationally efficient vector field approach is proposed in [64]. The vector field is generated in a distributed fashion using normal and sigmoid functions. The robots are required to continuosly sense or compute the centroid of the whole swarm. In [65], two mechanisms for robot swarm-

ing, namely, chains and vectorfield are provided. They are used to organize the robots into connected structures based upon visual information. Simulations and experiments are conducted to test different obstacle avoidance algorithms, the scalability of the mechanisms, fault tolerance and robustness to noisy conditions. A swarm aggregation control law for unicycles is proposed in [7]. The authors introduce a control algorithm composed of two terms: the first one is in charge of guaranteeing the collision avoidance while the second one leads to a compact configuration of the robots and preserves the links among them. Eventually, a bound on the size of the region of convergence is detailed. In [66], a decentralized formation control scheme that guarantees collision-free motion for a team of rovers with a leader is presented. In [67], instead, a swarming algorithm where the sensing graph is not restricted to be undirected or to have unitary weights associated to its edges is introduced. Indeed, the approach given in [5] is extended paving the way to a more generalized framework.

Some works consider the presence of actuator saturations, an inevitable limitation of actual mobile platforms. In [68], a set of control laws to drive the robots from any initial condition towards a desired configuration taking into account constraints on the inputs is provided. In [69], a behavior-based approach to formation maneuvers for groups of mobile robots that works under this assumption is proposed. In [70], a flocking algorithm for a multi-agent system with bounded control inputs is proposed; the agents are able to achieve all the same velocity under the assumption of the connectivity of the underlying communication graph. A formation control scheme for multiple unicycles with saturated inputs is described in [71]. However, as far as my knowledge, all the aforementioned works do not explicitly take into account both the modeling of the input saturations and the constraints of the local interactions giving an exhaustive theoretical analysis of the algorithms and solving the obstacle avoidance problem.

A mandatory requirement for the employment of the swarming algorithms is the ability for each robot to sense the distance/position of its neighbors. Within this thesis, a Radio Signal Strength and an Infrared based techniques are presented to fulfill this requirement. Different Radio Signal Strength based distance sensing techniques can be found in the literature. These techniques allow to retrieve distance information by exploiting the Radio Signal Strength Index (RSSI). In particular, the RSSI can be used in two different ways to determine the distance between a transmitter and a receiver: *fingerprinting*-based techniques and *propagation*-based techniques. Fingerprinting techniques consist of an offline learning phase and an online localization phase [72, 73, 74]. In the offline phase, RSSI values

corresponding to different anchor nodes are collected. The stored RSSI values are then used along with the known locations of the anchor nodes to construct an RF-fingerprint database. In the online phase, the target node measures RSSI values to different anchor nodes. At this point, the location of the target is determined by finding the closest recorded reference fingerprint values to the measured one (in signal space). The unknown location is then estimated to be the one paired with the closest reference fingerprint or in the (weighted) centroid of nearest reference fingerprints. The major drawback of this approach is the amount of time required to build the database of signatures. Propagation based techniques [75, 72, 76], instead, consist of a base station which measures the Signal Strength (SS), Time of Arrival (ToA), Time Difference of Arrival (TDoA) and Angle of Arrival (AoA) with respect to a target node. Distances are then retrieved by exploiting the radio propagation model. The performance of these techniques is significantly reduced by the presence of obstacles in the environment due to the multiple reflection phenomenon typical in RF signals. Both techniques present some advantages and disadvantages. Fingerprinting techniques provide better performances compared to the propagation techniques but they require a significant effort to build the radio signature of the environment during the offline phase [77]. Conversely, propagation techniques do not require any database, only a calibration of the radio parameters, but they are very sensitive to multi-path effects on the signal in indoor environments [72]. Indeed, the signal dispersion heavily depends on building dimensions, obstructions, partitioning materials and surrounding moving objects [78]. This makes the use of propagation model (free path loss) for accurate RSSI reporting very complicated. To summarize, the big advantage of RSS-based techniques is the possibility to use existing infrastructures to build a positioning system with minimum additional effort. Indeed, it is remarkably easier to obtain RSSI than the time or angle of arrival which require additional signal processing.

Several Infrared based approaches can be found in the literature for the estimation of relative distance and/or orientation among robots. Among the others, in [79] an infrared location system for relative pose (position and orientation) estimation is proposed. In this system, robots use the intensity and the bearing measurements of the received infrared signals to estimate the positions of other robots in polar coordinates. In addition, each robot has a unique modulation frequency from which each individual can be recognized. The location system performs position estimation by rotating a beam collector at constant rotation speed and by measuring the bearing and intensity of the received signal. Infrared signals are received through a small

aperture in the beam collector enabling accurate bearing measurements. In [80], an on-board robotic module for relative positions estimation among miniature robots is proposed. The module uses high-frequency modulated infrared emissions to enable nearby robots to determine the range, bearing and message of the sender with a rapid update rate. A CSMA protocol is employed for scalable operation.

Despite of its usefulness in cooperative control problems, little is available in the literature regarding the estimation of the left eigenvector associated with the zero eigenvalue of the Laplacian matrix for digraphs. The work in [81] possibly represents the best approach in this field. In this work, the authors propose a distributed approach for the estimation of the left eigenvector associated to the weight matrix and the expected consensus value. The estimate is then used in a control algorithm to improve the network convergence rate. However, the continuous time nature of the algorithm makes its implementation in a real world scenario challenging. Recently, the same authors proposed the discrete time version of this algorithm in [41]. This approach is used along this chapter to provide the left eigenvector estimation algorithm required by the average consensus one. Note that, being the algorithm in [41] asymptotic, the proposed average consensus has been developed to be run concurrently with it.

Finally, the average consensus on digraphs is discussed in several works [82, 83, 84, 85]. Among them, in [82] the fact that the weight matrix sums to zero over the columns at each step, guarantees that the average consensus can be performed in parallel with respect to the convergence of the weight matrix to a doubly stochastic form. However, this work requires each robot to know its out-neighborhood making the algorithm unpractical in pure broadcast communication scenarios. In [83, 84], the average consensus over a directed network topology is addressed. The proposed algorithms require an augmentation of the variables of each robot adding a "surplus" variable. Anyway, these approaches require the robots to exchange another set of values among themselves. In [85], the average consensus problem is addressed both in the continuous time and in the discrete time. Moreover, the topology of the network is assumed to be switching. However, the discrete time consensus algorithm requires the adjacency matrix to be doubly stochastic.

CHAPTER 3

Swarm Aggregation Control Law with Local Interactions

In this chapter, a swarm aggregation control law based on the assumption of local interactions among the robots is detailed. The notation used for the theoretical analysis of the proposed control law and some basic concepts are introduced in the next section. Therefore, the approach exploiting a fully connected graph to model the interactions is reviewed in Section 3.2. A proposed extension releasing the assumption of a fully connected topology is presented in Section 3.3. Eventually, in Section 3.4 a possible application of the proposed swarm aggregation algorithm to an Unmanned Surface Vehicles (USVs) system is described.

3.1 Preliminaries

Let us consider a swarm composed of n robots with the following dynamics:

$$\dot{x}_i(t) = u_i(t), \tag{3.1.1}$$

where $x_i(t) \in \mathbb{R}^d$ is the location of the i-th robot and $u_i(t) \in \mathbb{R}^d$ is the local control input. Usually this model is referred to as *kinematic agent* or *higher level* model. It turns out to be useful when dealing with higher level algorithms ignoring the low-level issues generated by the robots dynamics. Its outcome can be employed to generate reference trajectory to be tracked by a lower level robot control algorithm aware, for example, of the nonholonomic constrains imposed by the mechanical structure of the robot. Denote with $\chi(t) = [x_1^T(t) \dots x_n^T(t)]^T$ the collection of all the robots locations and

with $e_i(t) = x_i(t) - \bar{x}(t)$ the vector distance of robot i from the barycenter $\bar{x}(t) = \frac{1}{n}\sum_{i=1}^{n} x_i(t)$. Also, let us denote with $\mathbf{e}(t) = [e_1^T(t) \dots e_n^T(t)]^T$ the collection of all the distances from the barycenter. The interaction among the robots can be modeled by means of an undirected time-varying proximity graph $\mathcal{G}(t) = \{V, E(t)\}$ where $V = \{1, \dots, n\}$ are the vertices (robots) and $E(t) = \{\epsilon_{ij}(t)\}$ the set of edges representing the interaction between pairs of robots. An edge $\epsilon_{ij}(t)$ exists between a pair of robots i and j if and only if they are within the range of visibility of each other, that is:

$$\epsilon_{ij}(t) = \begin{cases} 1 & \text{iff } \|x_i(t) - x_j(t)\| \leq r, \\ 0 & \text{otherwise,} \end{cases} \tag{3.1.2}$$

where $\|\cdot\|$ is the Euclidean norm and $r > 0$ is the range of visibility.

Let us denote with $\mathcal{A}(\mathcal{G}(t))$ the adjacency matrix encoding $\mathcal{G}(t)$, the entries of which are defined as:

$$a_{ij}(t) = \begin{cases} 1 & \text{iff } \epsilon_{ij}(t) = 1, \\ 0 & \text{otherwise.} \end{cases} \tag{3.1.3}$$

Denote the set of neighboring robots for the i-th robot with

$$\mathcal{N}_i(t) = \{j \in V \setminus \{i\} \,:\, \epsilon_{ij}(t) = 1\}. \tag{3.1.4}$$

In addition, let $\mathcal{D}(\mathcal{G}(t)) = \mathtt{diag}(D_1(t), \dots, D_n(t))$ be the degree matrix of $\mathcal{G}(t)$, where $D_i(t) = |\mathcal{N}_i(t)|$ is the degree of the i-th robot. Finally, let us denote with $\mathcal{L}(\mathcal{G}(t)) = \mathcal{D}(\mathcal{G}(t)) - A(\mathcal{G}(t))$ the $n \times n$ Laplacian matrix of $\mathcal{G}(t)$. For the sake of readability the notation $\mathcal{L}(t)$, $\mathcal{A}(t)$, $\mathcal{D}(t)$ will be used in the rest of this thesis.

Let us now review some important properties of the Laplacian matrix $\mathcal{L}(t)$. First, let us recall that $\mathcal{L}(t)$ is a weakly diagonal dominant symmetric matrix where the row and the column sums are both equal to zero. This implies that there is always at least a zero structural eigenvalue whose corresponding eigenvector is $\mathbf{1}$, the n-vector with all unit components. Thus $\mathcal{L}(t)\,\mathbf{1} = \mathbf{0}$ and $\mathbf{1}^T\mathcal{L}(t) = \mathbf{0}^T$ for any $\mathcal{G}$. Furthermore, the number of zero eigenvalues corresponds to the number of connected components of $\mathcal{G}$, that is, $\mathtt{Rank}(\mathcal{L}(t)) = n - c$ with c the number of connected components. In addition, since the Laplacian matrix is symmetric, from the Gershgorin Circle Theorem it follows that all the eigenvalues of the Laplacian matrix are real and positive and they belong to $[0, 2\,D_{max}(t)]$, where $D_{max}(t) = \max_{i \in V}\{D_i(t)\}$ is the maximum degree of the nodes in the graph.

Among the others, the second smallest eigenvalue $\lambda_2(\mathcal{L}(t))$, called the algebraic connectivity, provides information about the connectedness of the graph. The reader is referred to [39] for further details on graph theoretic methods for multi-agent systems.

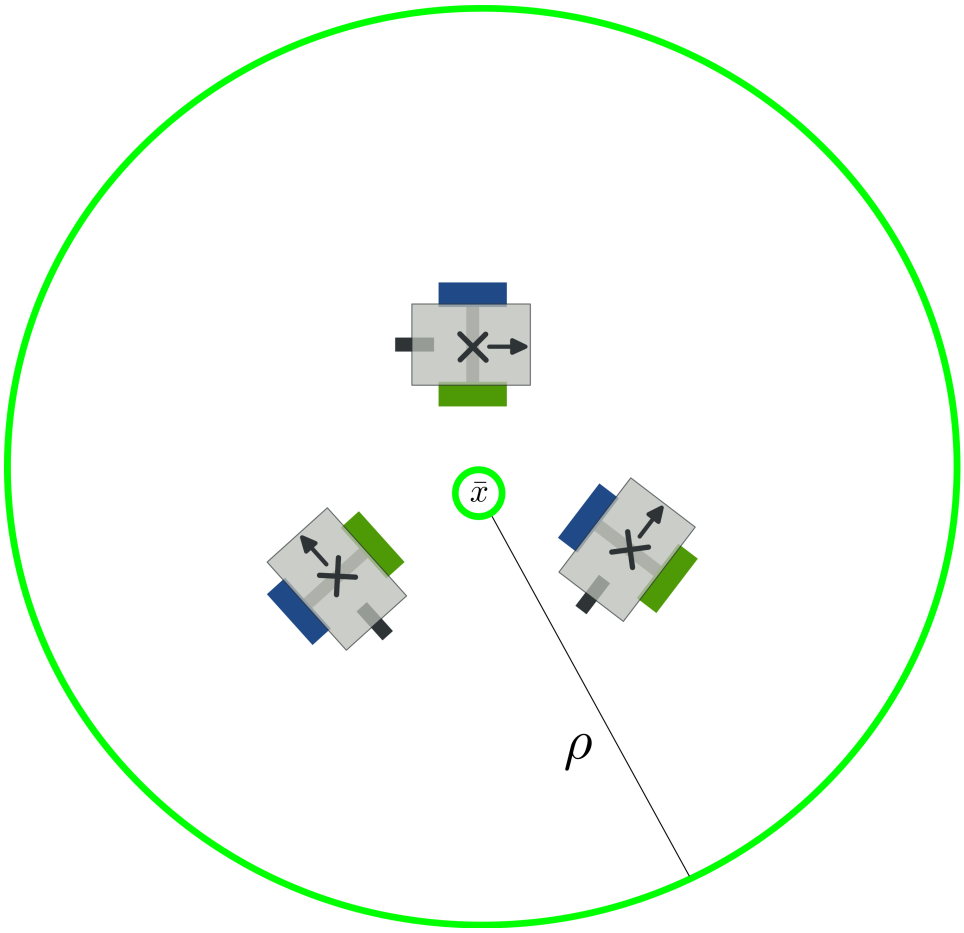

Figure 3.1: A representation of the convergence area for three robots.

For each proposed control law in this thesis, the bounded area where the swarm eventually converges into is characterized. In order to give a qualitative idea, let us consider Figure 3.1. The swarm of robots converges to the area delimited by a green line and described by a radius ρ. In the theoretical analysis carried out in the rest of the thesis, an upper bound to the radius ρ is given for each control law.

Let us now formalize the concept of *interaction function* according to the notation originally introduced in [19]. Denote with $g(\cdot) : \mathbb{R}^d \to \mathbb{R}^d$ the *interaction function* describing the interaction between a pair of robots.

It is defined as follows:

$$g(y) = -y\ (g_a(\|y\|) - g_r(\|y\|)), \quad y \in \mathbb{R}^d, \tag{3.1.5}$$

where:

- The term $g_a(\|y\|) : \mathbb{R} \to \mathbb{R}$ is called the *attraction* function.
- The term $g_r(\|y\|) : \mathbb{R} \to \mathbb{R}$ is called the *repulsion* function.

According to the biological aspects illustrated in Chapter 1, the interaction function has to satisfy the following properties:

- The interaction function is *odd*, i.e., $g(y) = -g(-y)$.
- On large distances, the attraction dominates the repulsion.
- On short distances, the repulsion dominates the attraction.

The first point is crucial because it leads to the aggregating behavior of the swarm. Its importance is emphasized in the rest of this chapter. The second one states that when some robots are getting further from the others, the attractive function should intervene to reunite the swarm. The third point deals with the collision avoidance problem. In fact, if two agents are too close to each other, the repulsive function should distance them.

The following assumption on g_a and g_r formalizes the requirements on the interaction function:

Assumption 1 (**A1**): There exists a unique distance δ at which $g_a(\delta) = g_r(\delta)$. Moreover, the following holds:

- $g_a(\|y\|) \geq g_r(\|y\|)$ for $\|y\| \geq \delta$,
- $g_r(\|y\|) > g_a(\|y\|)$ for $\|y\| < \delta$.

To further detail the characteristics of the interaction function, the following aspects are pointed out:

- The vector y defines the alignment, i.e., the direction on which the interaction acts.
- The term $yg_a(\|y\|)$ is called the *actual attraction.*
- The term $yg_r(\|y\|)$ is called the *actual repulsion.*

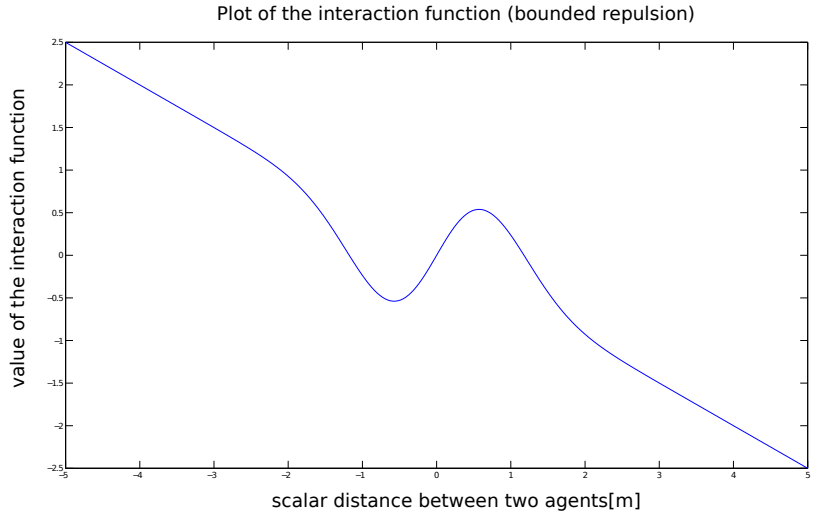

Figure 3.2: Plot of the interaction function with bounded repulsion with $a = 0.5, b = 2, c = 1$.

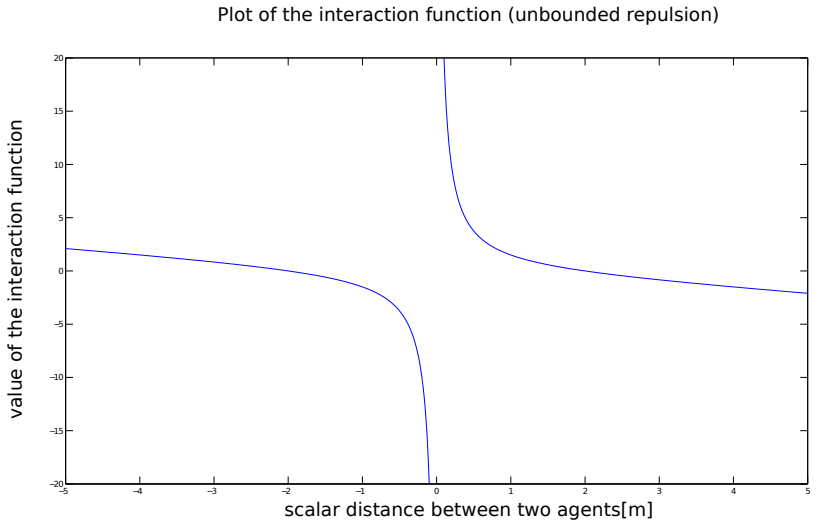

Figure 3.3: Plot of the interaction function with an unbounded repulsion and $a = 0.5, b = 2, c = 1$.

In the first point, the role of the vector y is clarified. As far as the last two points is concerned, they state that the whole term $yg_*(\|y\|)$ represents the actual attraction/repulsion, i.e., the whole vector with magnitude and direction.

In order to clarify the behavior of the interaction function, let us consider the following example, firstly introduced in [60]:

$$g(y) = -y\left[\underbrace{a}_{g_a(\|y\|)} - \underbrace{be^{-\left(\frac{\|y\|^2}{c}\right)}}_{g_r(\|y\|)}\right], \|y\| = \delta = \sqrt{c\ln\left(\frac{a}{b}\right)},$$

with $a, b, c \in \mathbb{R}^+$ constant gains. In Fig.3.2 a possible plot of the interaction function is proposed. Note that the distance vector y is assumed to be a scalar in order to simplify the plot. The equilibrium distance δ is reached in two symmetric (w.r.t. the vertical axis passing through the origin) points of the plot and in the origin, even if the latter is not a feasible configuration as it represents the collision of two robots. Moreover, it is possible to notice both the ranges of distance where the repulsion dominates the attraction and the other way round. In this figure, the repulsion between two agents is bounded, i.e., when the agents get closer to each other the repulsion is dominated by a finite value. Instead, in Fig. 3.3, the repulsion is unbounded because it tends to infinity as two agents get closer. Using an unbounded control law instead of a bounded one, guarantees the collision avoidance among the robots at the expense of an increased control effort. In the rest of this thesis, two saturated control laws are introduced to guarantee collision avoidance taking also into account the limited capabilities of the robots actuators.

In the next section, classical results on fully connected robot swarms are reviewed. For the sake of readability, the time-dependency will be omitted where not strictly required.

3.2 Fully Connected Topology Review

For the sake of clarity and completeness, the approach proposed by Veysel Gazi and Kevin M. Passino in [19] is reviewed in this section and the main properties arising from it are highlighted.

Let us suppose that the swarm interactions are encoded by a time unvarying fully connected undirected graph $\mathcal{G}\{V, E\}$. The dynamics of each

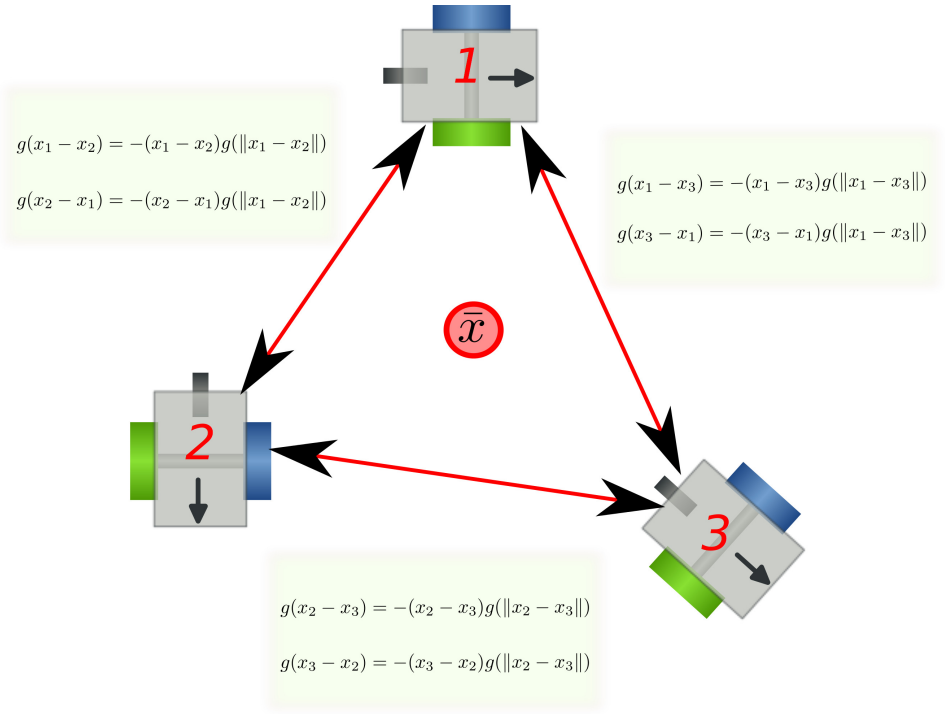

Figure 3.4: Example of fully connected swarm with 3 agents.

robot is given by the following equation:

$$\dot{x}_i = \sum_{j \neq i, j=1}^{n} g(x_i - x_j), \qquad i = 1, \ldots, n. \tag{3.2.1}$$

An example with 3 agents is illustrated in Fig.3.4.

A peculiar property of the fully connected topology is that the swarm barycenter is stationary over time. This characteristic is detailed in the following lemma:

Lemma 3.2.1. *The barycenter $\bar{x}(t)$ of the swarm consisting of agents with dynamics* (3.2.1) *with an attraction/repulsion function $g(\cdot)$ which is odd and satisfies the assumption **A1** is stationary for all t.*

Proof. Let us compute the time derivative of the barycenter:

$$\begin{aligned}\dot{\bar{x}} &= -\frac{1}{n}\sum_{i=1}^{n}\sum_{j=1,j\neq i}^{n}\left[g_a\left(\|x_i-x_j\|\right)-g_r\left(\|x_i-x_j\|\right)\right](x_i-x_j)\\ &= -\frac{1}{n}\sum_{i=1}^{n-1}\sum_{j=i+1}^{n}\Big[\left[g_a\left(\|x_i-x_j\|\right)-g_r\left(\|x_i-x_j\|\right)\right](x_i-x_j)+\\ &\quad+\left[g_a\left(\|x_j-x_i\|\right)-g_r\left(\|x_j-x_i\|\right)\right](x_j-x_i)\Big]=0\end{aligned}$$

□

Note that the last equation is obtained by using the assumption that the interaction function is odd. For the sake of analysis, let us consider the following assumption:

Assumption 2 (**A2**): There exist functions $J_a(\|y\|):\mathbb{R}^+\to\mathbb{R}^+$ and $J_r(\|y\|):\mathbb{R}^+\to\mathbb{R}^+$ such that $\nabla_y J_a(\|y\|)=y\,g_a(\|y\|)$ and $\nabla_y J_r(\|y\|)=y\,g_r(\|y\|)$.

In the following, the main theorems concerning the swarm aggregation algorithms for fully connected undirected communication graphs are reported. The proofs are omitted for the sake of brevity. For further details, the reader is referred to [21] .

Theorem 3.2.1. *Let us consider a swarm of robots whose dynamics is described by* (3.2.1) *under* ***A1,A2****. The swarm reaches a* steady configuration *as time goes to infinity, that is:*

$$\chi(t)\to\Omega_e,\ t\to\infty;\quad \forall\,\chi(0)\in\mathbb{R}^{dn}, \tag{3.2.2}$$

with $\Omega_e=\{\chi:\dot{\chi}(t)=\mathbf{0}\}$*, i.e., the set of the* equilibrium points*.*

Theorem 3.2.2. *Consider a swarm of n robots with dynamics given by* (3.2.1) *under assumptions* ***A1****,* ***A2****. Assume that the interaction function is composed of a linear attraction and a bounded repulsion, i.e.,* $g_a(\|y\|)=a$ *and* $g_r(\|y\|)\|y\|=b$ *with* $a,b>0$ *two real constant values. Then, the members of the swarm converges to the bounded area described by:*

$$B_r=\{x\in\mathbb{R}^d:\|x-\bar{x}(t)\|\leq\frac{b}{a}\}.$$

Moreover, the swarm eventually converges to the region B_r *in finite time, bounded by:*

$$\bar{t}\leq\max_{i\in\{1,\dots,n\}}\left\{-\frac{1}{2a}\ln\left(\frac{\xi^2}{2V_i(0)}\right)\right\} \tag{3.2.3}$$

with $\xi = \frac{b}{a}$.

Theorem 3.2.3. *Consider a swarm of n robots with dynamics given by* (3.2.1) *under assumptions **A1**, **A2**. Assume that the interaction function is composed of a linearly bounded from below attraction and an unbounded repulsion, i.e., $g_a(\|y\|) \geq a$ and $g_r(\|y\|) = \frac{b}{\|y\|^2}$ with $a, b > 0$ two real constant values. Then, the root mean square of the distances of the swarm members from the barycenter will satisfy:*

$$e_{rms} = \sqrt{\frac{1}{n}\sum_{i=1}^{n} \|e_i\|^2} \leq \sqrt{\frac{b}{2a}}.$$

Summarizing, the properties of the control algorithm in (3.2.1) are the following:

P1 The barycenter $\bar{x}$ of the swarm is stationary over time.

P2 The swarm converges to an equilibrium state.

P3 The swarm converges to a bounded region.

P4 The swarm reaches the bounded region in finite time.

In the next section, the control law in (3.2.1) is generalized to deal with fixed and time varying not fully connected undirected graphs. Therefore, in the rest of this thesis, the input to each agent is saturated to cope with the hardware limitations of the actuators and an effective obstacle avoidance algorithm is integrated.

3.3 Swarm Aggregation Control Laws with Local Interactions

In this section, the control law reviewed in Section 3.2 is extended preserving properties **P1**-**P4**. In particular, the interactions among the robots are limited by a range of view, i.e., each robot interacts only with its neighbors. Modeling the robot sensing capabilities using a limited range of view is of crucial importance as it allows to consider a realistic model for a broad range of distance measurement or relative pose sensors. This assumption becomes mandatory in the case of indoor environments where a GPS system can not be used by the robot. Therefore, the convergence of the fixed topology scenario is investigated. Eventually, the convergence of the more general case of switching topology is analyzed.

3.3.1 Fixed Topology

Let us consider a swarm composed of n robots with a fixed network topology described by an undirected graph $\mathcal{G} = \{V, E\}$ modeling the local interactions among the robots. The following dynamics is considered for each robot i:

$$\dot{x}_i = \sum_{j \in \mathcal{N}_i} g(x_i - x_j), \qquad i = 1, \ldots, n. \tag{3.3.1}$$

Note that in Eq.(3.3.1) the term $\mathcal{N}_i$ indicates that each robot i interacts only with its neighbors. Let us first provide a theorem which states that the swarm will converge towards a steady configuration as time goes to infinity.

Theorem 3.3.1. *Let us consider a swarm of robots whose dynamics is described by Eq.* (3.3.1) *with an interaction function $g(\cdot)$ defined according to Eq.* (3.1.5) *under **A1**-**A2**. If the graph $\mathcal{G}$ is connected, then the swarm reaches a steady configuration as time goes to infinity, that is:*

$$\chi(t) \to \Omega_e, \; t \to \infty; \quad \forall \chi(t_0) \in \mathbb{R}^{dn} \tag{3.3.2}$$

with $\Omega_e = \{\chi : \dot{\chi}(t) = 0\}$ the invariant set of equilibrium points.

Proof. The proof follows the same argument as in [5, Theorem 1], where the Lyapunov candidate function has been opportunely modified to take into account the fact that the robots interaction is limited according to the network topology. In particular, let us consider the following (generalized) Lyapunov candidate function:

$$V = \sum_{i=1}^{n-1} \sum_{\substack{j \in \mathcal{N}_i \\ j > i}} \Big[J_a(\|x_i - x_j\|) - J_r(\|x_i - x_j\|) \Big].$$

Let us now compute the gradient with respect to the i-th agent as follows:

$$\begin{aligned} \nabla_{x_i} V =& \sum_{j \in \mathcal{N}_i} \Big[\nabla_{x_i} J_a(\|x_i - x_j\|) - \nabla_{x_i} J_r(\|x_i - x_j\|) \Big] \\ =& \sum_{j \in \mathcal{N}_i} (x_i - x_j) \Big[g_a(\|x_i - x_j\|) - g_r(\|x_i - x_j\|) \Big] \\ =& -\dot{x}_i \end{aligned}$$

where **A2** has been used.

Let us now compute the time derivate $\dot{V}$ of the Lyapunov candidate

function as follows:

$$\dot{V} = [\nabla_{\chi} V]^T \dot{\chi} = \sum_{i=1}^{n} [\nabla_{x_i} V]^T \dot{x}_i = -\sum_{i=1}^{n} \|\dot{x}_i\|^2 \leq 0.$$

Therefore, the Lyapunov function V decreases over time until $\dot{\chi} = 0$, which implies that the swarm will eventually reach a steady state. In particular, by choosing $\Omega_0 = \{\chi : V \leq V(\chi(t_0)\}$ and using the LaSalle's Invariance Principle, it follows that as $t \to \infty$ the state χ converges towards the largest invariant subset of the set Ω_0, that is:

$$\Omega_e = \{\chi : \dot{V} = 0\} = \{\chi : \dot{\chi}(t) = 0\}.$$

□

Let us now further investigate the region where the swarm members will converge to and let us provide a bound on the size of the swarm for two scenarios involving different repulsive actions: (i) bounded repulsion, (ii) unbounded repulsion.

Bounded repulsion

The following assumption is used along this section:

Assumption 3 (**A3**): The norm of the total repulsive vector is bounded:

$$\|y\| g_r(\|y\|) \leq \beta. \tag{3.3.3}$$

In the following, the main result of this subsection is detailed:

Theorem 3.3.2. *Let us consider a swarm of robots whose dynamics is described by Eq.* (3.3.1) *with an interaction function $g(\cdot)$ defined according to Eq.* (3.1.5) *under **A1-A3**. If the graph $\mathcal{G}$ is connected, the swarm moves towards and remains within a bounded region defined as:*

$$\mathcal{B}_r = \left\{ x \in \mathbb{R}^d : \|x - \bar{x}\| \leq \frac{\beta\, \Delta_{\max}(\mathcal{G})\sqrt{n}}{\lambda_2(\mathcal{L}_{g_a,\mathcal{G}})} \right\}, \tag{3.3.4}$$

with $\Delta_{max}(\mathcal{G})$ the maximum degree among all the robots in the swarm.

Proof. Consider the following Lyapunov candidate function $V = \frac{1}{2}\sum_{i=1}^{n} \|e_i\|^2$ for which the following time derivative holds:

$$\dot{V} = \sum_{i=1}^{n} e_i^T \dot{e}_i. \tag{3.3.5}$$

For each robot i, the time derivative of the distance e_i from the barycenter is defined as follows:

$$\dot{e}_i = \sum_{j \in \mathcal{N}_i} g(e_i - e_j) \tag{3.3.6}$$

where the following facts have been used for the derivation:

- the center of mass $\bar{x}$ of the multi-robot system described by Eq. (3.3.1) with the interaction function $g(\cdot)$ given in Eq. (3.1.5) is stationary over time (Lemma 3.2.1[1],)

- the equality $(e_i - e_j) = (x_i - x_j)$ is obtained by simply adding and subtracting the quantity $\bar{x}$ to the term on the left side.

Note that, by substituting in Eq. (3.3.6) the definition of the interaction function given in Eq. (3.1.5), the following expression is obtained:

$$\dot{e}_i = \sum_{j \in \mathcal{N}_i} -(e_i - e_j)\left[g_a(\|e_i - e_j\|) - g_r(\|e_i - e_j\|)\right]. \tag{3.3.7}$$

At this point, by substituting Eq. (3.3.7) in Eq. (3.3.5) the derivative $\dot{V}$ of the Lyapunov candidate function can be re-written as follows:

$$\dot{V} = \sum_{i=1}^{n} e_i^T \sum_{j \in \mathcal{N}_i} -(e_i - e_j)\left[g_a(\|e_i - e_j\|) - g_r(\|e_i - e_j\|)\right]. \tag{3.3.8}$$

In order to study the convergence of the multi-robot system described by Eq. (3.3.1), let us decompose the derivative $\dot{V}$ of the Lyapunov function given in Eq. (3.3.8) in two terms as follows:

[1]Note that, although the swarm is assumed to be fully connected in Lemma 3.2.1, the lemma still holds for the considered scenario.

$$\begin{aligned}\dot{V} = &\underbrace{\sum_{i=1}^{n} e_i^T \sum_{j\in\mathcal{N}_i} -(e_i - e_j)\, g_a(\|e_i - e_j\|)}_{\dot{V}_a} \\ &+ \underbrace{\sum_{i=1}^{n} e_i^T \sum_{j\in\mathcal{N}_i} (e_i - e_j)\, g_r(\|e_i - e_j\|)}_{\dot{V}_r}.\end{aligned} \tag{3.3.9}$$

Let us now investigate the first of the two terms of the derivative $\dot{V}$, namely $\dot{V}_a$. Note that, the term $\dot{V}_a$ can be restated in a more convenient way for the stability analysis as follows:

$$\dot{V}_a = -\mathbf{e}^T \mathcal{L}^m_{g_a,\mathcal{G}}\, \mathbf{e}, \tag{3.3.10}$$

with $\mathcal{L}^m_{g_a,\mathcal{G}} = \mathcal{L}_{g_a,\mathcal{G}} \otimes I_m$, where $\mathcal{L}_{g_a,\mathcal{G}}$ is a time-varying weighted Laplacian matrix associated to $g_a(\cdot)$. It is obtained by considering the following coefficients for the adjacency matrix:

$$a_{ij} = \begin{cases} g_a(\|e_i - e_j\|) & \text{if } j \in \mathcal{N}_i, \\ 0 & \text{otherwise.} \end{cases} \tag{3.3.11}$$

Furthermore, $\otimes$ defines the Kronecker product and I_m an $m \times m$ identity matrix. At this point, since the Laplacian is a positive semi-definite matrix by construction, the following inequality holds:

$$\begin{aligned}\dot{V}_a &= -\mathbf{e}^T \mathcal{L}^m_{g_a,\mathcal{G}}\, \mathbf{e} \\ &\leq -\lambda_2(\mathcal{L}_{g_a,\mathcal{G}})\, \|\mathbf{e}\|^2, \forall\, \mathbf{e} \notin \text{span}\{\mathbf{1}\otimes\xi_1, \ldots, \mathbf{1}\otimes\xi_m\},\end{aligned} \tag{3.3.12}$$

with $\xi_i = [0, \ldots, \underbrace{1}_{i-th}, \ldots, 0]^T$ the i-th vector of the standard basis. Note that, the case $\mathbf{e} \in \text{span}\{\mathbf{1}\otimes\xi_1, \ldots, \mathbf{1}\otimes\xi_m\}$ is not considered as it implies:

$$\chi = [x_1^T, \ldots, x_n^T]^T \in \text{span}\{\mathbf{1}\otimes\xi_1, \ldots, \mathbf{1}\otimes\xi_m\},$$

that is $x_1 = \ldots = x_m$ which represents a trivial steady state for the interaction dynamics given in Eq. (3.3.1), namely all the robots are collapsed to the same point. Furthermore, it should be noticed that due to the repulsive component of the interaction function given in Eq. (3.1.5), this trivial steady state could be achieved only if all the robots were originally located at the same point, namely $\text{span}\{\mathbf{1}\otimes\xi_1, \ldots, \mathbf{1}\otimes\xi_m\}$ is an invariant subspace which is orthogonal to the swarm trajectories under the assumption

that $\chi(t_0)=[x_1^T(t_0),\,\ldots,\,x_n^T(t_0)]^T \notin \text{span}\{\mathbf{1}\otimes\xi_1,\,\ldots,\,\mathbf{1}\otimes\xi_m\}$.
Let us now investigate the second of the two terms of the derivative $\dot{V}$, namely $\dot{V}_r$:

$$\dot{V}_r = \sum_{i=1}^{n} e_i^T \sum_{j\in\mathcal{N}_i} (e_i - e_j)\, g_r(\|e_i - e_j\|). \tag{3.3.13}$$

At this point, by recalling **A3**, the term $\dot{V}_r$ can be bounded as follows:

$$\begin{aligned}
\dot{V}_r &= \sum_{i=1}^{n} e_i^T \sum_{j\in\mathcal{N}_i} (e_i - e_j)\, g_r(\|e_i - e_j\|) \\
&\leq \sum_{i=1}^{n} \|e_i\| \sum_{j\in\mathcal{N}_i} \|e_i - e_j\|\, g_r(\|e_i - e_j\|) \\
&\leq \sum_{i=1}^{n} \|e_i\| \sum_{j\in\mathcal{N}_i} \beta \leq \beta \sum_{i=1}^{n} \|e_i\| \Delta_i(\mathcal{G}) \\
&\leq \beta\, \Delta_{\max}(\mathcal{G}) \sqrt{n}\, \|\mathbf{e}\|
\end{aligned} \tag{3.3.14}$$

where the fact $\sum_{i=1}^{n} \|e_i\| \leq \sqrt{n}\,\|\mathbf{e}\|$ has been used.

Let us now substitute in Eq. (3.3.8) the bounds obtained for the two terms $\dot{V}_a$ and $\dot{V}_r$ respectively in Eq. (3.3.12) and Eq. (3.3.14) as follows:

$$\dot{V} = \dot{V}_a + \dot{V}_r \leq -\lambda_2(\mathcal{L}_{g_a,\mathcal{G}})\, \|\mathbf{e}\|^2 + \beta\, \Delta_{\max}(\mathcal{G}) \sqrt{n}\, \|\mathbf{e}\|. \tag{3.3.15}$$

Thus the derivative $\dot{V}$ is negative definite if the following holds:

$$\begin{aligned}
-\lambda_2(\mathcal{L}_{g_a,\mathcal{G}})\, \|\mathbf{e}\|^2 + \beta\, \Delta_{\max}(\mathcal{G}) \sqrt{n}\, \|\mathbf{e}\| &< 0 \\
\|\mathbf{e}\| \Big[-\lambda_2(\mathcal{L}_{g_a,\mathcal{G}})\, \|\mathbf{e}\| + \beta\, \Delta_{\max}(\mathcal{G}) \sqrt{n} \Big] &< 0
\end{aligned} \tag{3.3.16}$$

which implies:

$$\|\mathbf{e}\| > \frac{\beta\, \Delta_{\max}(\mathcal{G}) \sqrt{n}}{\lambda_2(\mathcal{L}_{g_a,\mathcal{G}})}. \tag{3.3.17}$$

Therefore, the solution of the system is uniformly bounded within the region:

$$\|x - \bar{x}\| \leq \frac{\beta\, \Delta_{\max}(\mathcal{G}) \sqrt{n}}{\lambda_2(\mathcal{L}_{g_a,\mathcal{G}})}. \tag{3.3.18}$$

□

Remark 3.3.1. *Note that, the term $\lambda_2(\mathcal{L}_{g_a,\mathcal{G}})$ is time-varying. This is due to the fact that no assumption has been made for the attractive function $g_a(\cdot)$. Indeed, a better bound can be obtained if further as-*

sumptions are made on the attractive term $g_a(\cdot)$. To this end, let us consider the following special case:

$$g_a(\|y\|) = a. \tag{3.3.19}$$

By having a linear attraction, Eq. (3.3.10) *can be modified as follows:*

$$\dot{V}_a = -a\, \mathbf{e}^T \mathcal{L}_{\mathcal{G}}^m\, \mathbf{e}, \tag{3.3.20}$$

As a result, the bound given in Eq. (3.3.18) *becomes:*

$$\|\mathbf{e}\| > \frac{\beta\, \Delta_{\max}(\mathcal{G})\sqrt{n}}{a\, \lambda_2(\mathcal{L}_{\mathcal{G}})}, \tag{3.3.21}$$

which implies:

$$\|x - \bar{x}\| \leq \frac{\beta\, \Delta_{\max}(\mathcal{G})\sqrt{n}}{a\, \lambda_2(\mathcal{L}_{\mathcal{G}})}. \tag{3.3.22}$$

Note that, this reflects the bound proposed in [86], where the convergence of the swarm dynamics given in Eq. (3.3.1)*, is investigated under the assumption of local communication among neighboring agents for a particular choise of attractive/repulsive functions originally proposed in [60], that is:*

$$g_a(\|y\|) = a, \quad g_r(\|y\|) \;\; = b \exp\left(-\frac{\|y\|^2}{c}\right) \tag{3.3.23}$$

with $\beta = b\sqrt{\frac{c}{2}} \exp\left(-\frac{1}{2}\right)$.

Unbounded repulsion

The following assumptions are used along this section:

Assumption 3b (**A3b**): The norm of the total repulsive vector is unbounded:

$$g_r(\|y\|) \leq \frac{\beta}{\|y\|^2}. \tag{3.3.24}$$

Assumption 4 (**A4**): The norm of the total attractive vector is bounded below by a linear function:

$$\|y\| g_a(\|y\|) \geq \alpha \|y\|. \tag{3.3.25}$$

In the following, the main result of this section is detailed:

Theorem 3.3.3. *Let us consider a swarm of robots whose dynamics is described by Eq.* (3.3.1) *with an interaction function $g(\cdot)$ defined according to Eq.* (3.1.5) *under **A1,A2,A3b** and **A4**. If the graph $\mathcal{G}$ is connected, then the swarm moves towards and remains within a bounded region defined as:*

$$\mathcal{B}_r = \left\{ x \in \mathbb{R}^d \,:\, \|x - \bar{x}\| \leq \sqrt{\frac{\beta\,|E|}{\alpha\,\lambda_2(\mathcal{L}_\mathcal{G})}} \right\} \tag{3.3.26}$$

Proof. Let us consider again the Lyapunov candidate function $V = \frac{1}{2}\sum_{i=1}^{n} \|e_i\|^2$ for which the following time derivative holds:

$$\begin{aligned} \dot{V} &= \sum_{i=1}^{n} e_i^T\, \dot{e}_i \\ &= \sum_{i=1}^{n} e_i^T \sum_{j\in\mathcal{N}_i} -(e_i - e_j)\,[g_a(\|e_i - e_j\|) - g_r(\|e_i - e_j\|)]. \end{aligned} \tag{3.3.27}$$

Note that, the derivative $\dot{V}$ could be restated with respect to the set of links E as follows:

$$\begin{aligned} \dot{V} &= -\sum_{(i,j)\in E} (e_i - e_j)^T (e_i - e_j)\,[g_a(\|e_i - e_j\|) - g_r(\|e_i - e_j\|)] \\ &= -\sum_{(i,j)\in E} [g_a(\|e_i - e_j\|) - g_r(\|e_i - e_j\|)]\,\|e_i - e_j\|^2. \end{aligned} \tag{3.3.28}$$

Therefore the time derivative $\dot{V}$ is negative definite if the following holds:

$$\sum_{(i,j)\in E} [g_a(\|e_i - e_j\|) - g_r(\|e_i - e_j\|)]\,\|e_i - e_j\|^2 \geq 0 \tag{3.3.29}$$

which can be restated as:

$$\sum_{(i,j)\in E} g_a(\|e_i - e_j\|)\,\|e_i - e_j\|^2 \geq \sum_{(i,j)\in E} g_r(\|e_i - e_j\|)\,\|e_i - e_j\|^2. \tag{3.3.30}$$

Recalling **A3b**, Eq. (3.3.30) can be re-written as follows:

$$\underbrace{\sum_{(i,j)\in E} g_a(\|e_i - e_j\|)\,\|e_i - e_j\|^2}_{H} \geq \beta|E| \tag{3.3.31}$$

where $|E|$ denotes the overall number of links for the graph $\mathcal{G} = \{V, E\}$.

Let us now consider an attractive function linearly bounded from below detailed in the following assumption:

The following inequality holds for H by using $\mathbf{A4}$:

$$\begin{aligned} H &= \sum_{(i,j)\in E} g_a(\|e_i - e_j\|)\,\|e_i - e_j\|^2 \\ &\geq \sum_{(i,j)\in E} \alpha\,\|e_i - e_j\|^2 = \alpha \sum_{(i,j)\in E} (e_i - e_j)^T (e_i - e_j) \\ &= \alpha \sum_{i=1}^{n} e_i^T \sum_{j\in\mathcal{N}_i} (e_i - e_j) = \alpha\,\mathbf{e}^T\,\mathcal{L}_{\mathcal{G}}^m\,\mathbf{e} \\ &\geq \alpha\,\lambda_2(\mathcal{L}_{\mathcal{G}})\,\|\mathbf{e}\|^2 \quad \forall\,\mathbf{e} \notin \text{span}\{\mathbf{1}\otimes\xi_1,\,\ldots,\,\mathbf{1}\otimes\xi_m\}, \end{aligned} \tag{3.3.32}$$

Therefore, Eq. (3.3.31) can be re-stated as follows:

$$\alpha\,\lambda_2(\mathcal{L}_{\mathcal{G}})\,\|\mathbf{e}\|^2 \geq \beta|E| \tag{3.3.33}$$

That is:

$$\|\mathbf{e}\|^2 \geq \frac{\beta}{\alpha\,\lambda_2(\mathcal{L}_{\mathcal{G}})}|E| \tag{3.3.34}$$

Therefore, the solution of the system is uniformly bounded within the region:

$$\|x - \bar{x}\| \leq \sqrt{\frac{\beta\,|E|}{\alpha\,\lambda_2(\mathcal{L}_{\mathcal{G}})}} \tag{3.3.35}$$

□

A few remarks are now in order.

Remark 3.3.2. *If the graph is fully connected, then $|E|=\frac{n(n-1)}{2}$. Furthermore, the Laplacian $\mathcal{L}$ has only two eigenvalues, namely $\sigma(\mathcal{L}) = \{\lambda_1 = 0,\,\lambda_2 = n\}$, with multiplicity respectively $\{\mu_1 = 1,\,\mu_2 = n-1\}$. This can be proven by looking at the particular structure of the matrices. In fact, for any symmetric matrix $A \in \mathbb{R}^{n\times n}$ with entries $a_{ii} = k$ and $a_{ij} = 1$, the determinant can be written in a closed form as $|A| = (k+n-1)\cdot(k-1)^{n-1}$. Details of the proof can be found in [46]. As a result, the bound given in Eq.* (3.3.35) *can be restated as follows:*

$$\|x - \bar{x}\| \leq \sqrt{\frac{\beta\,n}{\alpha\,2}} \tag{3.3.36}$$

which is exactly the result provided in [5].

Remark 3.3.3. *For sake of completeness, let us point out that in [5], also the case of almost constant attraction is investigated, that is* $g_a(\|x_i - x_j\|) \to 0$ *as* $\|x_i - x_j\| \to \infty$*. Indeed, this allows to model the fact that the interaction among agents vanishes as they move apart from each other. Note that, in this framework this peculiar behavior is obtained by limiting the agents interaction to their neighborhood, namely agents who are farther apart than a certain distance do not interact with each other. Therefore, the case of almost constant attraction will not be analyzed.*

3.3.2 Switching Topology

Let us now consider a swarm composed of n robots for which the network topology might change over time. In this scenario, the interaction among robots can be modeled by means of a time-varying undirected graph $\mathcal{G}(t) = \{V, E(t)\}$, where $E(t) = \{\epsilon_{ij}(t) : \|x_i(t) - x_j(t)\| \leq r\}$, with r the visibility radius. The interaction dynamics given in Eq. (3.3.1) can be modified accordingly as follows:

$$\dot{x}_i = \sum_{j \in \mathcal{N}_i(t)} g(x_i - x_j), \qquad i = 1, \ldots, n \tag{3.3.37}$$

where $\mathcal{N}_i(t)$ it the time-varying neighborhood of robot i. Note that, the result given in Theorem 3.3.1 still holds in the case of a switching network topology under the assumption that the graph $\mathcal{G}$ remains connected over time. Indeed, this can be easily proven by exploiting the same Lyapunov candidate function as the one given in the proof of Theorem 3.3.1. As for the case of a static network topology, let us now investigate the region where the swarm members will converge to and let us provide a bound on the size of the swarm for both a bounded and an unbounded repulsion.

Bounded Repulsion

For a scenario where the swarm has a network topology which can change over time and the repulsive term is assumed to be bounded, the following theorem holds.

Theorem 3.3.4. *Let us consider a swarm of robots whose dynamics is described by Eq.* (3.3.37) *with an interaction function* $g(\cdot)$ *defined according to Eq.* (3.1.5) *under* ***A1-A3****. If the graph* $\mathcal{G}$ *remains connected*

over time the swarm moves towards and remains within a bounded region defined as:

$$\mathcal{B}_r = \left\{ x \in \mathbb{R}^d \,:\, \|x - \bar{x}\| \leq \frac{\beta\, \Delta_{\max}(\mathcal{G})\sqrt{n}}{\lambda_2(\mathcal{L}_{g_a,\mathcal{G}(t)})} \right\} \tag{3.3.38}$$

Proof. In order to prove the theorem is sufficient to notice that the Lyapunov candidate function $V = \frac{1}{2}\sum_{i=1}^{n} \|e_i\|^2$ is a common Lyapunov function for the switching dynamics given in Eq. (3.3.37). Therefore, the same argument proposed for the proof of Theorem 3.3.2 can be used. □

Unbounded Repulsion

For a scenario where the swarm has a network topology which can change over time and the repulsive term is unbounded, the following theorem holds.

Theorem 3.3.5. *Let us consider a swarm of robots whose dynamics is described by Eq.* (3.3.37) *with an interaction function $g(\cdot)$ under **A1,A2, A3b** and **A4**. If the graph $\mathcal{G}$ remains connected over time the swarm moves towards and remains within a bounded region defined as:*

$$\mathcal{B}_r = \left\{ x \in \mathbb{R}^d \,:\, \|x - \bar{x}\| \leq \sqrt{\frac{\beta\,|E|}{\alpha\,\lambda_2(\mathcal{L}_{\mathcal{G}(t)})}} \right\}. \tag{3.3.39}$$

Proof. In order to prove the theorem is sufficient to notice that the Lyapunov candidate function $V = \frac{1}{2}\sum_{i=1}^{n} \|e_i\|^2$ is a common Lyapunov function for the switching dynamics given in Eq. (3.3.37). Therefore, the same argument proposed for the proof of Theorem 3.3.3 can be used. □

3.4 Unmanned Surface Vehicles Application

The aim of a continuous and widespread monitoring of large water areas, as well as intensive sampling and surveillance of oceans, harbors, lakes and rivers has brought in the recent years to the definition and the development of heterogeneous multi-vehicle frameworks, where a set of networked agents cooperates and coordinates themselves to achieve global objectives.
In particular, the need of fast-reliable, light-weight and low-cost vehicles is a key issue for the development of such multi-robot frameworks; the advantages with respect to huge and fully-equipped single-vehicle systems are

obvious: multi-vehicle systems allow surveying of wider areas in less time, different sensing devices can be mounted on different vehicles thus lowering the cost of each single vehicle and achieving a higher robustness of the entire framework, avoiding to jeopardize the entire mission if a single robot or sensor fails or gets damaged. Moreover, the tasks of each agent can be replanned to achieve different sampling resolution of the zones of interest. Being USVs the interface between water and air environments, they are often also used as mobile communication relays between Autonomous Underwater Vehicles (AUVs) and remote control stations. For this reason, a number of studies and researches are dedicated to the coordination of such kind of vehicles. The motion coordination of USVs with the aim of providing and maintaining a communication infrastructure is of relevant importance, as exploited in the AOSN (Autonomous Ocean Sampling Network) Project, presented in [87] and [88], where an extended interconnection between underwater, surface and aerial vehicles is provided. For all of these reasons, a number of approaches and techniques have been developed in order to guide and control the motion of teams of marine vehicles. First at-field experiments were carried out to test and validate collision avoidance strategies for USVs based on COLREGS rules, like in [89]. On September 2008 in Trondheimsfjord (Norway), the first full-scale vehicle-following experiment in a civilian setting worldwide was carried out. The experiment involved a manned vehicle, a 30 m long research vessel with upper speed of 13 knots, followed by a retrofitted leisure boat of length 8.5 m with a maximum speed of 18 knots as USV [90]. The following year the experiment was replicated with a couple of slave vehicles following the master vessel [91]. A similar experiment was carried out by CNR-ISSIA with the Charlie USV following the dual-mode ALANIS vessel [92] Successful results have been also gained by the European Project GREX [93] where one of the main project goals was the creation of a conceptual framework and middleware systems to coordinate a swarm of heterogeneous robotic vehicles.

The main goal of this section is to merge a virtual target based path-following guidance system developed in [94] for marine surface vehicle systems, with the swarm methodology proposed in Section 3.3.2. The intuitive idea is to rely on a simple potential-based attraction/repulsion swarm aggregation strategy, while using the path-following guidance system, not to control the motion of each single vehicle, but to directly drive the whole swarm onto a desired path. In the following, a brief introduction to the essential concepts of the virtual target based path-following approach for single-vehicle guidance is firstly given (further details, proofs and experimental results, can be found in [94] and references therein). Subsequently,

such path-following approach is applied to the task of swarm path-following, not guiding the motion of each vehicle but providing the convergence to and the following of the path of the whole swarm.

3.4.1 Single-Vehicle Virtual Target based Path-Following

With reference to Fig. 3.5 and assuming the vehicle's motion restricted to the horizontal plane, the task is to reduce to zero both the position error vector $\underline{d}$, i.e. the distance between the vehicle and the virtual target attached to the *Serret-Frenet* frame $< v >$, and the orientation error $\beta = \psi - \psi_p$, where ψ and ψ_p are the vehicle's direction of motion and local path tangent respectively, expressed with respect to the earth-fixed reference frame $< w >$. Performing some geometrical computations, the following kinematic

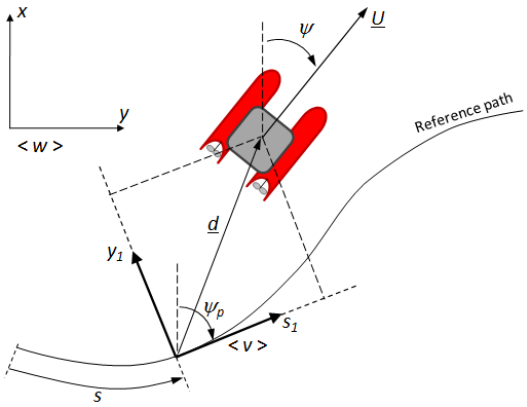

Figure 3.5: Path-following framework

error model is obtained and expressed with respect to the frame $< v >$:

$$\begin{cases} \dot{s}_1 &= -\dot{s}\,(1 - c_c y_1) + U\cos\beta \\ \dot{y}_1 &= -c_c \dot{s} s_1 + U\sin\beta \\ \dot{\beta} &= r - c_c \dot{s} \end{cases} \tag{3.4.1}$$

where $r = \dot{\psi}$, i.e. the yaw-rate of the vehicle which is also the control input for the kinematic system; c_c is the local path curvature and U is the norm of the vehicle's total velocity.
Posing the Lyapunov function $V = \frac{1}{2}(\beta - \varphi)^2$, $\dot{V}$ is negative-definite, with the following expression for r:

$$r^* = \dot{\varphi} - k_1(\beta - \varphi) + c_c \dot{s} \tag{3.4.2}$$

where k_1 is a positive controller gain, while φ is a suitable approach angle, function of the lateral error y_1, given by:

$$\varphi(y_1) = -\psi_a \tanh(k_\varphi\, y_1) \tag{3.4.3}$$

with $k_\varphi > 0$ and $0 < \psi_a < \frac{\pi}{2}$ parameters of the approach angle expression. The second step to guarantee the global convergence and the absence of singularities is to pose the Lyapunov function $V_e = \frac{1}{2}(s_1^2 + y_1^2)$, computing $\dot{V}_e$ and substituting first and second equations of (3.4.1), the following control signal guarantee $\dot{V}_e < 0$:

$$\dot{s}^* = U\cos\beta + k_2 s_1 \tag{3.4.4}$$

Such further control input regulates the speed of the virtual target, attached to the frame $< v >$, moving along the path.
The developed overall guidance system will reduce the lateral and orientation errors, y_1 and β respectively, driving the yaw-rate of the vehicle, while at the same time the speed regulation of the virtual target will reduce the longitudinal error s_1. The effect is that both the vehicle and the virtual target will converge one to each other.

3.4.2 Swarm Path-Following

The path-following behavior for the swarm is achieved modifying the control law in (3.3.37) by adding the swarm velocity input u_g computed by the path-following algorithm, i.e.:

$$\dot{x}_i = \sum_{j \in \mathcal{N}_i(t)} g(x_i - x_j) + u_g, \qquad i = 1, \ldots, n, \tag{3.4.5}$$

with $u_g \in \mathbb{R}^d$ the swarm guidance velocity input. In particular, the original single-vehicle path-following algorithm is initially adapted computing the cartesian error between the virtual target on the path and the coordinates of the center of mass of the swarm $\bar{x}$. The direction of motion of the swarm $\bar{\psi} = \dfrac{\sum_i \psi_i}{n}$ is not measured or estimated; being the swarm aggregation technique proven to converge to the velocity reference, the direction of the swarm motion is obtained by direct integration of the desired yaw rate obtained from Eq. (3.4.2) of the path-following controller, therefore $\bar{\psi} = \bar{\psi}^* = \int r^* dt$. Regarding the surge speed of the overall swarm, i.e. the norm of the desired velocity $|u_g|$, it is a priori defined and set by the user with a desired value $|u_g| = u_g^*$.

The reference velocity to be set as input for the swarm aggregation control system is then computed as:

$$u_g = \begin{bmatrix} |u_g| \cos \psi_b^* \\ |u_g| \sin \psi_b^* \end{bmatrix} \tag{3.4.6}$$

A simulation of the proposed integration between the swarm methodology and the path-following algorithm is given in Chapter 6

CHAPTER 4

Saturated Swarm Aggregation Control Laws with Local Interactions and Obstacle Avoidance

In this chapter, further extensions to the approach reviewed in Section 3.2 are introduced. Considering that the robot actuators have physical limitations by nature, i.e., they can not generate an arbitrarily large speed, the aforementioned approach is extended considering a bounded control input to the robot model in (3.1.1) using saturated inputs. A theoretical analysis of the implications of this choice is discussed in the rest of the chapter. A first approach integrating also an effective obstacle avoidance technique is detailed in the next section. In Section 4.2, instead, a refined control law with a single virtual robot for the obstacle avoidance is proposed. Note that, the notation introduced in Section 3.1 is used along this chapter.

4.1 Saturated Aggregation Law with Local Interactions and Obstacle Avoidance

In this section, a saturated swarm aggregation control law where the robot to robot interaction is limited by a visibility range r is proposed. The saturation is generated by adding a normalizing factor in the denominator of the control action of each robot i as follows:

$$\dot{x}_i(t) = k \frac{\sum_{j \in \mathcal{N}_i(t)} g(x_i(t) - x_j(t))}{1 + \left\| \sum_{j \in \mathcal{N}_i(t)} g(x_i(t) - x_j(t)) \right\|}, \tag{4.1.1}$$

where $k \geq 0$ is the saturation gain. Note that the visibility range r is used to define the neighborhood of the robot i as described by Equations (3.1.2)

and (3.1.4). Compared to the model reviewed in Section 3.2, the aggregation dynamics (4.1.1) has the following characteristics:

- The proximity graph encoding the interactions among the robots is time varying.
- Robots only interact within their visibility range.
- The control law is saturated to better comply with the actuators capabilities.

A consequence of these characteristics is the loss of property **P1**, i.e., the swarm barycenter is no longer stationary. This is due to the fact that, while the mutual effects of interacting robots are always symmetric in the model (3.2.1), this does not hold under limited visibility if saturation occurs. Nevertheless, it will be shown that model (4.1.1) still exhibits properties **P2–P4**.

4.1.1 Steady State Analysis

In this section, a convergence analysis for the control law given in (4.1.1) is provided. In particular, the following theorem shows the existence of a steady state configuration.

Theorem 4.1.1. *Consider a swarm of robots whose dynamics is described by* (4.1.1) *under* ***A1, A2****. Then the swarm reaches a steady state configuration for any given initial condition.*

Proof. Define $J(\|y\|) = J_a(\|y\|) - J_r(\|y\|)$, with $J_a(\cdot)$ and $J_r(\cdot)$ as in **A2**. Consider the following (generalized) Lyapunov candidate:

$$V(t) = \frac{1}{2} \sum_{(i,j)\in E(t)} J(\|x_i(t) - x_j(t)\|)$$

whose time derivative is:

$$\dot{V}(t) = \sum_{i=1}^{n} (\nabla_{x_i} V(t))^T \dot{x}_i(t). \tag{4.1.2}$$

By construction, the following is obtained:

$$\nabla_{x_i} V(t) = -\frac{\dot{x}_i(t)}{f(x_i(t))}, \tag{4.1.3}$$

with $f(x_i(t))$ defined as:

$$0 < f(x_i(t)) = \frac{1}{1 + \| \sum_{j \in \mathcal{N}_i(t)} g(x_i(t) - x_j(t)) \|} \leq 1. \tag{4.1.4}$$

Therefore, by substituting (4.1.3) in (4.1.2):

$$\dot{V}(t) = -\sum_{i=1}^{n} \frac{\|\dot{x}_i(t)\|^2}{f(x_i(t))} \leq 0.$$

Using LaSalle's Invariance Principle, it follows that as $t \to \infty$ the state $\chi(t)$ converges towards the largest invariant subset of the set where $\dot{V}(t) = 0$, that is:

$$\Omega_e = \{\chi : \dot{\chi}(t) = 0\}.$$

Since Ω_e is made of equilibrium points, the thesis follows. □

Note that, although Theorem 4.1.1 guarantees that the swarm converges to a steady state, it should be noticed that the computation of the equilibrium points in a closed form is impractical. Therefore, in the following section the area eventually achieved by the swarm of robots is characterized.

4.1.2 Cohesiveness Analysis

Let us now state a theorem concerning the bounded region where the swarm will eventually converge into.

Theorem 4.1.2. *Consider a swarm of robots whose dynamics is described by* (4.1.1) *under* ***A1-A3****. Then the swarm converges to the following bounded region:*

$$\mathcal{B}_r = \left\{ x \in \mathbb{R}^d \, : \, \|x - \bar{x}\| \leq \frac{\beta(n-1)}{\lambda_2(\mathcal{L}_{h_a, \mathcal{G}}(t))} \right\}.$$

Proof. Consider the following Lyapunov candidate:

$$V(t) = \frac{1}{2} \sum_{i=1}^{n} e_i(t)^T \, e_i(t). \tag{4.1.5}$$

Let us now consider the time derivative of the Lyapunov candidate as fol-

lows:

$$\dot{V}(t) = \sum_{i}^{n} e_i^T \dot{e}_i = \sum_{i=1}^{n} e_i^T (\dot{x}_i - \dot{\bar{x}}) = \underbrace{\sum_{i=1}^{n} e_i^T \dot{x}_i}_{\dot{V}_1} - \underbrace{\sum_{i=1}^{n} e_i^T \dot{\bar{x}}}_{\dot{V}_2}.$$

Let us first analyze the second term $\dot{V}_2$:

$$\dot{V}_2 = \sum_{i=1}^{n} e_i^T \dot{\bar{x}} = \left(\sum_{i=1}^{n} e_i^T \right) \dot{\bar{x}} = \mathbf{0}^T \dot{\bar{x}} = 0. \tag{4.1.6}$$

Note that, the motion of the barycenter does not affect the size of the region where the swarm will eventually aggregate. Interestingly enough, it only affects the location of such a region.

The term $\dot{V}_1$ is now investigated. Let $\bar{g}(\|e_i - e_j\|) = g_a(\|e_i - e_j\|) - g_r(\|e_i - e_j\|)$ and $k = 1$ with no lack of generality. By recalling that $x_i - x_j = e_i - e_j$, the following is obtained:

$$\begin{aligned}
\dot{V}_1 &= \sum_{i=1}^{n} e_i^T \frac{\sum_{j\in\mathcal{N}_i(t)} -(x_i - x_j)\,\bar{g}(\|x_i - x_j\|)}{1 + \| \sum_{j\in\mathcal{N}_i(t)} -(x_i - x_j)\,\bar{g}(\|x_i - x_j\|)\|} \\
&= \sum_{i=1}^{n} e_i^T \frac{\sum_{j\in\mathcal{N}_i(t)} -(e_i - e_j)\,\bar{g}(\|e_i - e_j\|)}{1 + \| \sum_{j\in\mathcal{N}_i(t)} -(e_i - e_j)\,\bar{g}(\|e_i - e_j\|)\|} \\
&= \sum_{i=1}^{n} f(x_i) e_i^T \sum_{j\in\mathcal{N}_i(t)} -(e_i - e_j)\bar{g}(\|e_i - e_j\|).
\end{aligned} \tag{4.1.7}$$

Therefore, Eq. (4.1.7) can be rewritten as follows:

$$\begin{aligned}
\dot{V}_1 &= \sum_{i=1}^{n} f(x_i) e_i^T \sum_{j\in\mathcal{N}_i(t)} -(e_i - e_j)\bar{g}(\|e_i - e_j\|) \\
&= \sum_{i=1}^{n} f(x_i) \left(-e_i^T \sum_{j\in\mathcal{N}_i(t)} (e_i - e_j) g_a(\|e_i - e_j\|) \right. \\
&\quad \left. + e_i^T \sum_{j\in\mathcal{N}_i(t)} (e_i - e_j) g_r(\|e_i - e_j\|) \right) \\
&= \sum_{i=1}^{n} \left(-e_i^T \sum_{j\in\mathcal{N}_i(t)} (e_i - e_j) h_a(\|e_i - e_j\|) + \right. \\
&\quad \left. + e_i^T \sum_{j\in\mathcal{N}_i(t)} (e_i - e_j) h_r(\|e_i - e_j\|) \right)
\end{aligned}$$

or

$$\dot{V}_1 = \underbrace{-\sum_{i=1}^{n} e_i^T \sum_{j\in\mathcal{N}_i(t)} (e_i - e_j) h_a(\|e_i - e_j\|)}_{\dot{V}_a} + \underbrace{\sum_{i=1}^{n} e_i^T \sum_{j\in\mathcal{N}_i(t)} (e_i - e_j) h_r(\|e_i - e_j\|)}_{\dot{V}_r}$$

where $h_a(\|e_i - e_j\|) = g_a(\|e_i - e_j\|) f(x_i)$ and $h_r(\|e_i - e_j\|) = g_r(\|e_i - e_j\|) f(x_i)$ are the attractive and repulsive terms, respectively.

Now, let us investigate the term $\dot{V}_a$:

$$\begin{aligned} \dot{V}_a &= -\sum_{i=1}^{n} e_i^T \sum_{j\in\mathcal{N}_i(t)} (e_i - e_j)\, h_a(\|e_i - e_j\|) \\ &= -\mathbf{e}^T \mathcal{L}^d_{h_a,\mathcal{G}}(t)\mathbf{e} \end{aligned} \tag{4.1.8}$$

where: $\mathcal{L}^d_{h_a,\mathcal{G}}(t) = \mathcal{L}_{h_a,\mathcal{G}}(t) \otimes I_d$ with $\otimes$ the Kronecker product and $\mathcal{L}_{h_a,\mathcal{G}}(t)$ the weighted Laplacian matrix related to the attractive term $h_a(\cdot)$:

$$\mathcal{L}_{h_a,\mathcal{G}}(t) = \mathcal{D}_{h_a,\mathcal{G}}(t) - \mathcal{A}_{h_a,\mathcal{G}}(t). \tag{4.1.9}$$

Here, $\mathcal{A}_{h_a,\mathcal{G}}(t)$ is the related adjacency matrix whose elements $\mathcal{A}^{ij}_{h_a,\mathcal{G}}(t)$ are defined as follows:

$$\mathcal{A}^{ij}_{h_a,\mathcal{G}}(t) = \begin{cases} h_a(\|e_i - e_j\|) & \text{if } (i,j) \in E(t), \\ 0 & \text{otherwise} \end{cases}$$

and $\mathcal{D}_{h_a,\mathcal{G}}(t)$ is the related degree matrix whose elements $\mathcal{D}^{ij}_{h_a,\mathcal{G}}(t)$ are defined as follows:

$$\mathcal{D}^{ij}_{h_a,\mathcal{G}}(t) = \begin{cases} \sum_{j\in\mathcal{N}_i(t)} h_a(\|e_i - e_j\|) & \text{if } i = j, \\ 0 & \text{otherwise.} \end{cases}$$

Note that, although the network topology encoding the robot-to-robot interaction is described by a time varying undirected graph $\mathcal{G}(t)$, the Laplacian matrix $\mathcal{L}_{h_a,\mathcal{G}}(t)$ related to the attractive term does not sum up to zero on both the columns and the rows but only on the rows as $f(x_i) \neq f(x_j)$ in general due to the saturations.

For the quadratic form in (4.1.8), the following inequality holds:

$$\begin{aligned} \mathbf{e}^T \mathcal{L}_{h_a}^d(\mathcal{G}(t))\mathbf{e} \geq \lambda_2(\mathcal{L}_{h_a,\mathcal{G}}(t))\|\mathbf{e}\|^2, \\ \forall\, \mathbf{e} \notin \text{span}\{\mathbf{1}\otimes\xi_1,\ldots,\mathbf{1}\otimes\xi_d\}. \end{aligned} \tag{4.1.10}$$

Using this fact, it is obtained:

$$\begin{aligned} \dot{V}_a &\leq -\lambda_2(\mathcal{L}_{h_a,\mathcal{G}}(t))\|\mathbf{e}\|^2 \\ &= -\lambda_2(\mathcal{L}_{h_a,\mathcal{G}}(t))\sum_{i=1}^{n}\|e_i\|^2. \end{aligned} \tag{4.1.11}$$

Recalling that:

$$\|x_i - x_j\|\, g_r(\|x_i - x_j\|) \leq \beta$$

or, equivalently:

$$\|e_i - e_j\|\, g_r(\|e_i - e_j\|) \leq \beta,$$

the following holds:

$$\begin{aligned} \dot{V}_r &= \sum_{i=1}^{n} e_i^T \sum_{j\in\mathcal{N}_i(t)} (e_i - e_j)\, h_r(\|e_i - e_j\|) \\ &\leq \sum_{i=1}^{n} e_i^T \sum_{j\in\mathcal{N}_i(t)} (e_i - e_j)\, f(x_i)\, \frac{\beta}{\|e_i - e_j\|} \\ &\leq \sum_{i=1}^{n} \|e_i\| \sum_{j\in\mathcal{N}_i(t)} \|e_i - e_j\|\, f(x_i)\, \frac{\beta}{\|e_i - e_j\|} \\ &\leq \sum_{i=1}^{n} \|e_i\|\, f(x_i)\beta|\mathcal{N}_i(t)| \leq \sum_{i=1}^{n} \|e_i\|\, f(x_i)\, \beta\,(n-1) \\ &\leq \sum_{i=1}^{n} \|e_i\|\, \beta\,(n-1). \end{aligned} \tag{4.1.12}$$

Now combine eqs. (4.1.11) and (4.1.12) to get:

$$\begin{aligned} \dot{V}_1 &= \dot{V}_a + \dot{V}_r \\ &\leq -\lambda_2(\mathcal{L}_{h_a,\mathcal{G}}(t))\sum_{i=1}^{n}\|e_i\|^2 + \sum_{i=1}^{n}\|e_i\|\,\beta\,(n-1) \\ &\leq -\sum_{i=1}^{n}\|e_i\|\left(\lambda_2(\mathcal{L}_{h_a,\mathcal{G}}(t))\|e_i\| - \beta\,(n-1)\right) \end{aligned} \tag{4.1.13}$$

which is negative definite if the following holds for each term $\|e_i\|$:

$$\|e_i\| \geq \frac{\beta\,(n-1)}{\lambda_2(\mathcal{L}_{h_a,\mathcal{G}}(t))}, \quad \forall\, i \in \mathcal{V}. \tag{4.1.14}$$

Therefore, the bound on the maximum ultimate swarm size is:

$$\|x - \bar{x}\| \leq \frac{\beta\,(n-1)}{\lambda_2(\mathcal{L}_{h_a,\mathcal{G}}(t))}, \tag{4.1.15}$$

with $x \in \mathcal{R}^d$. □

In view of the convergence time analysis, let us now further detail the bound given in (4.1.15) under the following hypothesis:

Assumption 5 (**A5**): Graph $\mathcal{G}(t)$ remains connected at all times. In particular, it is $\lambda_2(\mathcal{L}_{h_a,\mathcal{G}}(t)) \geq \lambda_{2,\min} > 0$, with $\mathcal{L}_{h_a,\mathcal{G}}(t)$ the weighted Laplacian matrix related to the attractive term $h_a(\cdot) = g_a(\cdot)f(x_i(t))$, with $f(x_i(t))$ defined as in (4.1.4).

Corollary 4.1.1. *Consider a swarm of robots whose dynamics is described by* (4.1.1) *under* ***A1-A5****. Then the swarm converges to the following bounded region:*

$$\mathcal{B}_r = \left\{ x \in \mathbb{R}^d \,:\, \|x - \bar{x}\| \leq \frac{\beta}{\alpha}\,\frac{(n-1)}{\lambda_{2,\min}} \right\}.$$

Proof. Let us consider equation (4.1.8). Using **A4**, it becomes:

$$\begin{aligned}
\dot{V}_a &= -\sum_{i=1}^{n} e_i^T \sum_{j \in \mathcal{N}_i(t)} (e_i - e_j)\, h_a(\|e_i - e_j\|) \\
&\leq -\alpha \sum_{i=1}^{n} e_i^T \sum_{j \in \mathcal{N}_i(t)} (e_i - e_j)\, f(x_i) \\
&\leq -\alpha\, \mathbf{e}^T\, \mathcal{L}^d_{f,\mathcal{G}}(t)\, \mathbf{e} \\
&\leq -\alpha\, \lambda_2(\mathcal{L}_{f,\mathcal{G}}(t)) \|\mathbf{e}\|^2 \\
&\leq -\alpha\, \lambda_2(\mathcal{L}_{f,\mathcal{G}}(t)) \sum_{i=1}^{n} \|e_i\|^2,
\end{aligned}$$

with $\mathcal{L}^d_{f,\mathcal{G}}(t) = \mathcal{L}_{f,\mathcal{G}} \otimes I_d(t)$ and $\mathcal{L}_{f,\mathcal{G}}(t)$ the Laplacian matrix defined as in (4.1.9), where the elements $\mathcal{A}^{ij}_{f,\mathcal{G}}(t)$ and $\mathcal{D}^{ij}_{f,\mathcal{G}}(t)$ of the adjacency and

degree matrices, respectively, are obtained by replacing the terms $h_a(\|x_i - x_j\|)$ with the terms $f(x_i)$. This implies that the condition given in (4.1.14) can be rewritten as:

$$\|e_i\| \geq \frac{\beta}{\alpha} \frac{(n-1)}{\lambda_2(\mathcal{L}_{f,\mathcal{G}}(t))}. \tag{4.1.16}$$

Using **A5**, the bound given in (4.1.15) becomes:

$$\|x - \bar{x}\| \leq \frac{\beta}{\alpha} \frac{(n-1)}{\lambda_{2,\min}}. \tag{4.1.17}$$

□

Noting that (4.1.16) and (4.1.17) depend on the algebraic connectivity of the Laplacian matrix encoding the graph modeling the robot-robot interactions and that the existence of an edge in the graph is discriminated by the range of visibility r, then there exists a strong relationship between the bounds and r. In particular, the higher r the bigger becomes the algebraic connectivity as the number of edges in the graph increases. Therefore, the given bounds decrease until the upper bound n is reached for the value of the algebraic connectivity. In order to establish some interesting relationship with the fully-connected scenario in [5], consider the behavior of the proposed interaction rule when approaching the equilibrium. Therefore, in the following the Laplacian matrix $\mathcal{L}_{f,\mathcal{G}}$ will be replaced with the Laplacian $\mathcal{L}_{\mathcal{G}}$ for the sake of the analysis. The time dependency is omitted in this analysis since the graph is assumed to be fully connected when approaching the equilibrium. Consider that if the graph is fully connected it can be proven that $\lambda_2(\mathcal{L}_{\mathcal{G}}) = n$. Hence, (4.1.15) becomes:

$$\|x - \bar{x}\| \leq \frac{\beta}{\alpha} \frac{(n-1)}{n} \leq \frac{\beta}{\alpha} \tag{4.1.18}$$

which is the same result obtained in [5].

In the following section, the time required for the swarm to move arbitrary close to the region in (4.1.17) is detailed.

4.1.3 Convergence in Finite Time

In the following theorem, it is shown the finite time convergence of the dynamics in (4.1.1) towards the bounded region.

Theorem 4.1.3. *Let us consider a swarm of robots whose dynamics is described by Eq.* (4.1.1) *under* ***A1-A5****. Then the swarm moves arbitrarily close to the bounded region $\mathcal{B}_r$ defined in Corollary 4.1.1 in*

finite-time t_f, that is:

$$t_f \leq -\frac{1}{2\,\vartheta\,\lambda_{2,\min}} \ln\left(\frac{\xi^2}{2V(0)}\right), \tag{4.1.19}$$

with ξ defined as follows:

$$\xi = (1+\eta)\frac{\beta\,(n-1)}{\lambda_{2,\min}},$$

where $\eta = \dfrac{\vartheta}{1-\vartheta}$ with $\vartheta \in (0,\,1)$.

Proof. Let us consider the upper bound given in (4.1.13) for the Lyapunov function:

$$\begin{aligned}
\dot{V}(t) &\leq -\lambda_2(\mathcal{L}_{h_a,\mathcal{G}}(t)) \sum_{i=1}^{n} \|e_i\|^2 + \sum_{i=1}^{n} \|e_i\|\,\beta\,(n-1) \\
&\leq -\lambda_{2,\min} \sum_{i=1}^{n} \|e_i\|^2 + \beta\,(n-1) \sum_{i=1}^{n} \|e_i\| \\
&\leq -(1-\vartheta)\,\lambda_{2,\min} \sum_{i=1}^{n} \|e_i\|^2 - \vartheta\,\lambda_{2,\min} \sum_{i=1}^{n} \|e_i\|^2 \\
&+\beta\,(n-1) \sum_{i=1}^{n} \|e_i\| \\
&\leq -\vartheta\,\lambda_{2,\min} \sum_{i=1}^{n} \|e_i\|^2 - \sum_{i=1}^{n} \|e_i\|\,[(1-\vartheta)\,\lambda_{2,\min}\,\|e_i\| \\
&-\beta\,(n-1)]
\end{aligned}$$

where $0 < \vartheta < 1$. If the following condition holds for each term $\|e_i\|$:

$$\|e_i\| \geq \frac{\beta\,(n-1)}{(1-\vartheta)\,\lambda_{2,\min}} = \xi$$

the time derivative of the Lyapunov function can be bounded as follows:

$$\begin{aligned}
\dot{V}(t) &\leq -\vartheta\,\lambda_{2,\min} \sum_{i=1}^{n} \|e_i\|^2 \\
&\leq -2\vartheta\,\lambda_{2,\min}\,V(t).
\end{aligned}$$

Thus, the swarm moves arbitrarily close to the bounded region in finite time:

$$t_f \leq -\frac{1}{2\vartheta\,\lambda_{2,\min}} \ln\left(\frac{\xi^2}{2V(0)}\right).$$

□

4.1.4 Obstacle Avoidance Integration

The swarm dynamics (4.1.1) does not take into account the avoidance of the obstacles in the environment. However, this is necessary to ensure a safe navigation of the swarm within the environment. Nowadays, most of the mobile robotics platforms are equipped with low level obstacle avoidance algorithms. The approach proposed in the following does not conflict with the equipped algorithms but offers a smooth potential based obstacle avoidance forming, together with the swarm aggregation algorithm, a stable navigation framework for robot swarms.

The key idea is to represent an obstacle as a set of virtual robots in the neighborhood of the detecting robot. The set of virtual agents are created on the boundary of the obstacle by projection, i.e., they are located on the boundary of the obstacle at the minimum distance from the detecting agent. In order to avoid an undesired attraction from the obstacle, it is sufficient to set δ in **A1** as the activation threshold for the obstacle avoidance algorithm. Furthermore, the number of virtual robots added in the neighborhood of the i-th agent has to be at least equal to the number of its current neighbors, i.e. $|\mathcal{N}_i(t)|$. This prevents any collision because the repulsion originated by the virtual agents will certainly counteract any possible influence due to the actual neighbors. Therefore, the dynamics in (4.1.1) is modified as follows:

$$\dot{x}_i = k\,\frac{\sum_{j\in\mathcal{N}_i^+(t)} g(x_i - x_j)\sigma(i,j,\mathcal{N}_i^+(t))}{1+\left\|\sum_{j\in\mathcal{N}_i^+(t)} g(x_i - x_j)\sigma(i,j,\mathcal{N}_i^+(t))\right\|},$$

where $\mathcal{N}_i^+(t) = \mathcal{N}_i(t)\cup\mathcal{N}_i^{obs}(t)$ with $\mathcal{N}_i^{obs}(t)$ the indexes of the local set of obstacles detected by the i-th robot and $\sigma(i,j,\mathcal{N}_i^+(t)) = |\mathcal{N}_i(t)|$ if $j \in \mathcal{N}_i^{obs}(t)$, $\sigma(i,j,\mathcal{N}_i^+(t)) = 1$ otherwise. As a result, the dynamics are characterized by a switching topology where sets of virtual robots, i.e., obstacles, are appropriately added or removed. For such dynamics, the result given in Theorem 4.1.2 still holds.

Remark 4.1.1. *Note that, in this chapter obstacles are assumed to be convex in order to ensure the repulsive action to be continuous. In*

the case of not convex obstacles, it is always possible to resort to well known convex decomposition techniques, see [95, Chapter 7], so that this assumption can be satisfied.

4.2 Saturated Aggregation Law with Local Interactions and a Single Virtual Robot Obstacle Avoidance

The swarm aggregation algorithm proposed in Section 4.1 requires an obstacle avoidance technique which projects a set of virtual robots on the obstacle to ensure a safe navigation. In this section, a more refined control law where the obstacle avoidance requires to project only one virtual robot rather than a set is introduced.

Let us consider a swarm of n mobile robots for which, as detailed in Section 3.1, the interaction is described by means of an undirected time-varying proximity graph $\mathcal{G}(t) = \{V, E(t)\}$. In particular, for each mobile robot i consider the following dynamics:

$$\dot{x}_i = \frac{\sum\limits_{j \in \mathcal{N}_i(t)} \gamma_{ij}\, g(x_i - x_j)}{\sum\limits_{j \in \mathcal{N}_i(t)} \gamma_{ij}}, \tag{4.2.1}$$

where γ_{ij} is the weighting factor between each pair of neighboring robots i and j defined as:

$$\gamma_{ij} = \frac{1}{\|x_i - x_j\|^{\alpha}}, \quad \text{with } \alpha \geq 1. \tag{4.2.2}$$

For the proposed dynamics, the attraction and repulsion functions are defined as follows:

$$\begin{aligned} g_a(\|y\|) &= a(1 - \Phi(\|y\|)), \\ g_r(\|y\|) &= b\ \Phi(\|y\|), \end{aligned} \tag{4.2.3}$$

where a, $b > 0$ are constant real values and $\Phi(\cdot) : \mathbb{R} \to \mathbb{R}$ is a suitable generalized function. Note that, the term $g_a(\|y\|) - g_r(\|y\|)$ by construction takes values within the range $[a,\ -b]$. Similarly to the control law proposed in Section 4.1, **P1** does not hold. However, in the rest of this section the fact that **P2**-**P4** are still valid for the control law in (4.2.1) is proven.

In order to analyze the characteristics of the proposed control law, the following assumption is made on the generalized function $\Phi(\cdot)$:

Assumption 6 (**A6**): A generalized function $\Phi(\cdot)$ must satisfy the fol-

lowing properties:

- monotonic function,
- $\lim_{\|y\|\to 0} \Phi(\|y\|) = 1$,
- $\lim_{\|y\|\to \infty} \Phi(\|y\|) = 0$.

Example 1. *As an example of generalized function* $\Phi(\cdot)$*, let us consider:*

- $\exp\left(-\dfrac{\|y\|^{\beta}}{c}\right)$ *with* $\beta \geq 1$ *and* $c > 0$,
- $\operatorname{sech}\left(-\|y\|^{\beta}\right)$ *with* $\beta \geq 1$.

It is worth pointing out that, compared to the approach in Section 4.1, the control law given in Eq. (4.2.1) has two major advantages:

1. It allows the input saturation to be asymmetric with respect to the forward and backward velocity to better comply with the hardware/software specifications.
2. It allows an easier and yet more natural integration of the obstacle avoidance.

The following assumption is required in the rest of this section:

Assumption 7 (**A7**): There exist the following functions:

$$J_a(\|y\|) : \mathbb{R}^+ \to \mathbb{R}^+,$$
$$J_r(\|y\|) : \mathbb{R}^+ \to \mathbb{R}^+$$

such that:

$$\nabla_y J_a(\|y\|) = \left(\frac{1}{\|y\|}\right)^{\alpha} \frac{y}{\|y\|}\, g_a(y),$$
$$\nabla_y J_r(\|y\|) = \left(\frac{1}{\|y\|}\right)^{\alpha} \frac{y}{\|y\|}\, g_r(y).$$

4.2.1 Steady State Analysis

In the following, the fact that the multi-robot system always reaches a steady state equilibrium for any given initial condition is proven.

Theorem 4.2.1. *Consider a swarm of robots whose dynamics is described by Eq.* (4.2.1) *under* ***A1, A6*** *and* ***A7****. Then the swarm converges to an equilibrium state for any initial condition.*

Proof. Define $J(\|y\|) = J_a(\|y\|) - J_r(\|y\|)$, with $J_a(\cdot)$ and $J_r(\cdot)$ as in **A7**. Consider the following (generalized) Lyapunov candidate:

$$V(t) = \frac{1}{2} \sum_{(i,j)\in E(t)} J(\|x_i(t) - x_j(t)\|)$$

whose time derivative is:

$$\dot{V}(t) = \sum_{i=1}^{n} (\nabla_{x_i} V(t))^T \dot{x}_i(t). \tag{4.2.4}$$

By construction, it follows that:

$$\nabla_{x_i} V(t) = -\left[\sum_{j\in\mathcal{N}_i(t)} \gamma_{ij}\right] \dot{x}_i(t). \tag{4.2.5}$$

Therefore, substituting (4.2.5) in (4.2.4) and deriving from (4.2.2) that:

$$\gamma_i = \sum_{j\in\mathcal{N}_i(t)} \gamma_{ij} > 0, \tag{4.2.6}$$

it is obtained:

$$\dot{V}(t) = -\sum_{i=1}^{n} \left[\sum_{j\in\mathcal{N}_i(t)} \gamma_{ij}\right] \|\dot{x}_i\|^2 \leq 0.$$

Hence, using LaSalle's Invariance Principle, it follows that as $t \to \infty$ the state $\chi(t)$ converges towards the largest invariant subset of the set where $\dot{V}(t) = 0$, that is:

$$\Omega_e = \{\chi : \dot{\chi}(t) = 0\},$$

which proves the thesis as Ω_e is made of equilibrium points. □

Example 2. *Consider the following generalized function* $\Phi(\|y\|) = \exp(-\frac{\|y\|^4}{c})$. *Then,* ***A7*** *is satisfied and the following (generalized) Lyapunov candi-*

date can be used in Theorem 4.2.1:

$$V(t) = \sum_{(i,j)\in E(t)} \left[-\frac{a}{2\left\|x_i - x_j\right\|^4} + (a-b)\left(-\frac{e^{-\frac{\|x_i - x_j\|^4}{c}}}{2\|x_i - x_j\|^2} - \frac{\sqrt{\pi}\ \mathrm{Erf}\left(\frac{\|x_i - x_j\|^2}{\sqrt{c}}\right)}{2\sqrt{c}} \right) \right]$$

with $\mathrm{Erf}(\cdot)$ *the error function defined as:*

$$\mathrm{Erf}(y) = \frac{2}{\sqrt{\pi}} \int_0^y e^{-t^2}\, dt.$$

4.2.2 Cohesiveness Analysis

In the following, the fact that the multi-robot system converges towards a bounded region whose size is a function of the parameters of the interaction function and of the network topology is proven. Time dependency is omitted for compactness.

Theorem 4.2.2. *Let us consider a swarm of robots whose dynamics is described by Eq.* (4.2.1) *under* ***A1, A6*** *and* ***A7****. Then the swarm moves towards and remains within a bounded region:*

$$\mathcal{B}_r = \left\{ x \in \mathbb{R}^d : \|x - \bar{x}\| \leq \frac{1}{\hat{\lambda}_2(\hat{\mathcal{L}})} \left(1 + \frac{b}{a}\right) \right\}. \tag{4.2.7}$$

Proof. Let us take into account the following Lyapunov candidate function:

$$V = \sum_{i=1}^{n} \frac{1}{2} e_i^T\ e_i.$$

Let us now analyze the time derivative of the Lyapunov candidate:

$$\dot{V} = \sum_{i=1}^{n} e_i^T\ \dot{e}_i. \tag{4.2.8}$$

From (4.1.6), it is possible to notice that due to the limited interaction range and to the saturation effects, the barycenter is no longer stationary.

Consequently, the previous equation becomes:

$$\dot{V} = \sum_{i=1}^{n} e_i^T(\dot{x}_i - \dot{\bar{x}}) = \underbrace{\sum_{i=1}^{n} e_i^T \dot{x}_i}_{V_1} - \underbrace{\sum_{i=1}^{n} e_i^T \dot{\bar{x}}}_{V_2}.$$

Similarly to what happens in (4.1.6), it can be noticed that the dynamics of the barycenter does not affect the value of the time derivative of the Lyapunov function, namely:

$$V_2 = \sum_{i=1}^{n} e_i^T \dot{\bar{x}} = \left(\sum_{i=1}^{n} e_i^T\right)(\dot{\bar{x}}) = \mathbf{0}^T(\dot{\bar{x}}) = 0. \tag{4.2.9}$$

Let us now consider the contribution V_i given by the i-th robot to the term V_1:

$$\begin{aligned}
\dot{V}_i =& e_i^T \frac{\sum\limits_{j\in\mathcal{N}_i(t)} -\gamma_{ij}\frac{(x_i-x_j)}{\|x_i-x_j\|}(g_a(\|x_i-x_j\|) - g_r(\|x_i-x_j\|))}{\gamma_i} \\
=& -\frac{e_i^T}{\gamma_i}\left[\sum_{j\in\mathcal{N}_i(t)} \gamma_{ij}\frac{(x_i-x_j)}{\|x_i-x_j\|}g_a(\|x_i-x_j\|)\right. \\
& \left. - \sum_{j\in\mathcal{N}_i(t)} \gamma_{ij}\frac{(x_i-x_j)}{\|x_i-x_j\|}g_r(\|x_i-x_j\|)\right]
\end{aligned}$$

At this point, by substituting $g_a = a(1-\Phi(\|x_i-x_j\|))$ and $g_r = b\ \Phi(\|x_i-x_j\|)$ in the previous equation it follows:

$$\begin{aligned}
\dot{V}_i =& -\frac{e_i^T}{\gamma_i}\left[\sum_{j\in\mathcal{N}_i(t)} \gamma_{ij}\frac{(x_i-x_j)\ a(1-\Phi(\|x_i-x_j\|))}{\|x_i-x_j\|}\right. \\
& \left. - \sum_{j\in\mathcal{N}_i(t)} \gamma_{ij}\frac{(x_i-x_j)\ b\ \Phi(\|x_i-x_j\|)}{\|x_i-x_j\|}\right] \\
=& \frac{e_i^T}{\gamma_i}\left[-a\sum_{j\in\mathcal{N}_i(t)} \gamma_{ij}\frac{(x_i-x_j)}{\|x_i-x_j\|}\right. \\
& \left. +(a+b)\sum_{j\in\mathcal{N}_i(t)} \gamma_{ij}\frac{(x_i-x_j)\ \Phi(\|x_i-x_j\|)}{\|x_i-x_j\|}\right]
\end{aligned}$$

$$\leq -\frac{a}{\gamma_i}\sum_{j\in\mathcal{N}_i(t)}\gamma_{ij}\frac{e_i^T(x_i-x_j)}{\|x_i-x_j\|} + \frac{(a+b)}{\gamma_i}\sum_{j\in\mathcal{N}_i(t)}\gamma_{ij}\frac{\|e_i\|\|x_i-x_j\|\ \Phi(\|x_i-x_j\|)}{\|x_i-x_j\|}$$

$$= -\frac{a}{\gamma_i}\sum_{j\in\mathcal{N}_i(t)}\gamma_{ij}\frac{e_i^T(x_i-x_j)}{\|x_i-x_j\|} + \frac{(a+b)}{\gamma_i}\sum_{j\in\mathcal{N}_i(t)}\gamma_{ij}\|e_i\|\ \Phi(\|x_i-x_j\|)$$

Now, by considering that $\Phi(\|x_i-x_j\|)\leq 1$, the following holds:

$$\dot{V}_i \leq -\frac{a}{\gamma_i}\sum_{j\in\mathcal{N}_i(t)}\gamma_{ij}\frac{e_i^T(x_i-x_j)}{\|x_i-x_j\|^{\hat{\alpha}}} + \frac{(a+b)}{\gamma_i}\|e_i\|\sum_{j\in\mathcal{N}_i(t)}\gamma_{ij}.$$

Noticing that the last term of the equation is equal to γ_i, the following is obtained:

$$\dot{V}_i \leq -\frac{a}{\gamma_i}\sum_{j\in\mathcal{N}_i(t)}\gamma_{ij}\frac{e_i^T(x_i-x_j)}{\|x_i-x_j\|} + (a+b)\|e_i\|. \tag{4.2.10}$$

Let us now recall that $x_i - x_j = e_i - e_j$. Thus, by substituting the previous equality in Eq. (4.2.10), it follows that:

$$= -\frac{a}{\gamma_i}\sum_{j\in\mathcal{N}_i(t)}\gamma_{ij}\frac{e_i^T(e_i-e_j)}{\|e_i-e_j\|} + (a+b)\|e_i\|. \tag{4.2.11}$$

It turns out that in order to have a semi-definite negative (SDN) time derivative of the Lyapunov function, the following condition must be satisfied:

$$-\frac{a}{\gamma_i}\sum_{j\in\mathcal{N}_i(t)}\gamma_{ij}\frac{e_i^T(e_i-e_j)}{\|e_i-e_j\|} + (a+b)\|e_i\| \leq 0,$$

or, in other terms:

$$(a+b)\|e_i\| \leq \frac{a}{\gamma_i}\sum_{j\in\mathcal{N}_i(t)}\gamma_{ij}\frac{e_i^T(e_i-e_j)}{\|e_i-e_j\|}.$$

Let us now consider all the elements of the term V_1:

$$\dot{V}_1 = \sum_{i=1}^{n} \left[-\frac{a}{\gamma_i} \sum_{j \in \mathcal{N}_i(t)} \gamma_{ij} \frac{e_i^T (e_i - e_j)}{\|e_i - e_j\|} + (a+b)\|e_i\| \right] \leq 0.$$

The previous equation can be restated as follows:

$$(a+b) \sum_{i=1}^{n} \|e_i\| \leq \sum_{i=1}^{n} \left[\frac{a}{\gamma_i} \sum_{j \in \mathcal{N}_i(t)} \gamma_{ij} \frac{e_i^T (e_i - e_j)}{\|e_i - e_j\|} \right]. \tag{4.2.12}$$

Basically, a lower bound of the term

$$a \sum_{i=1}^{n} \left[w_i \sum_{j \in \mathcal{N}_i(t)} \gamma_{ij} \frac{e_i^T (e_i - e_j)}{\|e_i - e_j\|} \right], \tag{4.2.13}$$

is required, where $w_i = \dfrac{1}{\gamma_i}$ has been used. To this aim, let us take into account the following error Laplacian matrix $\hat{\mathcal{L}}$:

$$\hat{l}_{ij} = \begin{cases} \sum\limits_{j \in \mathcal{N}_i(t)} \gamma_{ij} \dfrac{w_i}{\|e_i - e_j\|}, & j = i \\ -\gamma_{ij} \dfrac{w_i}{\|e_i - e_j\|}, & j \in \mathcal{N}_i(t) \\ 0 & \text{otherwise.} \end{cases} \tag{4.2.14}$$

Note that in this Laplacian, only the row sum is equal to zero. Equation (4.2.13) can be restated in terms of the algebraic connectivity of the Laplacian matrix $\hat{\mathcal{L}}$ as follows:

$$a \sum_{i=1}^{n} \left[w_i \sum_{j \in \mathcal{N}_i(t)} \gamma_{ij} \frac{e_i^T (e_i - e_j)}{\|e_i - e_j\|} \right] = a\, \mathbf{e}^T \hat{\mathcal{L}}^d \mathbf{e}, \tag{4.2.15}$$

where $\hat{\mathcal{L}}^d = \hat{\mathcal{L}} \otimes I_d$. An upper bound to the term $a\, e^T \hat{\mathcal{L}}^d e$ can be obtained similarly to (4.1.10). Let us substitute this bound to (4.2.12). The following is obtained:

$$(a+b) \sum_{i=1}^{n} \|e_i\| \leq a \hat{\lambda}_2(\hat{\mathcal{L}}) \|\mathbf{e}\|^2. \tag{4.2.16}$$

Note that, the previous equation can be equivalently stated as:

$$(a+b) \sum_{i=1}^{n} \|e_i\| \leq a \hat{\lambda}_2(\hat{\mathcal{L}}) \sum_{i=1}^{n} \|e_i\|^2. \tag{4.2.17}$$

At this point, since the previous inequality can be rewritten as:

$$-\|e\| \left[a\hat{\lambda}_2(\hat{\mathcal{L}})\|\mathbf{e}\| - (a+b)\sum_{i=1}^{n}\|e_i\| \right] \leq 0,$$

and by recalling that $\dot{V}_2 = 0$ due to (4.2.9), it follows that the derivative of the Lyapunov candidate is semi-definite negative if the following condition holds:

$$\|e_i\| \geq \frac{(a+b)}{a\,\hat{\lambda}_2(\hat{\mathcal{L}})} = \frac{1}{\hat{\lambda}_2(\hat{\mathcal{L}})}\left(1+\frac{b}{a}\right) \tag{4.2.18}$$

Therefore, the bound on the maximum ultimate swarm size is:

$$\|x - \bar{x}\| \leq \frac{1}{\hat{\lambda}_2(\hat{\mathcal{L}})}\left(1+\frac{b}{a}\right)$$

with $x \in \mathcal{R}^d$.

□

Remark 4.2.1. *Note that, differently from the bound given in Theorem 4.1.2, the bound in Theorem 4.2.2 does not depend upon the number of robots n due to the weighting factor in* (4.2.2).

It is worth to point out that the algebraic connectivity $\hat{\lambda}_2(\hat{\mathcal{L}})$ is a function of the Laplacian matrix thus it depends upon the errors $e_i, \forall i \in V$. Nevertheless, it is possible to derive a bound which does not depend upon $\mathbf{e}$ by exploiting the following assumption:

Assumption 8 (**A8**): The graph $\mathcal{G}(t)$ remains connected all the time. Furthermore, it is $\hat{\lambda}_2(\hat{\mathcal{L}}(t)) \geq \lambda_{2,\min}(\hat{\mathcal{L}}(t))$ with $\hat{\mathcal{L}}$ the error Laplacian matrix whose elements definition is given in Eq. (4.2.14).

Corollary 4.2.1. *Let us consider a swarm of robots whose dynamics is described by Eq.* (4.2.1) *under **A1, A6-A8**. Then the swarm moves towards and remains within a bounded region:*

$$\mathcal{B}_r = \left\{ \|x(t) - \bar{x}\| \leq \frac{1}{\lambda_{2,min}(\hat{\mathcal{L}})}\left(1+\frac{b}{a}\right) \right\}. \tag{4.2.19}$$

Proof. Applying **A8** to (4.2.17), it is obtained:

$$(a+b)\sum_{i=1}^{n}\|e_i\| \leq a\hat{\lambda}_{2,\min}(\hat{\mathcal{L}})\sum_{i=1}^{n}\|e_i\|^2. \tag{4.2.20}$$

The thesis follows by an algebraic computation similar to the one performed in Theorem 4.2.2. □

4.2.3 Convergence in Finite Time

In the following, the fact that the multi-robot system moves arbitrarily close the bounded region given in Corollary 4.2.1 in finite-time is proven.

Theorem 4.2.3. *Let us consider a swarm of robots whose dynamics is described by Eq.* (4.2.1) *under* ***A1,A6-A8****. Then the swarm moves arbitrarily close to the bounded region $\mathcal{B}_r$ defined in Corollary 4.2.1 in finite-time t_f, that is:*

$$t_f \leq -\frac{1}{2\,\vartheta\,a\,\hat{\lambda}_{2,\min}(\hat{\mathcal{L}})} \ln\left(\frac{\xi^2}{2V(0)}\right) \tag{4.2.21}$$

with ξ defined as follows:

$$\xi = (1+\eta)\,\frac{1}{\hat{\lambda}_{2,\min}(\hat{\mathcal{L}})}\left(1+\frac{b}{a}\right), \tag{4.2.22}$$

where $\eta = \dfrac{\vartheta}{1-\vartheta}$ with $\vartheta \in (0,\,1)$.

Proof. In order to prove the lemma, let us consider the bound given in Eq. (4.2.20):

$$\begin{aligned}
\dot{V} &\leq -a\,\hat{\lambda}_{2,\min}(\hat{\mathcal{L}}) \sum_{i=1}^{n} \|e_i\|^2 + (a+b) \sum_{i=1}^{n} \|e_i\| \\
&\leq -a(1+\vartheta-\vartheta)\,\hat{\lambda}_{2,\min}(\hat{\mathcal{L}}) \sum_{i=1}^{n} \|e_i\|^2 + (a+b) \sum_{i=1}^{n} \|e_i\| \\
&\leq -\vartheta\,a\,\hat{\lambda}_{2,\min}(\hat{\mathcal{L}}) \sum_{i=1}^{n} \|e_i\|^2
\end{aligned}$$

$$- (1-\vartheta)\, a\, \hat{\lambda}_{2,\min}(\hat{\mathcal{L}}) \sum_{i=1}^{n} \|e_i\|^2 + (a+b) \sum_{i=1}^{n} \|e_i\|$$

$$\leq -\vartheta\, a\, \hat{\lambda}_{2,\min}(\hat{\mathcal{L}}) \sum_{i=1}^{n} \|e_i\|^2$$

$$- \sum_{i=1}^{n} \|e_i\| \left[(1-\vartheta)\, a\, \hat{\lambda}_{2,\min}(\hat{\mathcal{L}}) \sum_{i=1}^{n} \|e_i\| - (a+b) \right]$$

At this point, if the following condition holds for each robot i:

$$(1-\vartheta)\, a\, \hat{\lambda}_{2,\min}(\hat{\mathcal{L}}) \sum_{i=1}^{n} \|e_i\| - (a+b) > 0$$

that is:

$$\|e_i\| > \frac{1}{(1-\vartheta)} \frac{(a+b)}{a\, \hat{\lambda}_{2,\min}(\hat{\mathcal{L}})} = \frac{1}{(1-\vartheta)\hat{\lambda}_{2,\min}(\hat{\mathcal{L}})} \left(1 + \frac{b}{a}\right) = \xi.$$

Then:

$$\dot{V} \leq -\vartheta\, a\, \hat{\lambda}_{2,\min}(\hat{\mathcal{L}}) \sum_{i=1}^{n} \|e_i\|^2$$

$$\leq -2\, \vartheta\, a\, \hat{\lambda}_{2,\min}(\hat{\mathcal{L}}) V(t)$$

Thus, the swarm moves arbitrarily close to the bounded region in finite time:

$$t_f \leq -\frac{1}{2\, \vartheta\, a\, \hat{\lambda}_{2,\min}(\hat{\mathcal{L}})} \ln \left(\frac{\xi^2}{2\, V(0)} \right)$$

□

4.2.4 Obstacle Avoidance Integration

An effective way to integrate the obstacle avoidance has been presented in Section 4.1.3 where an obstacle is represented as a set of virtual robots created on the boundary of the closest obstacle by projection, i.e. they are located on the boundary of the obstacle at the minimum distance from the detecting robot. Furthermore, the cardinality of this set of virtual robot has to be at least equal to the current neighborhood of the considered robot. Indeed, this would prevent any collision because the repulsion originated by the virtual robots will certainly counteract any possible influence by the

actual neighbors.

Conversely, by using the control law given in Eq. (4.2.1), only one virtual robot has to be projected on the closest obstacle. This can be explained by the fact that the control law proposed in this work relies on the presence of weighting factors γ_{ik}. To better understand this concept, let us denote with x_k the location of a virtual robot representing an obstacle detected by a given robot i. It is worthy to recall that, also in this case, the virtual robot is projected on the closest obstacle only if the distance from the actual robot to the obstacle itself is shorter than equilibrium distance of (4.2.1), i.e., the distance for which the repulsive and attractive actions balance. Then, the closer the robot i moves to the virtual robot x_k, the greater the term $\gamma_{ik} = \frac{1}{\|x_i - x_k\|^\alpha}$ becomes. Hence, the control contribution due to the interaction with the virtual robot becomes more relevant and this allows to prevent a collision with the virtual robot k associated to a certain obstacle regardless of the cardinality of the current true neighborhood of robot i. Clearly, a normalization γ_i for each robot i (as defined in (4.2.6)) is required to ensure the boundedness of input.

Note that, in the case of non convex obstacles the same arguments as in Remark 4.1.1 can be used.

CHAPTER 5

Distributed Consensus Algorithms for Robot Swarms over Directed Communication Graphs

In this chapter, the average consensus algorithms over directed communication graphs for robot swarms is presented. As stated in Chapter 1, modeling the robots communications using a digraph appears to be realistic in all those situations where the robots transmit with varying gains and varying interference levels appear. In Section 5.1 some preliminary tools coming from the algebraic graph theory are reviewed. In Section 5.2 the algorithm for the estimation of the left eigenvector of a Laplacian matrix encoding a Strongly Connected Weighted Digraph is reviewed and a necessary and sufficient condition to verify the strongly connectedness of the communication digraph in a distributed fashion is introduced. Eventually, in Section 5.3, the main contribution of this chapter, namely, a technique to achieve the average consensus on strongly connected digraphs is presented.

5.1 Preliminaries

5.1.1 Notation

In the following, further concepts concerning the digraphs are introduced to integrate the notation given in Section 3.1.

Let us consider a set of n robots whose communication network is described by a *digraph* $\mathcal{G}(\mathcal{V}, \mathcal{E})$ where $\mathcal{V} = \{1, \cdots, n\}$ is the set of nodes and $\mathcal{E} \subseteq \mathcal{V} \times \mathcal{V}$ is the set of directed edges, i.e., ordered pairs of nodes. Let us define the *weighted adjacency matrix* $\mathcal{A}(\mathcal{G}) \in \mathbb{R}^{n \times n}$ as follows: $\mathcal{A}_{ij}(\mathcal{G}) > 0$ if $(j, i) \in \mathcal{E}$, $\mathcal{A}_{ij}(\mathcal{G}) = 0$ otherwise. Note that $\mathcal{A}_{ij}(\mathcal{G}) > 0$ if

the robot i can receive data from the robot j. In general, the existence of $(j,i) \in \mathcal{E}$ does not imply the existence of $(i,j) \in \mathcal{E}$. It is worthy to point out that the previously defined adjacency matrix is based on the incoming edges of each node. It is assumed that no self loops exist in the network, i.e., $(i,i) \notin \mathcal{E}$. The in-degree and the out-degree of a node k are given by $d_{in}(k) = \sum_j \mathcal{A}_{kj}(\mathcal{G})$ and $d_{out}(k) = \sum_j \mathcal{A}_{jk}(\mathcal{G})$, respectively. The *Laplacian matrix* is defined as follows:

$$\mathcal{L}(\mathcal{G}) = \mathcal{D}(\mathcal{G}) - \mathcal{A}(\mathcal{G}),$$

with $\mathcal{D}(\mathcal{G})$ the *diagonal in-degree matrix* defined as

$$\mathcal{D}(\mathcal{G}) = \begin{bmatrix} d_{in}(1) & & \\ & \ddots & \\ & & d_{in}(n) \end{bmatrix},$$

and $\mathcal{D}_{ij}(\mathcal{G}) = 0$ whenever $i \neq j$. Note that this definition of Laplacian matrix is different from the one given in Section 3.1 due to the nature of the degree and adjacency matrices encoding $\mathcal{G}$. For the sake of readability, the dependency on the graph $\mathcal{G}$ will be omitted in the rest of the chapter. Let us now review some properties of the Laplacian matrix. Generally speaking, the Laplacian matrix is a non-symmetric weakly diagonal dominant matrix. It has a zero structural eigenvalue for which the corresponding right eigenvector is the vector of ones of appropriate size, i.e., $\mathcal{L}\mathbf{1} = \mathbf{0}$. Let us now introduce the following definitions:

Definition 5.1.1. *A matrix $\mathcal{Q} \geq 0$ is called* nonnegative *if all the elements are strictly nonnegative.*

Definition 5.1.2. *A matrix $\mathcal{Q} > 0$ is called* positive *if all the elements are strictly positive.*

Note that a nonnegative matrix is not the same as a positive semidefinite matrix and a positive matrix is not the same as a positive definite matrix. The following definitions will be used throughout the rest of the paper:

Definition 5.1.3. *Two vertices $i, j \in \mathcal{V}$ are* adjacent *iff $(i,j) \in \mathcal{E}$.*

Definition 5.1.4. *A* path *from vertex $i \in \mathcal{V}$ to vertex $j \in \mathcal{V}$ is a sequence of distinct adjacent vertices.*

Definition 5.1.5. *For $i, j \in \mathcal{V}$, the* distance *$d(i,j)$ from i to j is the number of edges of the shortest i-j path in $\mathcal{G}$.*

Definition 5.1.6. *For $i \in \mathcal{V}$, the* eccentricity $e(i)$ *of i is the distance from i to the farthest vertex.*

Definition 5.1.7. *The* diameter $d = diam(\mathcal{G})$ *of a graph $\mathcal{G}$ is the maximum eccentricity among the vertices.*

Definition 5.1.8. *A digraph is called* weakly connected *if and only if any two distinct nodes in the vertex set can be connected by a path regardless of the direction of the edges.*

Definition 5.1.9. *A digraph is called* strongly connected *if and only if any two distinct nodes in the vertex set can be connected by a path which follows the direction of the edges of the digraph.*

Definition 5.1.10. *A weighted digraph is said to be* balanced *if:*

$$d_{in}(i) = d_{out}(i),\ \forall i \in \{1, \dots, n\}.$$

Note that, this definition can be equivalently expressed in terms of the Laplacian matrix as follows: $\mathcal{L}\mathbf{1} = \mathbf{0}$ and $\mathbf{1}^T\mathcal{L} = \mathbf{0}^T$.

Definition 5.1.11. *A non negative matrix $\mathcal{Q} \in \mathbb{R}^{r\times r}$, with $r \geq 2$, is reducible if there exists a permutation matrix $P \in \mathbb{R}^{r\times r}$ such that:*

$$\bar{\mathcal{Q}} = P^T\mathcal{Q}P = \begin{bmatrix} \mathcal{Q}_{11} & \mathcal{Q}_{12} \\ 0 & \mathcal{Q}_{22} \end{bmatrix}, \tag{5.1.1}$$

being $\mathcal{Q}_{11}$ and $\mathcal{Q}_{22}$ two squared matrices. Otherwise the matrix is said to be irreducible*. Moreover, being P an orthogonal matrix, i.e., $P^T = P^{-1}$, the previous equation can be restated as:*

$$\bar{\mathcal{Q}} = P^{-1}\mathcal{Q}P. \tag{5.1.2}$$

The link between the definition of an irreducible matrix and digraphs is given by the following results (see [96, Ch.4]).

Proposition 5.1.1. *The adjacency matrix $\mathcal{A}$ is an irreducible matrix if and only if its associated digraph $\mathcal{G}$ is strongly connected.*

Definition 5.1.12. *A non negative matrix $\mathcal{Q}$ is said to be* primitive *if there exist a positive integer k s.t. $\mathcal{Q}^k > 0$.*

Eventually, from the Perron-Frobenius theorem it follows that for any primitive matrix $\mathcal{Q}$ the following holds:

$$\lim_{k\to\infty}\left(\frac{\mathcal{Q}}{r}\right)^k = \frac{v\,w^T}{w^T\,v} > 0, \tag{5.1.3}$$

where v is the right eigenvector and w^T is the left eigenvector both associated with the eigenvalue r.

5.1.2 Assumptions

Let the following assumptions be satisfied throughout the rest of this chapter:

A1 A unique identifier is associated to each robot i of the network, e.g., the MAC address.

A2 Each robot sends n variables.

A3 Each robot does not know the number of robots receiving its information (i.e., its out degree).

A4 The network topology of the considered multi-robot system is described by a static Strongly Connected Weighted Digraph.

In **A1**, it is assumed that each robot can distinguish the information coming from the other robots according to the identifier of the sender. For example, the MAC address of the robot communication device can be used in order to avoid burdening the estimation process with extra neighborhood identification algorithms and thus preserving the scalability of the system. In **A2**, it is assumed that each robot has enough storage size for the values coming from its in-neighbors. Therefore, the number of robots belonging to the network is known by each robot. In **A3**, it is stated that each robot can not count the number of its out-neighbors. Eventually, in **A4** it is assumed that the information produced by one node is propagated within the network. In this thesis, an effective way to verify the satisfaction of the last assumption is provided.

5.2 Decentralized Estimation of the Left Eigenvector

In this section, a decentralized algorithm for the estimation of the left eigenvector associated to the zero structural eigenvalue of the Laplacian matrix encoding a SCWD originally proposed in [41] is reviewed. To this aim, a distributed algorithm for the computation of the powers of a matrix is now discussed. Further details can be found in [97, 98].

Let us now introduce the concept of matrix compatibility with a digraph.

Definition 5.2.1. *A matrix $\mathcal{Q} \in \mathbb{R}^{n\times n}$ is* compatible *with a digraph $\mathcal{G}$ if $\mathcal{Q}_{ij} = 0$ iff $(j,i) \notin \mathcal{E}$ and $j \neq i$.*

Loosely speaking, this definition of compatibility guarantees that $\mathcal{Q}_{ij}$ is equal to 0 whenever the robot i cannot receive any data from the robot j.

Let each robot i have a variable $\delta_i(k) = [\delta_{i1}(k) \ \dots \ \delta_{in}(k)]^T$ with initial values

$$\delta_{ij}(0) = \begin{cases} 1 & \text{if } i = j, \\ 0 & \text{otherwise} \end{cases} \tag{5.2.1}$$

and let $\mathcal{Q} = [\mathcal{Q}_{ij}]$ be a weighted matrix which is *compatible* with the communication graph. At each iteration, the robots update their variables as follows:

$$\delta_{ij}(k+1) = \sum_{p \in \mathcal{N}_i \cup i} \mathcal{Q}_{ip}\delta_{pj}(k), \tag{5.2.2}$$

with $\mathcal{N}_i$ the in-neighborhood of robot i, i.e., $\mathcal{N}_i = \{j \in \mathcal{V} : (j,i) \in \mathcal{E}\}$. Update rule (5.2.2) can be put in vectorial form as

$$\Delta(k+1) = \mathcal{Q}\Delta(k),$$

with:

$$\Delta(k) = \begin{bmatrix} \delta_1(k)^T \\ \vdots \\ \delta_n(k)^T \end{bmatrix}.$$

Noting that $\Delta(0) = \mathcal{I}$, it is easy to see that at iteration k, the variable $\delta_i(k)$ contains exactly the value of the i^{th} row of the matrix $\mathcal{Q}^k$. Let us remark that the algorithm is fully distributed, in the sense that each robot only uses its previous value and the data sent by its in-neighbors to update the variable $\delta_i(k)$.

The update law in (5.2.2) is applied on the following matrix $\mathcal{C}$ compatible with the graph in order to estimate the left eigenvector associated to the zero eigenvalue:

$$\mathcal{C} = \mathcal{I} - \beta\,\mathcal{L}, \quad 0 < \beta < \frac{1}{\Psi}, \tag{5.2.3}$$

where $\Psi = \max_i\{\sum_{j\neq i} \mathcal{A}_{ij}\}$. The matrix $\mathcal{C}$ is commonly denoted as *Perron matrix* and corresponds to the state matrix of the discrete time version of the consensus algorithm.

Let us notice that the eigenvalues $\lambda_{\mathcal{C}}$ of the matrix $\mathcal{C}$ and the eigenvalues of the Laplacian matrix $\lambda_{\mathcal{L}}$ are related as follows:

$$\lambda_{\mathcal{C}_i} = 1 - \beta\,\lambda_{\mathcal{L}_i},$$

where $\lambda_{\mathcal{C}_i}$ and $\lambda_{\mathcal{L}_i}$ are the i^{th} eigenvalues of the $\mathcal{C}$ and $\mathcal{L}$ matrices respectively. It follows that the two matrices also share the same set of eigenvectors. In particular for the eigenvalue of maximum modulus, namely $\lambda_{\mathcal{C}_1}$, the following holds:

$$\mathcal{C}\,\mathbf{1} = \lambda_{\mathcal{C}_1}\mathbf{1},$$
$$w^T\,\mathcal{C} = \lambda_{\mathcal{C}_1}\,w^T,$$

with w^T the left eigenvector associated to $\lambda_{\mathcal{C}_1}$ and $\lambda_{\mathcal{L}_1}$. The following proposition proves the convergence to this eigenvector:

Proposition 5.2.1. *Let us consider a strongly connected weighted digraph. Moreover, let us assume that an initial value $\delta_{ij}(0)$, as defined in* (5.2.1)*, is associated to each robot i. Then if the robots apply the update rule in* (5.2.2) *using the compatible with the graph matrix $\mathcal{C}$, as defined in* (5.2.3)*, then*

$$\lim_{k\to\infty}\Delta(k) = \frac{\mathbf{1}\;w^T}{w^T\mathbf{1}} \tag{5.2.4}$$

or, in other terms, $\delta_i(k)$ will tend to the normalized left eigenvector w of the Laplacian matrix encoding the digraph.

Proof. Using Lemma 3 in [99], it is possible to state that the matrix $\mathcal{C}$ is primitive. Then, the proof follows from the application of the Perron-Frobenius theorem reported in Section 5.1.1. □

Algorithm 1 shows the pseudo-code of the left eigenvector estimation algorithm. Note that the algorithm requires the digraph to be strongly connected. This ensures the Perron matrix built according to (5.2.3) to be irreducible and diagonally positive. Regarding the pseudo-code, the variable max_iter represents the predefined maximum value of the algorithm's iterations. The matrix $\Delta(max\_iter)$ is the output of the algorithm; each row i represents the estimation performed by the i^{th} robot. Line 1 describes the variables initialization. Each robot sets its corresponding component to 1 and the other components to 0. In the second step, the Perron matrix is computed according to its definition in (5.2.3). Lines 3-5 represent an implementation of the update rule introduced in (5.2.2).

5.2.1 Strongly Connectedness Verification

In order to estimate the left eigenvector, the communication digraph is required to be strongly connected. In the following, the relationship between

Algorithm 1 Left Eigenvector Estimation Algorithm

Require: $\mathcal{G}$ SCWD, $\mathcal{L}$, $0 < \beta < \frac{1}{\Psi}$, max_iter
Ensure: $\Delta_i(max\_iter) \rightarrow \mathbf{1w^T}$
1: $\delta_{ij}(0) = 1$ if $i = j$; $\delta_{ij}(0) = 0$ otherwise
2: $\mathcal{C} \leftarrow \mathcal{I} - \beta\mathcal{L}$
3: **for** $k = 0, \ldots, max\_iter$ **do**
4: $\quad \delta_{ij}(k+1) = \sum_{p \in \mathcal{N}_i \cup i} \mathcal{C}_{ip}\delta_{pj}(k)$
5: **end for**

a weakly connected digraph and the presence of null elements in the d^{th} power of the Perron matrix is disclosed, where $d = diam(\mathcal{G})$.

Proposition 5.2.2. *Let us consider a multi-robot system running the algorithm given in* (5.2.2)*. The communication digraph is not strongly connected if and only if at least one robot has one or more zeros in its estimation of the left eigenvector after d step.*

Proof. Let us take into account the Perron matrix $\mathcal{C}$. It can be rewritten as follows:

$$\begin{aligned}\mathcal{C} &= \mathcal{I} - \beta\mathcal{L} = \mathcal{I} - \beta(\mathcal{D} - \mathcal{A}) = (\mathcal{I} - \beta\mathcal{D}) + \beta\mathcal{A} \\ &= \mathcal{H} + \beta\mathcal{A},\end{aligned}$$

where $\mathcal{H} = \mathcal{I} - \beta\mathcal{D}$ is a nonnegative diagonal matrix. Let us now consider the equation describing the algebraic expansion of powers of a binomial applied to this case:

$$(\mathcal{H} + \beta\mathcal{A})^d = \sum_{q=0}^{d} \binom{d}{q} \beta^{d-q}\mathcal{H}^q\mathcal{A}^{d-q}. \tag{5.2.5}$$

It can be noticed that the d^{th} power of (5.2.5) is composed by the summation of the matrix products of all the powers of $\mathcal{H}$ and $\mathcal{A}$ up to d. Note also that being $\mathcal{H}$ diagonal, the null elements in $\mathcal{A}$ are preserved after the matrix product $\mathcal{H}^q\mathcal{A}^{d-q}$. According to [100, Lemma 1.32], the generic q^{th} power of the adjacency matrix contains the number of directed paths of length q in the digraph. If the digraph is not strongly connected then some elements in the rows of the powers of $\mathcal{A}$ corresponding to the set of unreachable robots are equal to zero. Therefore the following holds:

$$\mathcal{C}_{ij}^d = 0 \iff \mathcal{A}_{ij}^k = 0, \forall k \leq d,\ \forall i, j \in \mathcal{V}.$$

The thesis follows. □

Remark 5.2.1. *In Proposition 5.2.2, it is explicitly stated that if an element of the d^{th} power of the Perron matrix is null, i.e., $C_{ij}^{d} = 0$, then there is no path up to length d between i and j. Being the diameter d the longest shortest path among two robots in $\mathcal{G}$, it means that also all the elements C_{ij}^{k} with $k > d$ are null.*

Remark 5.2.2. *In order to know the diameter of the digraph $\mathcal{G}$, an robot has to be aware of the topology of the network. However, it is known that $d \leq n$, i.e., the diameter of the digraph is upper bounded by the number of robots. Using this fact, each robot can perform the technique suggested in Proposition 5.2.2 only knowing the number n of robots in the network.*

5.2.2 Weakly Connectedness Notification

A proposition which relies on the strong connectivity of the graph in order to estimate the left eigenvector of the Laplacian matrix has been given in Section 5.2 . In the following, it will be shown that each robot, which cannot detect the weak connectivity of the graph according to Proposition 5.2.2, can made aware of it by means of notification.

Proposition 5.2.3. *Each robot becomes aware of the weak connectivity of the graph in at most $2\,d$ steps either by self detection or through notification.*

Proof. Let us consider a multi-robot system running Algorithm 1 over a weakly connected graph $\mathcal{G}$. According to Proposition 5.2.2, there must be at least one node with one or more zeros in its estimation of the left eigenvector after d step. It should be noticed that after d steps for each robot two scenarios are possible: either the robot has one or more zeros in its estimate and thus it can self detect the weak connectivity of the graph or all the elements are greater then zero and thus the weak connectivity can be notified to it by any other robot. □

In Algorithm 2, the implementation of the finite-time verification of the strong connectivity and the weakly connectivity notification are shown. First of all the diameter of the graph is required along with the Perron matrix C. Note that, according to the previous remark, d can be set equal to n. In step 3, each robot i verifies if its corresponding row of C^{d} contains at least a value equal to 0. If this happen, in step 4 all the elements in its row are set to zero for all the iterations $k > d$. In this way all the robots receiving a 0 since the d^{th} step are aware of the absence of strong connectivity of the digraph $\mathcal{G}$.

Algorithm 2 Finite-Time Strong Connectivity Verification and Weakly Connectivity Notification

Require: d, C
1: Compute C^d using Algorithm 1.
2: **for** $i = 1 \dots n$ **do**
3: **if** C_i^d contains 0 **then**
4: $\delta_{ij}(k) = 0, \forall j \in \mathcal{N}_i, \forall k > d$
5: **end if**
6: **end for**

5.3 Average Consensus Algorithm Over Digraphs

In this section, a solution to the average consensus problem on a digraph using the left eigenvector estimation algorithm proposed in Section 5.2 is presented. First of all, let us suppose that with each robot $i \in \mathcal{V}$ an initial value $x_i(0) \in \mathbb{R}$ is associated. Note that for the sake of simplicity and without loss of generality, the state of each robot is assumed to be a scalar and the elements of the adjacency matrix are unitary. Let us refer to $x(k) \in \mathbb{R}^n$ as the state vector $x(k) = [x_1(k)\ x_2(k)\ \dots\ x_n(k)]^T$ and to $x(0) \in \mathbb{R}^n$ as the initial conditions of the system $x(0) = [x_1(0)\ x_2(0)\ \dots\ x_n(0)]^T$.

Briefly speaking, the average consensus on a digraph is the problem of computing $\mu = \sum_i x_i(0)/n$, where each robot uses only its locally available information. The discrete time update law used to solve the consensus problem on digraphs is given by the following equation:

$$x_i(k+1) = x_i(k) + \beta \sum_{j \in \mathcal{N}_i^-} (x_j(k) - x_i(k)). \tag{5.3.1}$$

Let us remark that, for each robot, the required information to compute (5.3.1) is obtained by its in-neighbors. The previous equation can be rearranged in terms of the product between a matrix and a vector as follows:

$$x(k+1) = C\,x(k). \tag{5.3.2}$$

It is a well established result that with a balanced digraph, the classical consensus algorithm leads to an average consensus, [101]. Unfortunately, the same statement does not hold for the general case of digraphs, where the consensus value is given by $\bar{\mu} = \sum_i w_i x_i(0) \neq \mu$, being w_i the i^{th} coefficient of the left eigenvector.

In order to reach the average in the case of a general SCWD, the initial

conditions can be opportunely modified as follows:

$$\mu = \frac{1}{n}\sum_{i=1}^{n} x_i(0) = \sum_{i=1}^{n} w_i \left(x_i(0) + \Gamma_i\right), \tag{5.3.3}$$

with $\Gamma = [\Gamma_1 \ \dots \ \Gamma_n]^T$ the extra term that needs to be adjusted. In particular, each component of the initial conditions is required to satisfy:

$$\frac{x_i(0)}{n} = w_i \left(x_i(0) + \Gamma_i\right),$$

which leads to

$$\Gamma_i = x_i(0)\left(\frac{1}{n\,w_i} - 1\right) = x_i(0)\left(\frac{1 - n\,w_i}{n\,w_i}\right). \tag{5.3.4}$$

In the following proposition, it is shown that if the initial conditions is modified according to (5.3.3) and (5.3.4) then the average consensus is achieved.

Proposition 5.3.1. *Let us assume the initial conditions modified as follows:*

$$\tilde{x}(0) = x(0) + \Gamma,$$

then the consensus value is equal to μ.

Proof. Let us consider the final value of the consensus algorithm:

$$\bar{\mu} = \sum_{i=1}^{n} w_i\, \tilde{x}_i(0)$$

by substituting $\tilde{x}_i(0) = x_i(0) + \Gamma_i$ with Γ_i defined according to Eq. (5.3.4), it follows:

$$\begin{aligned}
\bar{\mu} &= \sum_{i=1}^{n} w_i \left(x_i(0) + x_i(0)\left(\frac{1 - n\,w_i}{n\,w_i}\right)\right) \\
&= \sum_{i=1}^{n} w_i \left(x_i(0)\left(1 + \frac{1 - n\,w_i}{n\,w_i}\right)\right) \\
&= \sum_{i=1}^{n} w_i \left(x_i(0)\left(\frac{1}{n\,w_i}\right)\right) \\
&= \sum_{i=1}^{n} \frac{x_i(0)}{n} = \mu.
\end{aligned}$$

□

Let us now assume the left eigenvector to be available at time $k = 0$. This implies that the vector Γ can be also computed. Therefore, the av-

erage consensus over a digraph can be achieved by following two different approaches:

1. fixing the initial conditions $x(0)$ before starting the algorithm,
2. injecting a suitable exogenous input at any given step k.

To properly design the second strategy the following Proposition is required:

Proposition 5.3.2. *The correction term Γ can be equivalently injected at any iteration, such that:*

$$\langle x(0) + \Gamma,\, w \rangle = \langle x(k) + \Gamma,\, w \rangle\,,$$

where $\langle \cdot, \cdot \rangle$ denotes the inner product in $\mathbb{R}^n$.

Proof. First of all, let us resort to the well-known property of the left eigenvector for discrete time systems:

$$\langle x(k),\, w \rangle = \lambda^k\ \langle x(0),\, w \rangle\,.$$

In particular, being $\lambda = 1$, the previous equality becomes:

$$\langle x(k),\, w \rangle = \langle x(0),\, w \rangle\,.$$

By linearity of the inner product, it follows that:

$$\begin{aligned} \langle x(0) + \Gamma,\, w \rangle &= \langle x(0),\, w \rangle + \langle \Gamma,\, w \rangle \\ &= \langle x(k),\, w \rangle + \langle \Gamma,\, w \rangle \\ &= \langle x(k) + \Gamma,\, w \rangle\,. \end{aligned}$$

□

By assuming the estimate of the eigenvector w to be asymptotic, it follows that a possible technique to asymptotically achieve the consensus is to modify the update rule given in Eq. (5.3.1) as follows:

$$\begin{aligned} x_i(k+1) = x_i(k) + \epsilon_i(k) \\ + \beta \sum_{j \in \mathcal{N}_i} \Big(x_j(k) + \epsilon_j(k) - x_i(k) - \epsilon_i(k) \Big) \end{aligned} \tag{5.3.5}$$

where the iterative error $\epsilon_i(k)$ is defined as:

$$\epsilon_i(k) = \tilde{\Gamma}_i(k) - \tilde{\Gamma}_i(k-1) \tag{5.3.6}$$

with:

$$\tilde{\Gamma}_i(k) = x_i(0)\left(\frac{1}{n\,\delta_{ii}(k)} - 1\right).$$

and $\tilde{\Gamma}_i(-1) = 0$. Clearly, from an implementation standpoint, each robot i broadcasts the quantity $\hat{x}_i(k) = x_i(k) + \epsilon_i(k)$ at each time step k.

The modified consensus algorithm can be expressed in vector form as:

$$x(k+1) = C\left(x(k) + \epsilon(k)\right) \tag{5.3.7}$$

with $x(k) = [x_1(k), \ldots, x_n(k)]^T$ the state vector at time k and $\epsilon(k) = [\epsilon_1(k), \ldots, \epsilon_n(k)]^T$ the error vector at time k.

Proposition 5.3.3. *Let us assume the multi-robot system applies the modified consensus algorithm given in Eq.* (5.3.7)*. Then it follows that:*

$$\lim_{k\to\infty} x_i(k) = \mu \quad \forall\, i \in \mathcal{V}. \tag{5.3.8}$$

Proof. Let us consider the update at time k

$$\begin{aligned}
\langle x(k+1),\, w\rangle &= \langle x(k) + \epsilon(k),\, w\rangle \\
&= \langle x(k),\, w\rangle + \langle \epsilon(k),\, w\rangle \\
&= \langle x(k-1) + \epsilon(k-1),\, w\rangle + \langle \epsilon(k),\, w\rangle \\
&\;\;\vdots \\
&= \langle x(0),\, w\rangle + \langle \epsilon(0) + \epsilon(1) + \ldots \epsilon(k),\, w\rangle \\
&= \langle x(0),\, w\rangle + \langle \sum_{i=0}^{k} \epsilon(i),\, w\rangle
\end{aligned}$$

The term $\sum_{i=0}^{k} \epsilon(i) = \epsilon(0) + \epsilon(1) + \ldots + \epsilon(k)$ is a telescoping series:

$$\begin{aligned}
\sum_{i=0}^{k} \epsilon(i) &= \tilde{\Gamma}(0) + \left(\tilde{\Gamma}(1) - \tilde{\Gamma}(0)\right) + \ldots + \left(\Gamma - \tilde{\Gamma}(k-1)\right) \\
&= \tilde{\Gamma}(k)
\end{aligned}$$

Therefore, it follows that:

$$\langle x(k+1),\, w\rangle = \langle x(0),\, w\rangle + \langle \tilde{\Gamma}(k),\, w\rangle$$

At this point by adding and subtracting the quantity $\langle \Gamma,\, w\rangle$ to the right-

hand side, it follows:

$$\langle x(k+1),\, w\rangle = \langle x(0),\, w\rangle + \langle \Gamma,\, w\rangle + \langle \zeta(k),\, w\rangle$$

where $\zeta(k) = [\zeta_1(k),\, \ldots,\, \zeta_n(k)]^T$ with $\zeta_i(k) = \tilde{\Gamma}_i(k) - \Gamma_i$.

Therefore, since

$$\lim_{k\to\infty} \zeta_i(k) = 0, \quad \forall\, i \in \mathcal{V},$$

it follows that:

$$\lim_{k\to\infty} \langle x(k),\, w\rangle = \langle x(0),\, w\rangle + \langle \Gamma,\, w\rangle$$

which ensure that:

$$\lim_{k\to\infty} x_i(k) = \mu, \quad \forall\, i \in \mathcal{V}.$$

□

The iteration rule in (5.3.7) can also be used to computed any desired weighted mean of the initial conditions. Concerning this the following corollary is introduced:

Corollary 5.3.1. *Let $w^* = [w_1^*, \ldots, w_n^*]$ be a vector such that $\sum w_i^* = 1$ and $w_i^* > 0$ for all i, that contains the desired weights of the initial conditions of each robot. If the robots design their inputs by*

$$\Gamma_i(k) = x_i(0)\left(\frac{w_i^*}{w_i} - 1\right). \tag{5.3.9}$$

and $\epsilon_i(k)$ as in (5.3.6)*, then the final value reached by all the robots is equal to*

$$\lim_{k\to\infty} x_i(k) = \sum w_i^* x_i(0) \tag{5.3.10}$$

In Algorithm 3, the implementation of the average consensus algorithm is illustrated. The algorithm requires the number of robots n, the Perron matrix C, the number of iterations max_iter and the initial state of the system $x(0)$. The result of the algorithm is the average of $x(0)$ obtained in a distributed fashion. Line 2 represents the computation of the k^{th} power of C according to the algorithm provided in section 5.2. In lines 3-5, the exogenous input ϵ_i is computed by each robot relying upon the current estimation of the i^{th} component of the left eigenvector, the number of the robots and the initial conditions of the system. Line 6 represents the modified consensus step. Note that, as stated above, line 2 and lines 3-6 can be performed in parallel.

Algorithm 3 Average Consensus Algorithm

Require: $n, C, max\_iter, x(0)$

Ensure: $x(max\_iter) = \left(\frac{1}{n}\mathbf{1}^T x(0)\right)\mathbf{1}$

1: **for** $k = 1 \dots max\_iter$ **do**
2: Compute C^k using Algorithm 1.
3: **for** i=1...n **do**
4: $\epsilon_i(k) \leftarrow \frac{x_i(0)}{n}\left(\frac{C_{ii}(k-1) - C_{ii}(k)}{C_{ii}(k-1)C_{ii}(k)}\right)$
5: **end for**
6: $x(k+1) = C\left(x(k) + \epsilon(k)\right)$
7: **end for**

Currently, the convergence rate of this algorithm is under investigation and will be part of upcoming publications.

CHAPTER 6

Simulations and Experiments

In this chapter, the simulations and the experiments carried out to show the effectiveness of the proposed approaches are shown. In the first section, the SAETTA mobile robotic platform used in the experiments is introduced. Then, in Sections 6.2 and 6.3, a distance and a relative position measurement technique are discussed along with the main differences with other works in the literature. In Section 6.4 simulations ad experiments regarding the control law in Chapter 3 are proposed while in Section 6.5 the same approach is applied to simulate the behavior of a USV swarm. Simulations and experiments for the control laws in Chapter 4 are in Section 6.6. In Section 6.7, simulations concerning the left eigenvector estimation along with the average consensus algorithm are detailed. Where available, links to extra materials like videos are given.

6.1 SAETTA Mobile Robotic Platform

The SAETTA robotic hardware platform developed at the Robotics Lab of the University of "Roma TRE" is a low-cost mobile robot. It features a complete sensorial system, a very accurate traction in indoor environment, and a ZigBee transceiver for multi-robot applications. The platform shown in Figure 6.1 has been reproduced into 12 units.

The SAETTA architecture can be conceptually decomposed into a two-tiers architecture. The first tier is constituted by the interaction between low level components, such as traction and sensorial system, while the other is in charge of executing high level tasks. This conceptual division has an immediate correspondence in the hardware realization: each tier is realized

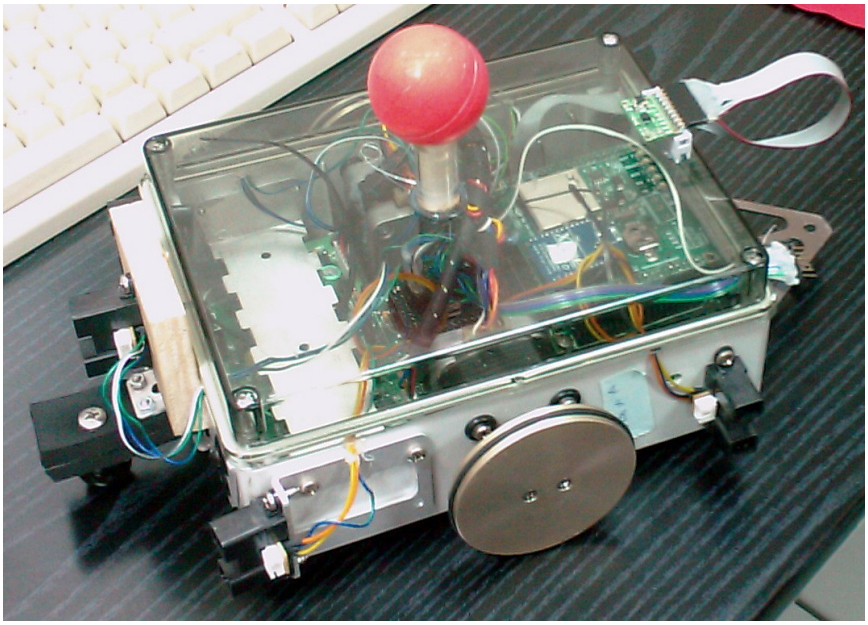

Figure 6.1: The low-cost SAETTA robotic hardware platform developed at the Robotics Lab of the University of "Roma TRE".

on an electronic board and equipped by a CPU unit. The low level is managed by a Programmable Interface Controller (PIC) while the high level is a Linux embedded board (FOX Board G20) from Acme Systems. The first board, which manages strictly time constrained tasks, has a control cycle (25ms) shorter than the other one (250ms) that is supported, on the other hand, by a more powerful CPU to implement higher level tasks. In particular, the FOX Board G20 is a Linux Embedded Single Board Computer built around an Atmel AT91SAM9G20 micro-controller based on the ARM926EJ-S processor, with a clock speed of 400MHz.

The inter-board communication is realized by exploiting a RS232 channel. At the moment, a gyroscope, a magnetometer, an accelerometer and 5 infrared (IR) sensors are present. Furthermore, an additional infrared sensor along with a webcam both pointing to the ceiling has been considered for the measurement of relative distance and orientation among robots.

Regarding the traction system, a very convenient choice has been the use of stepper motors instead of the more common d.c. motors. They offer several advantages, first of all the absence of tachometers or encoders and, as a consequence, of the circuitry associated with the transducer. Moreover, a stepper motor requires low supply voltages as it has a very low back EMF. For further information about the SAETTA platform, the reader is referred

to [102].

6.2 A RSSI-based Inter-Distance Measurement System for Robot Swarms

In this section, the attention is focused on providing a reliable technique to compute inter-distances among robots by exploiting Zigbee radio transceivers. Any attempt to use Zigbee devices to achieve this goal has hardly produced satisfactory performances so far. Several experiments, carried out by exploiting Xbee-Pro modules, have been performed to show the effectiveness of the proposed technique. Note that, the approach described in the following does not require extra hardware devices as other works in the literature, for example [103].

In the following, first the Radio Propagation Model is discussed along with the hardware specification of the Xbee Pro communication devices. Then the data acquisition technique is introduced. Results for outdoor and indoor experiments using the hardware platform described in 6.1 are shown. Eventually, two case studies based on the trilateration and the Kalman Filtering techniques are discussed. The experiments were carried out using a custom

6.2.1 Radio Propagation Model

A radio propagation model is an empirical mathematical model to characterize the radio wave propagation as a function of the distance. This model typically predicts the path loss along a link or the effective coverage area of a transmitter. The simplest method to relate the received signal power P_r to the distance d between the transmitter and the receiver is by assuming that the received power P_r is proportional to such a distance d raised to a certain exponent α, referred to as the *distance-power gradient*. This can be expressed as:

$$P_r = P_0 \, d^{-\alpha} \tag{6.2.1}$$

where P_0 is the received power at a given reference distance (usually 1 meter) from the transmitter. The parameter α is generally assumed to be $\alpha = 2$ for free-space. For indoor and urban-radio channels, the distance-power relationship will change due to the presence of buildings and street layouts. Generally, the variations in the value of the parameter α in different outdoor areas are smaller compared to the variations observed in indoor areas. The distance-power relationship given in Eq. (6.2.1) can be re-written in decibels

(dB) as:

$$10\ \log_{10}(P_r) = 10\ \log_{10}(P_0) - 10\,\alpha\ \log_{10}(d), \tag{6.2.2}$$

where the term $10\,\alpha\ \log_{10}(d)$ represents the power-loss in dB with respect to the received power at 1 meter, namely $10\ \log_{10}(P_0)$. For sake of clarity, let us rewrite this equation as:

$$L_r = L_0 - 10\,\alpha\ \log_{10}(d). \tag{6.2.3}$$

where L_r is the received signal strength in dB and the parameter α must be generally fit for each environment. Note that, this model can be further detailed by adding an additional term, usually referred to as X, which describes the effect of the *shadow-fading*, i.e., the effect by which several measures referred to the same distance might present some variations.

A different normalized equation is occasionally used in the literature to represent the distance-power relationship. Let us assume P_t to be the transmitted power. If the path-loss in dB at a distance of one meter is defined as $\bar{L}_0 = 10\ \log_{10}(P_t) - 10\,\alpha \log_{10}(P_0)$, the total path loss L_p in dB is given by:

$$L_p = \bar{L}_0 + 10\,\alpha\ \log_{10}(d). \tag{6.2.4}$$

This presents the total path-loss as the path-loss in the first meter plus the loss relative to the power received at one meter. The received power in dB is the transmitted power in dB minus the total path loss L_p. In this section the model given in Eq. (6.2.3) will be used. For a complete overview of the characteristics of wireless medium the reader is referred to [104] and the references therein.

6.2.2 Radio Specification

The Zigbee radio transceiver exploited for the experiments was the Xbee-Pro 802.15.4 RF Module produced by Digi. The Xbee-Pro 802.15.4 is an IEEE 802.15.4 compliant solution that satisfies the unique needs of low-cost, low-power wireless sensor networks. The module is easy-to-use, requires a minimal power and provides reliable delivery of critical data between devices. The XBee-Pro 802.15.4 module operates within the ISM 2.4 GHz frequency band. Zigbee is a communication protocol built for low-power radios based on the IEEE 802.15.4 standard which handles all of the physical and media access control layer operation that is important to this work. IEEE 802.15.4 dictates that each node operates in a carrier sense, multiple access/collision avoidance (CSMA/CA) paradigm. Crucial for the experiments is that both radios provide methods for reporting the RSSI. The

specification returns this measurement directly as an integer ranging from -36 dBm to receiver sensitivity (-100 dBm for the Xbee-Pro).

6.2.3 Experiments

In this section experiment using the Zigbee radio transceivers equipped on the SAETTA robotic platform are provided. They have been carried out both in indoor and outdoor environments.

Data Acquisition Technique

The proposed data acquisition technique relies on spatial and frequency averaging in order to reduce the effect of multi-path for both indoor and outdoor environments. A similar technique to deal with the localization problem for IEEE 802.11 b/g Wireless LAN was proposed in [105]. Besides the different hardware requirements and applications context, the main difference is that the spatial movement while performing the channel hopping to further reduce the multi-path effect to the received radio signal strength is explicitly taken into account.

The key idea is very simple. As stated in [106] the multi-path components at a given frequency add or subtract at the receiving antenna according with their phases that in turn are linked to the ratio between the path length and the wavelength. This permits to compute by averaging a RSS value which is closer to the expected true readings. Considering that for IEEE 802.15.4 radio devices operating at 2.4 GHz the wavelength is in the order of 125 mm, a comparable position variation can provide even more uncorrelated readings and hence further improve the estimate. In a multi-robot context, this can be achieved letting robots perform a particular maneuver, e.g., moving in circle, while collecting measurements. Therefore, compared to [105], here two parameters to get more uncorrelated readings near a given position are modified.

In the following, a comparison between results achievable by exploiting RSS data with (only) frequency averaging and RSS data with both spatial and frequency averaging is reported. The transmission frequency was set to 5Hz while the acquisition time was set to 10s.

Outdoor Environment

In this experiment, data was collected in an outdoor environment using a transmission power level fixed at 18 dBm. Figure 6.2a and Figure 6.2b show the data-fitting with respect to the radio propagation model given in

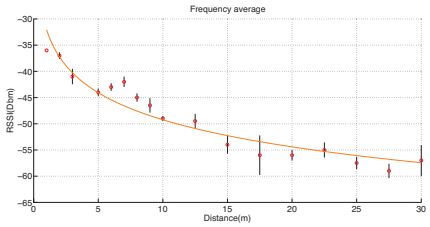

(a) Data fitting for the frequency averaging data set. Transmitter power level 18 dBm.

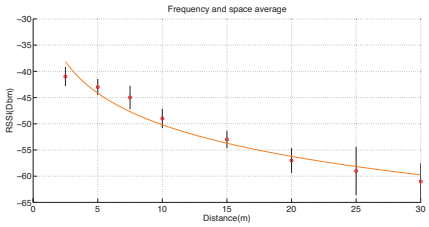

(b) Data fitting for the frequency and space averaging data set. Transmitter power level 18 dBm.

Figure 6.2: Outdoor Scenario Data Fitting.

Eq. (6.2.3) for frequency averaging data only and both spatial and frequency averaging data.

According to the obtained results, the proposed data acquisition technique significantly outperforms the technique proposed in [105] which relies only on frequency averaging. In particular, Figure 6.2a, which depicts the data-fitting obtained changing the frequency only, shows a remarkable fluctuation with respect to the ideal radio propagation model due to the effect of multi-path. Conversely Figure 6.2b, which depicts the data-fitting obtained by adding a motion of the reader on a circumference having a 90 mm radius, shows a better matching with the ideal radio propagation model.

Indoor Environment

In this experiment, data was collected in an indoor environment using a transmission power level fixed at 12 dBm. Figure 6.3a and Figure 6.3b show the data-fitting with respect to the radio propagation model given in Eq. (6.2.3) for frequency averaging data only, and both spatial and frequency averaging data. According to the obtained results, also in this scenario the proposed data acquisition technique is more promising than the technique proposed in [105]. However, it should be noticed that compared to the previous scenario a significant degradation of the performance due to the multi-path phenomenon is experienced.

6.2.4 Case Study

In this section, two simple applications to test the reliability of the proposed data acquisition technique are proposed. In the first scenario, a static localization technique based on trilateration is described. In the second scenario, a mobile localization technique based on the Kalman Filter is described.

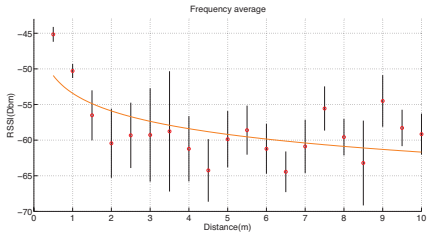

(a) Data fitting for the frequency averaging data set. Transmitter power level 12 dBm.

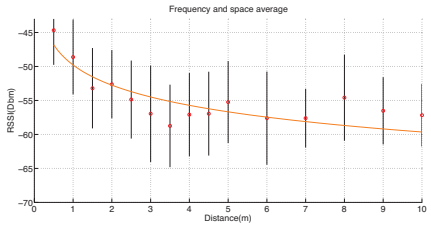

(b) Data fitting for the spatial and frequency averaging data set. Transmitter power level 12 dBm.

Figure 6.3: Indoor Scenario Data Fitting

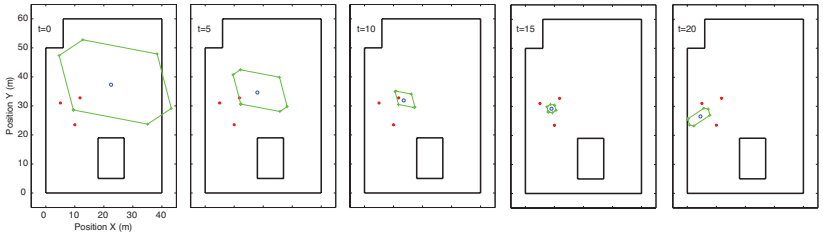

Figure 6.4: Outdoor Scenario (40m $\times$ 60m). Trilateration-based localization. Three robots (let say A, B and C) act as base stations and a fourth robot (let say D) acts as the receiver.

Trilateration-based localization

In this case study, it is shown that proposed data acquisition technique can be used to improve a trilateration-based localization approach. To this end, let us suppose to have a swarm of n robots (emitters) whose spatial deployment can be described by means of a set of points $\left\{P_b = (x_b, y_b) | x_b \in \mathbb{R}, y_b \in \mathbb{R}\right\}$ where $b = 1, \cdots, n$. Furthermore, let us assume that a set of range measurements $R_b = \{r_b\}$, where $r_b \in \mathbb{R}$, is available for an additional target robot.

Trilateration is a method to obtain the position of such a target robot (receiver) with respect to the set of range measurements R_b. The location of each robot P_b can be seen as the center of a circle, while the distance measurement r_b can be considered as the radius of such a circle. The location of the target can then be achieved as the intersection of these circles. However, due to the various errors affecting the measurements, the areas of all these circles rarely intersect, in a real context. In this case, trilateration can be seen as an optimization problem which can be solved using, for instance, a least square approach [107]. Obviously, in order to have an unique solution

to the trilateration problem, at least 3 emitters must be available for the receiver.

From a mathematical standpoint, this problem can be formulated as follows:

$$\begin{cases} (x_1 - x)^2 + (y_1 - y)^2 = r_1^2 \\ (x_2 - x)^2 + (y_2 - y)^2 = r_2^2 \\ \vdots \\ (x_n - x)^2 + (y_n - y)^2 = r_n^2 \end{cases} \tag{6.2.5}$$

where x and y are the coordinates of the target robot. This system can be linearized by subtracting the last equation to the previous $n-1$ equations. The resulting system can be written in a matrix from by re-ordering the elements as follows:

$$A = \begin{bmatrix} 2(x_1 - x_n) & 2(y_1 - y_n) \\ 2(x_2 - x_n) & 2(y_2 - y_n) \\ \vdots & \vdots \\ 2(x_{n-1} - x_n) & 2(y_{n-1} - y_n) \end{bmatrix}$$

and

$$b = \begin{bmatrix} x_1^2 - x_n^2 + y_1^2 - y_n^2 + r_n^2 - r_1^2 \\ x_2^2 - x_n^2 + y_2^2 - y_n^2 + r_n^2 - r_2^2 \\ \vdots \\ x_{n-1}^2 - x_n^2 + y_{n-1}^2 - y_n^2 + r_n^2 - r_{n-1}^2 \end{bmatrix}$$

where A is a $n \times m$ matrix and, in this bi-dimensional case, $m = 2$. It is worth to note that $m < n$, so the solution can be obtained by using the left inverse matrix:

$$x = (A^T A)^{-1} A^T b \tag{6.2.6}$$

Furthermore, this solution is able to minimize the distance from each circumference exploiting the least square method.

In this experiment, three robots act as base stations (let say A, B and C) and a fourth robot acts as the receiver (let say D) in an outdoor environment (parking lot) whose size was 40 m $\times$ 60 m. During the trials the receiver has been placed at different spots and its location has been worked out by exploiting the trilateration-based technique previously introduced. Figure 6.4 describes the localization accuracy in terms on uncertainty area achieved by the receiver with respect to different locations. In particular, at time $t = 0$

the receiver achieves very poor localization as it is located far away from the base stations. This can be explained by the fact that trilateration-based techniques significantly suffer from the collinearity problem. Indeed, the further the base stations are, the more collinear their deployment looks. At time $t = 10$, the receiver approaches the base stations and the localization accuracy drastically improves. At time $t = 15$ the receiver is within the triangular area delimited by the base stations and the best localization accuracy is achieved. Finally, at time $t = 20$ the receiver is moving away from the base stations and the localization accuracy downgrades again.

Kalman Filter

In this case study, it is shown how the proposed data acquisition technique can be used to improve a Kalman Filter-based localization approach.

Two robots act as base stations (let say A and B) and a third robot acts as the receiver (let say C). Two different environments (one indoor and one outdoor) have been taken into account for the experiment. In both cases, during the trials the receiver has been driven from the base station A to the base station B moving along a linear path. A Kalman filter has been applied to estimate the position and the velocity of the receiver exploiting the distances data retrieved from the radio signal strength information of the base stations. Note that, as the receiver was moving along a straight line, the simple kinematics model of an integrator chain has been used for sake of simplicity.

Let us define the state vector of the robot C moving along a linear path as:

$$x = \begin{bmatrix} p \\ v \end{bmatrix}, \tag{6.2.7}$$

where $p \in \mathbb{R}$ is the position of the robot and $v \in \mathbb{R}$ is its linear velocity.

In the prediction step, the prediction estimate $\hat{x}_{k|k-1}$ and its uncertainty $P_{k|k-1}$ are computed as:

$$\hat{x}_{k|k-1} = A\,\hat{x}_{k-1|k-1} + B\,u_k \tag{6.2.8}$$

$$P_{k|k-1} = A_k\,P_{k-1|k-1}\,A_k^T + B\,Q_k\,B^T \tag{6.2.9}$$

where $\hat{x}_{k|k-1}$ is composed by the position $\hat{p}_{k|k-1}$ and the velocity $\hat{v}_{k|k-1}$of the receiver; the input $u(t) \sim \mathcal{N}(0, Q)$ is a random acceleration and the

dynamic matrix A and the input matrix B are respectively:

$$A = \begin{bmatrix} 1 & \Delta t \\ 0 & 1 \end{bmatrix} \tag{6.2.10}$$

and

$$B = \begin{bmatrix} \Delta t^2/2 \\ \Delta t \end{bmatrix} \tag{6.2.11}$$

where Δt represents the sampling time.

During the update step, the expected observation $\hat{z}_k$, namely the power of the signals coming from the base stations, is computed by means of the nonlinear mapping $h(\cdot)$ given in Eq. (6.2.3):

$$\hat{z}_k^A \triangleq h(d_k^A) = L_0 - 10\alpha \log_{10}(d_k^A) \tag{6.2.12}$$

$$\hat{z}_k^B \triangleq h(d_k^B) = L_0 - 10\alpha \log_{10}(d_k^B) \tag{6.2.13}$$

where $d_k^A = \left\|\hat{p}_{k|k-1} - p_A\right\|$ and $d_k^B = \left\|\hat{p}_{k|k-1} - p_B\right\|$ are the Euclidean distances between the base stations and the receivers. The update estimate and its uncertainty are obtained as follows:

$$K_k = P_{k|k-1} {J_x^h}^T \left[J_x^h P_{k|k-1} {J_x^h}^T + R\right]^{-1} \tag{6.2.14}$$

$$\hat{x}_k = \hat{x}_{k|k+1} + K_k(z_k - \hat{z}_k) \tag{6.2.15}$$

$$P_k = P_{k|k-1} - K_k\left[J_x^h P_{k|k-1} {J_x^h}^T + R\right] K_k^T \tag{6.2.16}$$

where J_x^h is the Jacobian matrix of the function $h(\cdot)$ with respect to x_k, and R represents the observation uncertainty.

A validation gate is set up to discard outliers, using Mahalanobis distance and χ-square test:

$$(z_k - \hat{z}_k)^T \left[J_x^h P_{k|k-1} {J_x^h}^T + R\right]^{-1} (z_k - \hat{z}_k) \leq \gamma^2 \tag{6.2.17}$$

where the parameter γ is tuned to obtain a region of acceptance such that 5% of true measurements are rejected.

Figure 6.5a, Figure 6.5b and Table 6.1 describe the results of the experiments. In the indoor scenario, the receiver covered about 30 m moving at a constant speed of roughly 0.16 m/s and receiving a signal from the two base stations at sampling time $T_{in} = 0.1$ sec. In the outdoor scenario, the receiver covered a shorter path of 19 m moving again at a constant speed

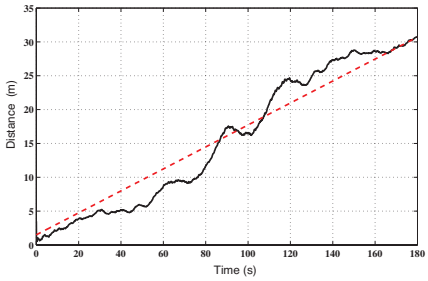

(a) Trajectory of the receiver during indoor test: real path (red dashed line), Kalman estimate (black solid line)

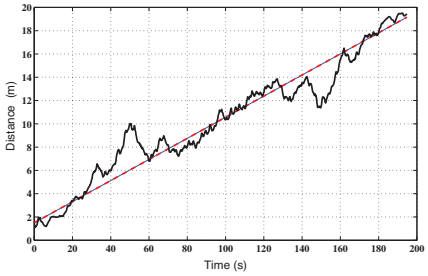

(b) Trajectory of the receiver during outdoor test: real path (red dashed line), Kalman estimate (black solid line)

of 0.1 m/s but receiving a signal from the two base stations at sampling time $T_{out} = 0.2$ sec. Both experiments lasted 3 minutes. In addition, in the indoor scenario the base stations were transmitting at the power level of 14 dBm, while in the outdoor scenario the base stations were transmitting at the power level of 18 dBm.

Table 6.1: Kalman localization indoor and outdoor

	e_{p0} [m]	e_{v0} [m/sec]	min($\lvert e_p \rvert$) [m]	max($\lvert e_p \rvert$) [m]	$\hat{e}_p$ [m]	Cov e_p [m^2]	Outlier %
In	3.5	0.10	0.005	4.29	0.42	5.01	5.45
Out	2.5	0.04	0.001	3.90	0.02	1.51	2.90

As it is reported in Tab. 6.1, the effects of the multi-path phenomenon are evident indoor, where the covariance of the estimate is higher as well as the percentage of the outliers. The Kalman estimate downgrades in the middle of the path (see Fig. 6.5a –6.5b), due to the logarithmic relation between the distance and the power signal described by Eq. (6.2.3).

Note that, the range information coming from the proposed data acquisition technique improves dead reckoning localization both in outdoor and indoor environments. Indeed, due to the initial error, dead reckoning estimate should result biased.

6.3 An Infrared-based Inter-Distance Measurement System for Robot Swarms

In this section, the experiments of a low-cost indoor relative position measurement system for robot swarms are introduced. The idea is to equip each robot with a light emitter along with a camera both pointing to the ceiling to retrieve the information concerning the relative position and orientation. Differently from other works appeared in the literature (see [108, 109]), this approach does not require the robots to send the IR beam directly towards each other thus reducing the measurement error due to the discretization of the bearing. Clearly it is assumed that in the application scenario a ceiling is available at measurable distance. Experiments are provided to show the effectiveness of the proposed relative localizing system for typical multi-robot applications.

In the following, the hardware setup of the proposed infrared based system is detailed along with the algorithms running on it. Therefore, accuracy tests are shown before some observations on the proposed localization system. Experiments have been carried out to corroborate the effectiveness of the approach.

6.3.1 The Proposed Low-Cost Indoor Relative Position Localizing System

The proposed low-cost indoor relative position localizing system is composed of a light emitter and a camera. In this way, each robot can see on the ceiling a constellation with its own position at the azimuth and the (relative) positions of its neighbors falling in its visual field. The spot can be emitted by a red laser or by an infrared focused source. Both have been tested and have shown different pros and cons.

Note that, in the current realization this system does not recognize the identity of a neighbor or its orientation. Nevertheless, this system could be easily improved in different ways, for instance, by using special lens that project easy to recognize shapes.

Image Processing

The image processing for the proposed localizing system consists of three steps:

- blob detection,

- centroid computation,
- coordinates extrapolation.

Note that, being the FOX Board G20 equipped only with full-speed USB ports, the image acquisition resolution was limited to 176x144 pixels. Indeed, this significantly affects the achievable estimation accuracy.

Blob Detection

The detection of the blobs is highly influenced by the camera settings. Typically, using automatic contrast and white balancing provide poor results with both type of lights, namely red laser and infrared source. On the one hand, the laser spot is very intense but covers very few pixels. Therefore, since the camera driver sets the exposure suitable for the average environment, the laser pixels saturate resulting in a white spot with some red fringes that are useless for the recognition. However, the software drivers available (Video4Linux) allows for an easy manual regulation of all the involved parameters. Thus, some simple tests are enough to determine a proper sets of values. On the other hand, in order to use the infrared light with enough sensitivity, the infrared filter located between the lens and the sensor must be removed (a rather tricky operation when a low-cost webcam is used). The infrared spot was obtained by a collimated LED and produces a larger spot that cannot be confused with noise and is easily detected even with coarse exposure settings, as shown in Figure 6.5. As a result, the blob detection is based on a simple thresholding process with respect to the luminance and the chrominance values. Pixels whose value is within a predefine range of values are marked. As a result a binary matrix is obtained.

Centroid Computation

The centroid computation is based on a labeling process by which all the connected component representing the detected robots are identified. In order to avoid erroneous detection, too small components (less than three pixels) are not considered. As a result a list of centroid coordinates in terms of pixels is obtained.

Coordinates Extrapolation

The coordinates extrapolation is based on a geometrical relationship between pixel matrix of the CCD camera and the local reference frame of the

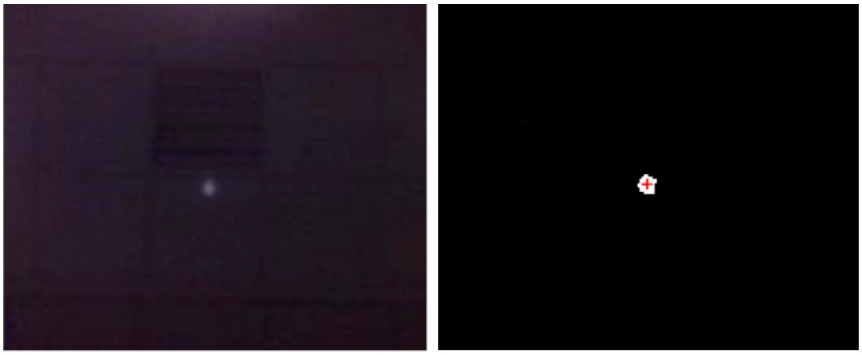

Figure 6.5: Image processing: a) the snapshot obtained by removing the infrared-filter, b) the detected blob.

observing robot. Assuming a perfect optics, the relationship is quite simple owing to the parallelism of the image plane and of the ceiling. If the optic aberrations were introduced, it would be much more complicated to compute [110].
A couple of assumptions concerning the localizing system implementation are now in order:

- the height of the ceiling is assumed to be available,
- the emitter and the camera axes are assumed to be orthogonal to the ceiling.

These limitations can be overcome adding more sensors. In particular, while the first assumption can be easily released by exploiting a range finder, e.g. an ultrasonic one, which provides reliable results in a typical office-like environment, the second one is more problematic. Indeed, if a robot violates this assumption, its measures would be affected by an offset. Unfortunately, adding three accelerometers to sense the gravity direction could only help the violating robot but not the others, as the spots are not associated with the single robots. Therefore, the only way to overcome this problem is to mount the laser and the camera on a (maybe passive) stabilized platform, a solution that would impinge the simplicity as well as the cost of the hardware setup.

Webcam Calibration

The systematic error sources for the proposed indoor relative position localizing system are mainly due to the optical aberrations and to the misalignments. Both can be reduced by a proper calibration.

On the one hand, lens aberration can be reduced by a calibration procedure, for instance by using the one in Matlab, that provides a calibration matrix mapping the pixels space in the world space. Although, the calibration procedure is lengthily, the obtained calibration matrix can be easily used in real time.

On the other hand, the alignment is more difficult to obtain and calibrate. Moreover, as it has been discussed above, it cannot be compensated by post-processing. Although, a good initial alignment can be ensured by a well-designed mechanics, it is expensive and demand for costly optical devices that have suitable mounting provisions. Therefore an adaptable rest device were used and adjusted to obtain satisfying results, as described in the experimental part below.

Accuracy tests

The proposed localizing system has been evaluated to find out the achievable accuracy. The test started with the alignment of the camera and of the emitter along the vertical direction. This step was necessary as no precision rest was used to support these two items. The residual error measured on the ceiling is roughly 20mm. The camera was left still at coordinates $(0, 0)$, while the emitter was moved in nine known points. Figure 6.6 shows the obtained results, where stars represent the "true" locations and pluses describe the measured ones. The radial and the angular errors have been computed, their average and standard deviation are respectively $16, 39$ mm and $-1.9, 2.9$ degrees. With the used webcam the field of view is about 2.5×2m. It should be noticed that the error distribution shows no similarity with the usual optic aberration of lenses, this can be ascribed to random causes such as small misalignments in the floor tiles.

Real-Time Processing: Observations

A crucial aspect is the capability to perform the processing in real-time. Indeed, this is mandatory to perform almost any task which requires the relative position and orientation among the robots. From a computation perspective, the dominant operation is represented by the second step, namely the centroid computation, as it requires a labeling process to detect all the connected components. For this step, the approach proposed in [111], whose complexity grows linearly with the number of pixels, has been exploited.

In the proposed architecture, the FOX Board G20 is in charge of the management of the high-level tasks with a control cycle of 250 ms. Experimental results have show that with a resolution of 176x144 pixels, the

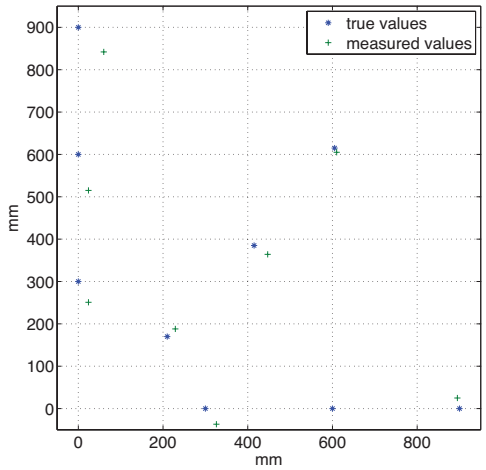

Figure 6.6: Accuracy test. The camera was left still at coordinates $(0, 0)$, while the emitter was moved in nine known points.

image processing takes roughly 70ms. Indeed, this allows to have roughly 180ms left for any other task. In order to have a term of comparison for the cpu usage, it is sufficient to notice that an Extended Kalman filter with 5 infrared takes only 7ms at each time step. Indeed, the video processing has turned out to be an order of magnitude heavier than any other implemented task so far.

6.3.2 Experiments

Experiments have been carried out to show the effectiveness of the proposed low-cost indoor relative position localizing system. Figure 6.7 shows the hardware setup, that is a Sharp GP2Y0A02YK infrared sensor along with a Logitech C300 webcam.

Three different experiments have been considered in the following. First a simple scenario where two robots play the role of landmarks for a third robot is considered. Successively a more refined scenario, where the three robots perform rendezvous relying only on the information provided by the proposed localizing system is described. Finally, a formation control task where the three robots must reach a line-shaped formation is considered. Note that, these experiments represent a possible application scenario for the proposed inter-robot localization system aiming only to provide ideas for possible use cases. The code used to control the robots behavior will be subject of future publications. Videos concerning these experiments can be found at

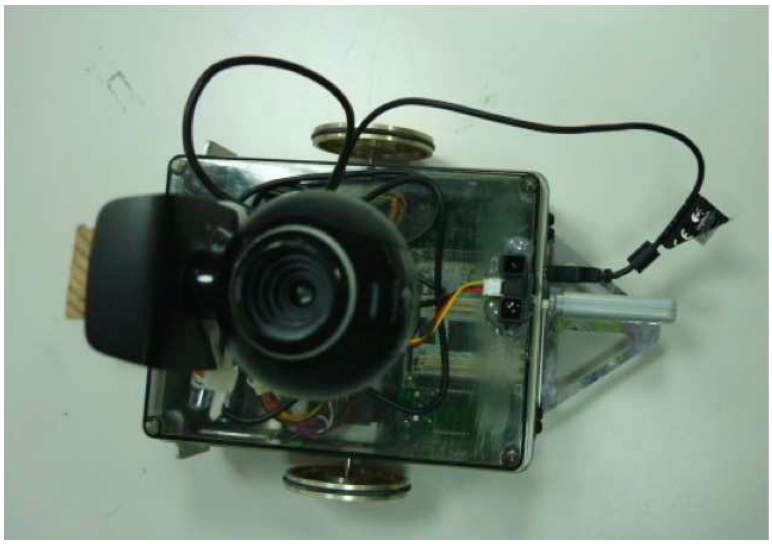

Figure 6.7: The proposed low-cost indoor relative position localizing system composed of a Sharp GP2Y0A02YK infrared sensor along with a Logitech C300 webcam.

`http://www.dia.uniroma3.it/~gasparri/med11.html` .

Passing-Through

In this scenario, two robots are assumed to play the role of landmarks, while a third one has to drive through them. This simple task could be useful in a multi-robot mapping context to more easily perform the map merging process.

Figure 6.8 shows a snapshot of the experiments: the landmark robots are placed to the sides of a door to point the way out to the third robot.

Figure 6.9 shows the odometry (blue) rectangles of the robot passing through the other two (red) ellipses. Note that, at the beginning only the closest among the two robots playing the role of landmarks was visible to the third robot. The implemented strategy to deal with this case was very simple: move closer to the visible robot in order to let the second one enter within the field of visibility.

Rendezvous

In this scenario, three robots have to drive towards a common location, i.e., the rendezvous coordination problem. This task can be performed by applying a consensus-like algorithm. Furthermore, no direct communication

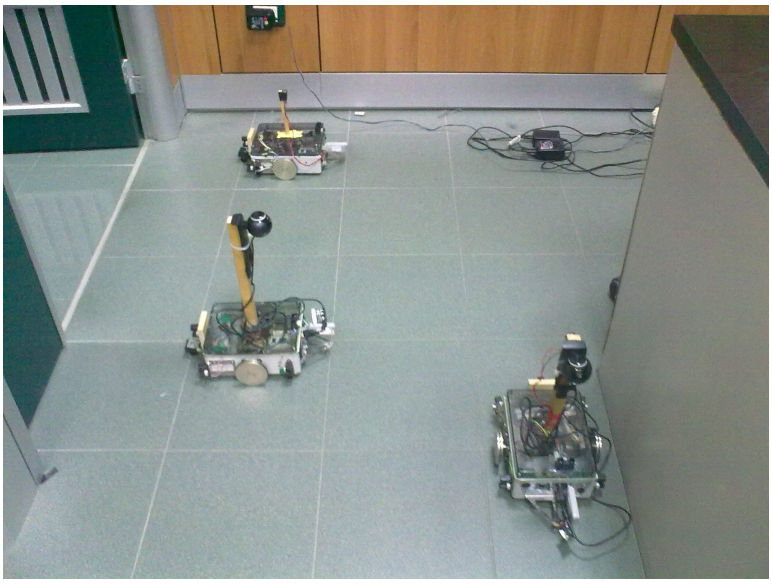

Figure 6.8: Experiment one: two robots play the role of landmarks while a third one has to drive through them.

among the robot is required by using the proposed localizing system, as at each time-step each robot drives itself toward the center of mass of all the robots detected in its field of view. In particular, the control law proposed in [112] has been used for this task. Indeed, it requires the availability of the relative distances among the robots, and the relative orientation of a robot with respect to the line of sight with another one.

Figure 6.10 shows a snapshot of the experiments: the three robots are moving toward the center of mass of all the detected centroids. Note that, the experiment would stop when all the robots have reached an area of radius ρ with respect to the rendezvous point. In particular, Figure 6.10-a) shows the robots at their starting locations, while Figure 6.10-b) shows the robots once the rendezvous area has been reached.

Figure 6.11 shows the odometry of the three robots where the small circle represents the heading direction of each robot. In particular, it should be noticed how all the robots reach the rendezvous area, a circle located at the rendezvous point (marked with a cross) of radius ρ. Note that for sake of simplicity, no obstacle avoidance has been considered for the experiment. Indeed, two out of the three robots end up bumping each other.

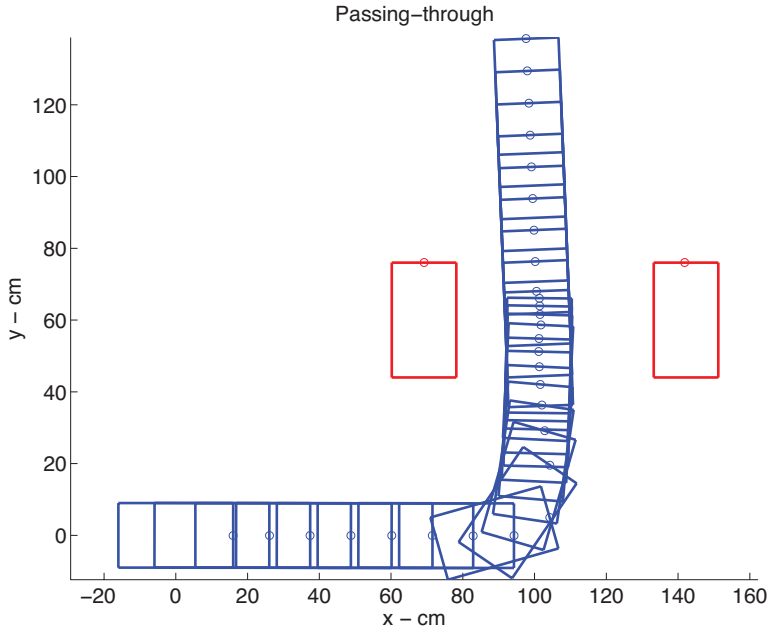

Figure 6.9: Experiment one: the (red) ellipses represent the two robots playing the role of landmarks while the (blue) rectangles describe the odometry of third one passing through them.

Formation Control

In this scenario, a simple formation control task has been considered. Three three robots have to move in a line-shaped formation by means of a leader-follower approach where the first robot follows a predefined path while the other two must follow it keeping themselves at a safe distance.

Figure 6.12 shows a snapshot of the experiments where the three robots are moving in a line-shaped formation with the leader on the left-side.

6.4 Swarm Aggregation Control Laws with Local Interactions: Simulation and Experiment

Simulations and experiments of the framework proposed in 3.3 have been carried out. Simulations have been considered to investigate the scalability of the proposed framework, while experiments have been considered to show its effectiveness in a real context.

The Kinect®-based Supervisory Control System described in [46] has been implemented to issue guidance commands to the swarm. Finite State Machines (FSMs) have been used for the dynamic hand gesture recognition.

a) b)

Figure 6.10: Experiment two: three robots have to drive towards a common location, a) robots are at the starting locations b) robots have reached the rendezvous area.

For a comprehensive overview about FSMs the reader is referred to [113]. Eight motion commands (North, North-West, West, South-West, South, South-East, East, North-East) to drive the swarm across the 2-dimensional environment and two interaction commands, namely "get closer" and "spread out", to modify the interaction among the robots have been considered. Finally a high priority "stop command" to be immediately recognized by the system has been included.

A bounded repulsive function and a linear attraction function were used in both the simulations and the experiments for modeling the agents interaction, i.e. $g_a(\|y\|) = a$, $g_r(\|y\|) = -be^{-\|y\|^2}$. In order to avoid obstacles, a virtual agent is projected on the closest obstacle w.r.t. the detecting robot. An unbounded repulsive action is associated with this virtual agent. An activation threshold coinciding with the equilibrium distance between attraction and repulsion is used. The difference between this approach and the more refined one in Section 4.2.4 is that the latter uses a single control law for both the interaction among the actual robots and the virtual ones. Therefore, less effort is required in the design of the control laws. The initial values of the parameters of the agents interaction function and the obstacle avoidance function are: $a = 0.5$, $b = 1$. In the following section, how the

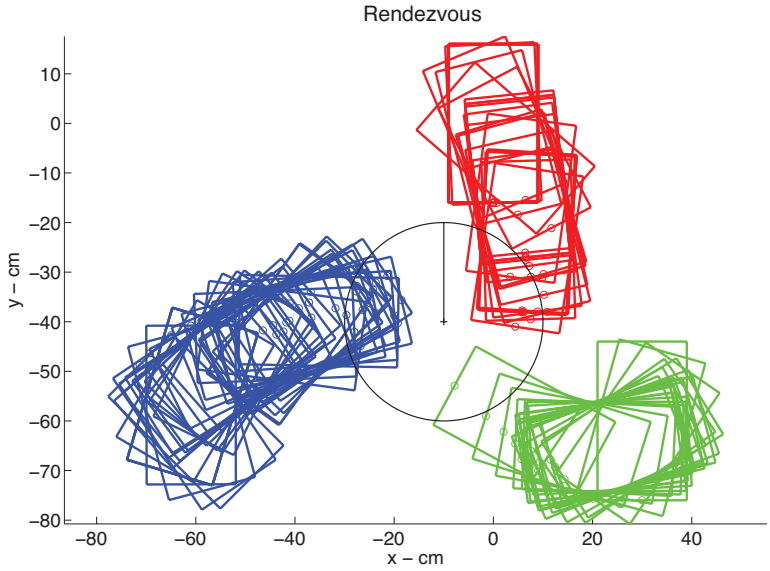

Figure 6.11: Experiment two: All the robots reach the rendezvous area, i.e., a circle located at the rendezvous point (marked with a cross) of radius ρ.

remote operator commands are fused in the swarming algorithm is detailed for the sake of completeness.

6.4.1 Simulations

Simulations have been carried out by interfacing the Kinect® hardware with the Player/Stage simulation environment. In this way, a real-time gesture recognition was possible for an effective guidance of the swarm. A swarm composed of 20 mobile robots has been deployed within an environment filled with obstacles to test the obstacle avoidance. Regarding the obtained results, the swarm safely moves within the environment according to the guidance commands issued by the human operator. For a more comprehensive understanding of the swarm behavior, the reader is referred to the following video: `http://www.dia.uniroma3.it/~priolo/simulation_full_res.avi`.

6.4.2 Experiments

For the experiments five mobile robotic platforms SAETTA have been exploited. The Kinect®-based remote control system has been implemented on a central unit equipped also with a low-cost vision system to retrieve the

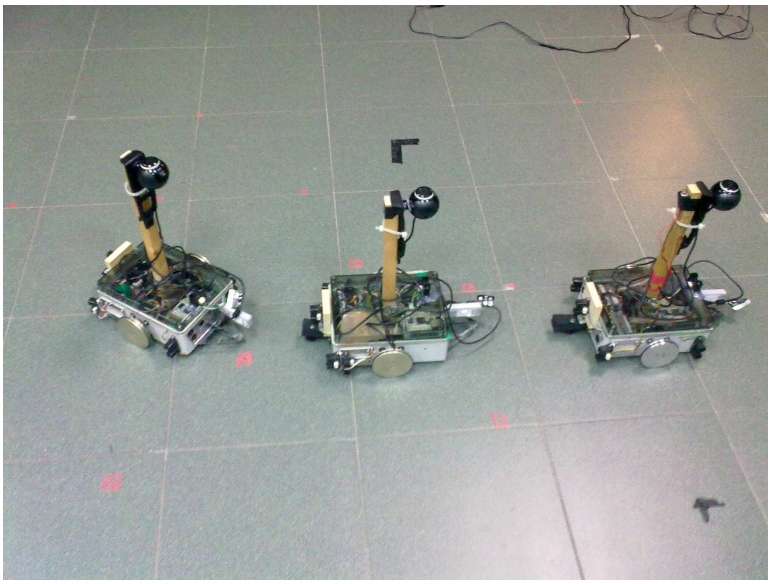

Figure 6.12: Experiment three: three robots have to move in a line-shaped formation.

relative distance among robots. Communication between the central unit and the swarm has been realized by means of a wifi channel. In Fig. 6.13, four screenshots of the algorithm execution are depicted. In Fig. 6.13a the initial configuration of the swarm is shown. In Fig. 6.13b, the robots are avoiding an obstacle within the environment. Then the robots get closer to each other after the obstacle is cleared as depicted in Fig. 6.13c. Eventually, the final configuration achieved by the swarm is shown in 6.13d.

The video of the experiment can be found at: `http://www.dia.uniroma3.it/~priolo/experiment_full_res.avi`.

6.5 USV Simulations

In this section, the simulations carried out using the framework proposed in 3.3 are discussed. Experimental trials at sea will be carried out with the aim of reporting at-field results and will appear in future publications.
The first simulation, is relative to a scenario where four vehicles are required to assume the desired formation, which is determined by the two following

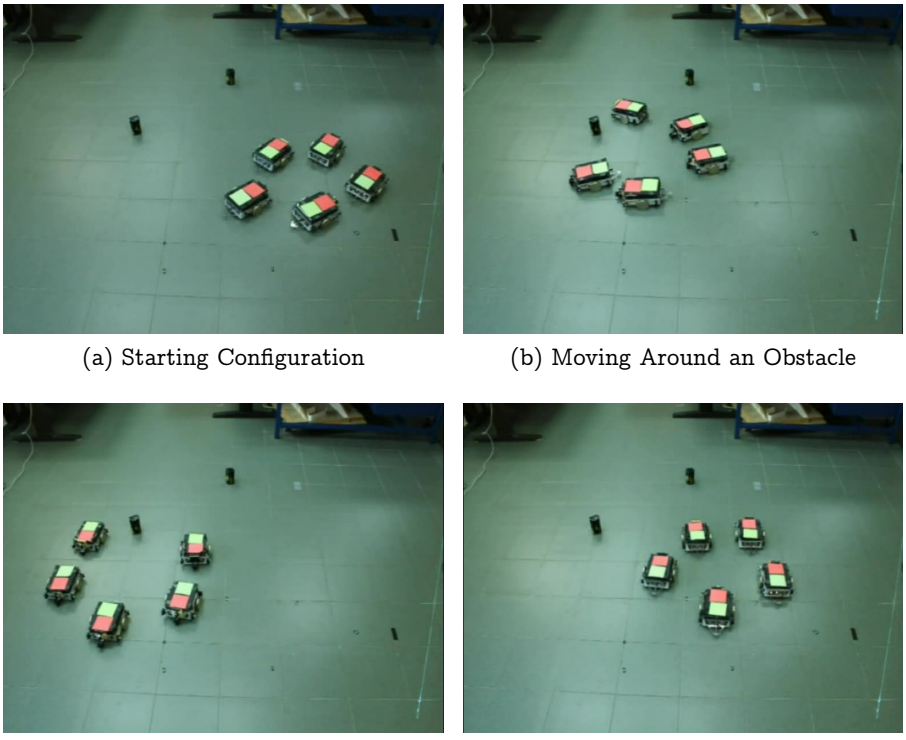

(a) Starting Configuration

(b) Moving Around an Obstacle

(c) Grouping after obstacles

(d) Final configuration

Figure 6.13: Four screenshots of the experiments concerning the swarm aggregation algorithms with local interactions.

attractive and repulsive potential functions respectively:

$$g_a(\|y\|) = a$$
$$g_r(\|y\|) = b \exp\left(\frac{-\|y\|^2}{c}\right) \tag{6.5.1}$$

where $a = 0.1$, $b = 1.0$ and $c = 1.0$.
In order to prevent collisions among the robots, a safety threshold $\bar{d}$ in the distance computation has been inserted, basically computing the value of $\|y\|$ of the attractive and repulsive functions in the following way:

$$\|y\| = \|\bar{y} - \bar{d}\| = \sqrt{(\bar{y}_1 - \bar{d}_1)^2 + (\bar{y}_2 - \bar{d}_2)^2} \tag{6.5.2}$$

where $\bar{y} = [\bar{y}_1 \bar{y}_2]^T$ and $\bar{d} = [\bar{d}_1 \bar{d}_2]^T$, with the desired threshold $\|\bar{d}\| = \sqrt{\bar{d}_1^2 + \bar{d}_2^2}$ set to the value of 3.0 meters.
While the vehicles are forming and maintaining the swarm configuration, the swarm barycenter is required to converge to and follow a desired geometrical path-a 6^{th} order polynomial parameter curve.
Figure 6.14 reports the motion of the four vehicles (blue, red, green and cyan lines); they initially start from random positions, modulating their speeds to reach the formation, while the path-following algorithm drives the formation itself towards the desired path (black dashed line). The small circle close to the vehicles represents the barycenter of the formation.
As it can be noticed from Figure 6.14, the simulation proves the convergence and maintenance of the combined formation-keeping and path-following tasks for the robot team. In Figure 6.15 the speed profiles assumed by each robot during the simulation are reported. As expected, a modulation of the speed for each robot is required to converge to the swarm configuration and it is then stabilized to a constant cruise speed of 1 m/s for the proposed experiments.
A second simulation is reported with the aim of proving the validity of the concept proposed in this work, also in the presence of obstacles in the operative scenario. For the sake of simplicity, a fixed obstacle with dimension comparable with robots' one is considered in the reported simulation. A generic obstacle dimension is again taken into account properly changing the safety threshold value $\bar{d}$. Under these hypothesis, the combined swarm and path-following technique is employed, obtaining the result reported in Figure 6.16, where the deviated motion of the vehicles, due to the obstacle presence, can be observed. After the obstacle avoidance, the formation is again driven back along the desired path.

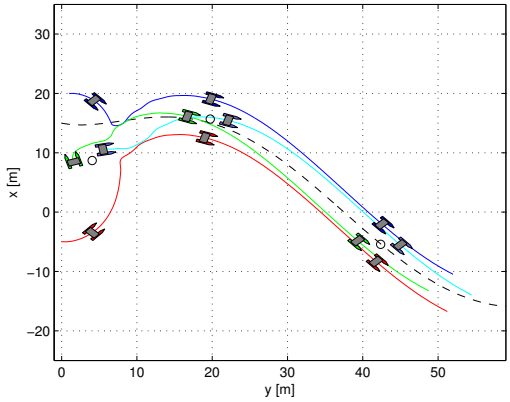

Figure 6.14: USV motions during swarm & path convergence and maintenance

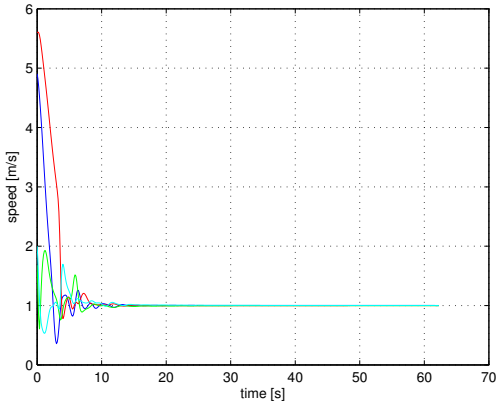

Figure 6.15: USV speed profiles assumed during swarm & path convergence and maintenance

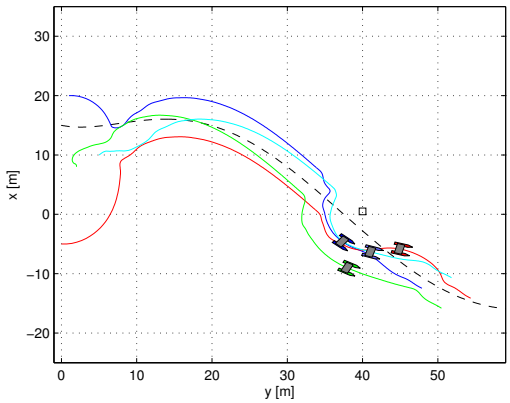

Figure 6.16: USV Swarm & path-following algorithm tested in presence of an obstacle

6.6 Saturated Swarm Aggregation Control Laws with Local Interactions and Obstacle Avoidance: Simulations and Experiments

In this section, simulations and experiments regarding the aggregation laws given in Sections 4.1 and 4.2 are described. As far as the control law in 4.1 is concerned, a bounded repulsive vector and a linear attraction vector, i.e. $g_a(\|y\|) = \alpha$, $g_r(\|y\|) = -\beta/\|y\|$, were used. The values of the parameters of the agents interaction function used along both the experiments and the simulations are: $\alpha = 1.5$, $\beta = 1$. For the control law in 4.2, the following functions and parameters are used in both the simulations and the experiments:

$$\Phi(\|y\|) = \exp\left(-\frac{\|y\|^4}{0.02}\right),$$

$$\gamma_i = \frac{1}{\|x_i - x_j\|^3},$$

$$[-a,\ b] = [-4,\ 0.4].$$

In Figure 6.17, four screen-shots of the experiments led by using the algorithm in 4.2 are shown. Figure 6.17a depicts the initial configuration for the swarm which is about to move towards the north of environment. Figure 6.17b depicts the swarm approaching an obstacle on the east of the environment, it can be noticed how the swarm is approaching the obstacle in order to move around it as a whole. Figure 6.17c depicts the swarm splitting around an obstacle. Finally, Figure 6.17d depicts the swarm moving between two obstacles. It can be noticed how the swarm, according to the fact that only one robot can safely move between two obstacles, shapes itself roughly as a line.

For both the control laws, the videos showing the simulations and the experiments can be found at the following URLs:

`http://www.dia.uniroma3.it/~priolo/set_virtual.mp4`,

`http://www.dia.uniroma3.it/~priolo/single_virtual.mp4`.

6.7 Distributed Left Eigenvector Estimation and Average Consensus over Digraphs: Simulations

In this section two simulations with an increasing number of robots are proposed for the framework introduced in Chapter 5. In each simulation, all the robots perform both the classical discrete time consensus and the

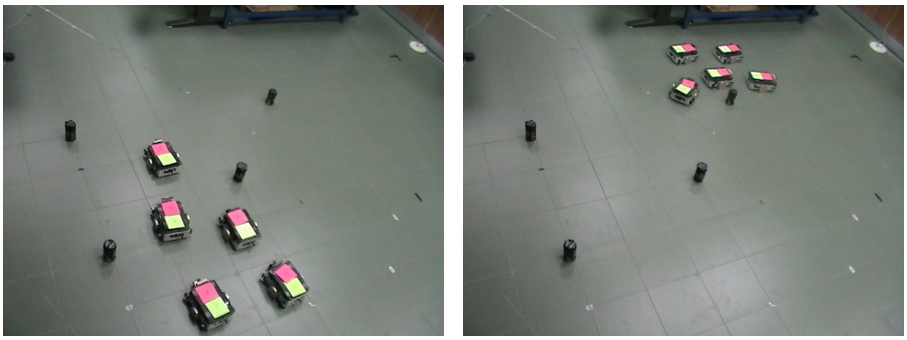

(a) Starting Configuration

(b) Moving Around an Obstacle

(c) Splitting Around an Obstacle

(d) Moving Between Two Obstacles

Figure 6.17: Four screenshots of the experiments concerning the swarm aggregation algorithms with input saturation and obstacle avoidance.

modified discrete time average consensus presented in Section 5.3 along with the required left eigenvector estimation algorithm. The first simulation involves 6 robots performing both consensus algorithms.

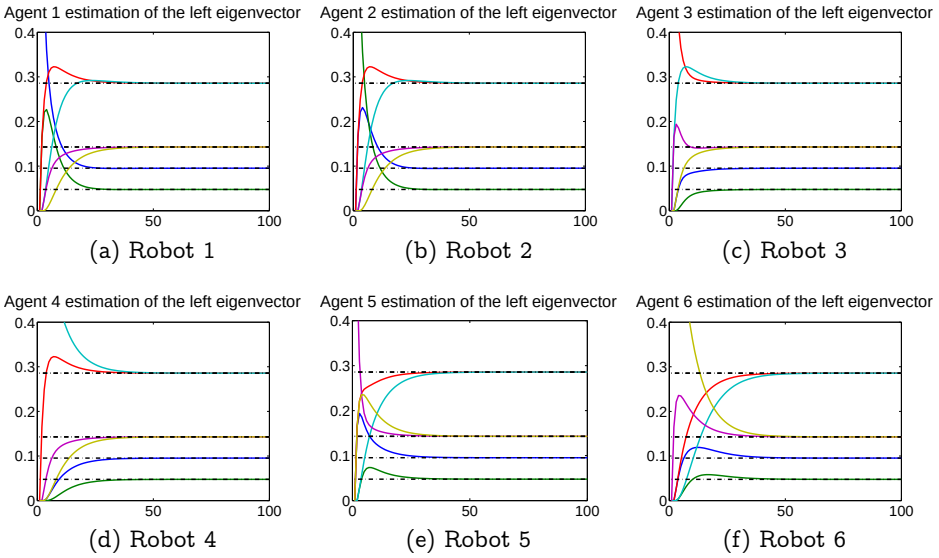

(a) Robot 1 (b) Robot 2 (c) Robot 3

(d) Robot 4 (e) Robot 5 (f) Robot 6

Figure 6.18: Left Eigenvector Estimate for 6 robots.

The network topology is described by the graph in Fig. 6.19a. The initial conditions of the robots are $x(0) = [64, 79, 4, 32, 9, 60]^T$, leading to $\mu = 41.3333$. In Fig. 6.18 the estimation process of the left eigenvector associated to the zero eigenvalue of the Laplacian matrix is illustrated. For every robot, the estimation process of each element of the vector is plotted. It can be noticed that the robots asymptotically achieve the same values. In Fig. 6.19b the execution of the consensus algorithm is shown. It is worthy to notice that in this case the robots can achieve a consensus because the digraph strongly connected, but the consensus value is different from μ. Instead, in Fig. 6.19c the execution of the consensus using the modified algorithm is given. In this case, all the robots obtain μ as their consensus value.

The same simulation, but considering 20 robots, is depicted in Fig. 6.20 and the following random initial conditions are used: $x(0) = [26, 34, 12$ $94, 10, 19, 44, 20, 34, 89, 68, 89, 59, 21, 63, 81, 81, 84, 13, 23]^T$, leading to $\mu = 48.2$. Note that also in this case the average consensus is reached. In Fig. 6.21, the corresponding left eigenvector estimation process is illustrated for a single robot. The robots achieve the same values of the estimated components of the left eigenvector w^T. This estimate is exploited in the executions

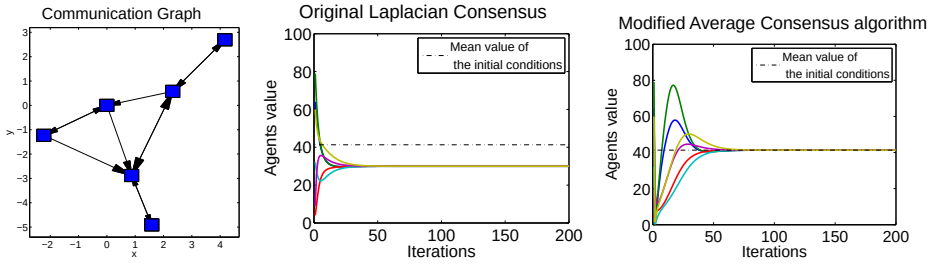

Figure 6.19: Iterations of the classical consensus protocol and the modified one. The case of 6 robots. Fig. 6.19-(a) depicts the underlying communication graph describing the interaction among the six robots. Fig. 6.19-(b) shows the classical consensus protocol with 6 robots. The dotted line represents the average value. Fig. 6.19-(c) shows the consensus protocol using the proposed consensus protocol with 6 robots. The dotted line represents the average value.

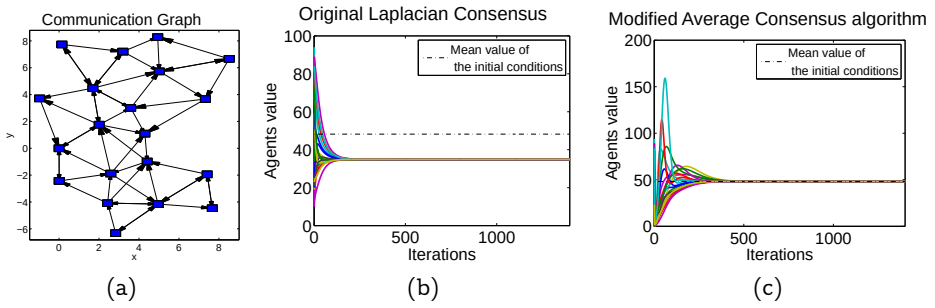

Figure 6.20: Iterations of the classical consensus protocol and the modified one. The case of 20 robots. Fig. 6.20-(a) depicts the underlying communication graph describing the interaction among the twenty robots. Fig. 6.20-(b) shows the consensus protocol using consensus protocol with 20 robots. The dotted line represents the average value. Fig. 6.20-(c) shows the proposed consensus protocol with 20 robots. The dotted line represents the average value.

of the consensus protocol depicted in 6.20c. As far as the modified average consensus is concerned, both in the case of 6 robots and the case of 20 robots the estimated consensus values decrease rapidly. This is due to the occurring of an abrupt change in the estimation of the left eigenvector during the first two steps. However, this behavior does not affect the achievement of the average consensus value.

Finally, the iterations of Algorithm 5.2.2 w.r.t. the powers of the Perron matrix in the case of a weakly connected digraph are shown. Let us consider again the network depicted in Figure 6.19a and let us remove the directed link that ends to the robot placed at the right upper part of the figure from its only out-neighbor. In this way, this robot is sending its information to another robot but it is not receiving any data from the others, resulting in a weakly connected topology. Figure 6.22 shows the values of the elements in the rows corresponding to the robot in the upper right part of Figure 6.19a and its only out-neighbor. The vertical bar indicates the n^{th} iteration of the algorithm, namely, the upper bound of the graph diameter. It is possible to notice that the first robot is aware of the weakly connectivity at step n due to the presence of one zero in its estimation. This is coherent with the theoretical analysis carried out in Section 5.2.1. Moreover, the structure of the left eigenvector follows from the peculiar choice of the digraph topology. In fact, there is an robot with only an outgoing edge and no incoming ones. Therefore, this robot is the one "imposing" its value in the consensus, i.e., the value initially assigned to it is the eventually achieved consensus value.

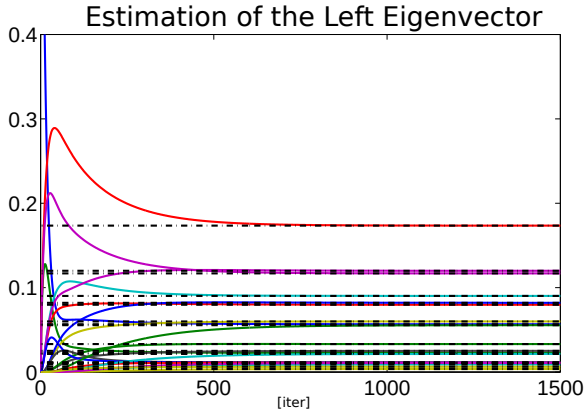

Figure 6.21: Left eigenvector estimation in the case of 20 robots.

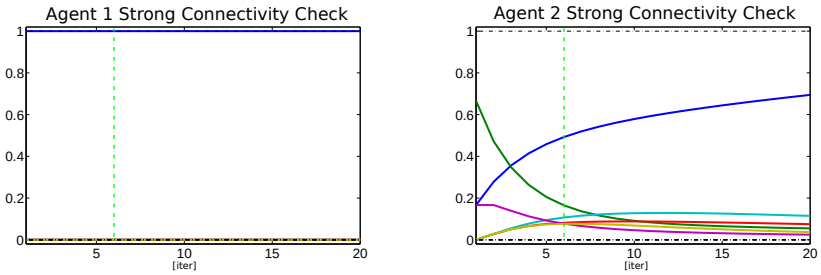

Figure 6.22: Strong connectivity verification

Conclusions

In this thesis, novel contributions in the field of multi-robot systems have been proposed. First of all, the framework proposed by Gazi and Passino in [5] was extended to deal with the limited sensing capabilities of the robots within the swarm. The main motivation behind this choice was a more realistic modeling of the constrains imposed by common sensor devices, especially in indoor environments where the GPS system can not be used. Then, two control laws were introduced to explicitly consider the physical limitations of the actuators equipped on the robots by using a saturation in the robot kinematic model. Two effective obstacle avoidance techniques were proposed based on the projection of one or a set of virtual robots on the closest obstacle w.r.t. the detecting unit. The proposed approaches do not conflict with the low level obstacle avoidance algorithms usually equipped on mobile robotic platforms but offer a smooth potential based obstacle avoidance forming, together with the swarm aggregation algorithm, a stable navigation framework for robot swarms. A novel contribution in the field of multi-robot systems where the communication is modeled as a digraph was given as well. A necessary and sufficient condition to check the strong connectivity of a weighted digraph in finite-time was proposed as a useful stopping condition for the asymptotic left eigenvector estimation algorithm. Then, the information coming from it was used by each robot to perform a modified average consensus algorithm which can be run concurrently to the estimation process. Eventually, a distance and a relative position measurement technique used to retrieve the necessary inputs for the swarming algorithms based on the Zigbee and the IR technologies were introduced. The former does not require any extra hardware to be equipped on the robot but it uses the same devices employed for the communication. The latter showed satisfactory performances in all those scenarios where a ceiling is available and measurable as it does not require the IR beam to be directed exactly towards the robot thus avoiding angular discretization errors. A complete theoretical analysis was carried out while simulations and exper-

iments were shown to corroborate the theoretical findings. Future work will be mainly focused on adding nonholonomic constrains to the kinematic model of the robots in order to show the overall system stability even in their presence. The left eigenvector algorithm will also be subject of future work. In particular, an algorithm working with switching topologies without the need of being reset after each switch is under investigation. Distributed strategies to check the rigidity of the communication graph are currently under development as well and will be used in the localization field. A porting of the IR relative localization system to the OpenCV library is under development as well. Eventually, a rigorous experimental validation should be addressed for the proposed swarming aggregation algorithms in order to validate the theoretical findings contained within this thesis.

Bibliography

[1] Y. U. Cao, A. S. Fukunaga, and A. Kahng. Cooperative mobile robotics: Antecedents and directions. *Autonomous Robots*, 4:7–27, 1997.

[2] J.P. Desai, J. Ostrowski, and V. Kumar. Controlling formations of multiple mobile robots. In *IEEE International Conference on Robotics and Automation*, volume 4, pages 2864 –2869 vol.4, may 1998.

[3] J.P. Desai, J.P. Ostrowski, and V. Kumar. Modeling and control of formations of nonholonomic mobile robots. *IEEE Transactions on Robotics and Automation*, 17(6):905 –908, dec 2001.

[4] M. Egerstedt and Xiaoming Hu. Formation constrained multi-agent control. *IEEE Transactions on Robotics and Automation*, 17(6):947 –951, dec 2001.

[5] V. Gazi and K. M. Passino. A class of attractions/repulsion functions for stable swarm aggregations. *International Journal of Control*, 77(18):1567–1579, 2004.

[6] D. Wenjie and J.A. Farrell. Cooperative control of multiple nonholonomic mobile agents. *IEEE Transactions on Automatic Control*, 53(6):1434 –1448, july 2008.

[7] D.V. Dimarogonas and K.J. Kyriakopoulos. Connectedness preserving distributed swarm aggregation for multiple kinematic robots. *IEEE Transactions on Robotics*, 24(5):1213 –1223, oct. 2008.

[8] P. Brass, F. Cabrera-Mora, A. Gasparri, and Jizhong Xiao. Multirobot tree and graph exploration. *IEEE Transactions on Robotics*, 27(4):707–717, 2011.

[9] A. Dhariwal, G.S. Sukhatme, and A. A.G. Requicha. Bacterium-inspired robots for environmental monitoring. In *Proceedings of IEEE International Conference on Robotics and Automation*, volume 2, pages 1436–1443. IEEE, 2004.

[10] S. Rutishauser, N. Correll, and A. Martinoli. Collaborative coverage using a swarm of networked miniature robots. *Robotics and Autonomous Systems*, 57(5):517–525, 2009.

[11] Xue Songdong and Zeng Jianchao. Sense limitedly, interact locally: the control strategy for swarm robots search. In *IEEE International Conference on Networking, Sensing and Control*, pages 402 –407, 2008.

[12] A. Shia, F.B. Bastani, and Yen I-Ling. A highly resilient framework for autonomous robotic swarm systems operating in unknown, hostile environments. In *10th International Symposium on Autonomous Decentralized Systems,*, pages 147 –153, march 2011.

[13] Liu Yanfei and K.M. Passino. Stable social foraging swarms in a noisy environment. *IEEE Transactions on Automatic Control*, 49(1):30 – 44, jan. 2004.

[14] N.R. Hoff, A. Sagoff, R.J. Wood, and R. Nagpal. Two foraging algorithms for robot swarms using only local communication. In *IEEE International Conference on Robotics and Biomimetics*, pages 123 –130, 2010.

[15] V. Kumar and F. Sahin. Cognitive maps in swarm robots for the mine detection application. In *Systems, Man and Cybernetics, 2003. IEEE International Conference on*, volume 4, pages 3364–3369. IEEE, 2003.

[16] R. Fruergaard-Pedersen and B.H. Mayoh. *Optimal demining using a swarm of low-cost robotic units*. PhD thesis, Citeseer, 2007.

[17] E. Şahin. Swarm robotics: From sources of inspiration to domains of application. In *Swarm Robotics*, pages 10–20. Springer, 2005.

[18] L. Steels. Cooperation between distributed agents through self-organisation. In *Proceedings of IEEE International Workshop on Intelligent Robots and Systems*, pages 8–14. IEEE, 1990.

[19] V. Gazi and K.M. Passino. Stability analysis of social foraging swarms. *IEEE Transactions on Systems, Man, and Cybernetics, Part B: Cybernetics*, 34(1):539–557, 2004.

[20] J. Fredslund and M. J. Mataric. A general algorithm for robot formations using local sensing and minimal communication. *IEEE Transactions on Robotics and Automation*, 18(5):837–846, 2002.

[21] V. Gazi and K.M. Passino. *Swarm Stability and Optimization*. Springer, 2011.

[22] Sahin E. and Winfield A. Special issue on swarm robotics. *Swarm Intelligence*, 2(2-4):69–72, 2008.

[23] V. Trianni, S. Nolfi, and M. Dorigo. Cooperative hole avoidance in swarm-bot. *Robotics and Autonomous Systems*, 54(2):97–103, 2006.

[24] Roderich Groß, Michael Bonani, Francesco Mondada, and Marco Dorigo. Autonomous self-assembly in swarm-bots. *IEEE Transactions on Robotics*, 22(6):1115–1130, 2006.

[25] K. Warburton and J. Lazarus. Tendency-distance models of social cohesion in animal groups. *Journal of Theoretical Biology*, 150(4):473–488, June 1991.

[26] D. Grunbaum, A. Okubo, and S. A. Levin. Modelling social animal aggregations. In *Frontiers in Theoretical Biology: Lecture nNotes in Biomathematics*. Springer-Verlag, 1994.

[27] M. Ballerini, N. Cabibbo, R. Candelier, A. Cavagna, E. Cisbani, I. Giardina, A. Orlandi, G. Parisi, A. Procaccini, M. Viale, and V. Zdravkovic. Empirical investigation of starling flocks: a benchmark study in collective animal behaviour. *Animal Behaviour*, 76(1):201 – 215, 2008.

[28] S. Camazine. *Self-Organization in Biological Systems*. Princeton Studies in Complexity. Princeton University Press, 2003.

[29] A. Khozaee, A.H. Aminaiee, and A. Ghaffari. A swarm robotic approach to distributed object pushing using fuzzy controllers. In *IEEE International Conference on Robotics and Biomimetics*, pages 1117 –1122, feb. 2009.

[30] N. Correll and A. Martinoli. Robust Distributed Coverage using a Swarm of Miniature Robots. In *IEEE International Conference on Robotics and Automation*, pages 379 – 384, 2007.

[31] I. Navarro and F. Matía. An introduction to swarm robotics. *ISRN Robotics*, 2013:10, 2013.

[32] A. FT Winfield and J. Nembrini. Safety in numbers: fault-tolerance in robot swarms. *International Journal of Modelling, Identification and Control*, 1(1):30–37, 2006.

[33] F. Mondada, G. C Pettinaro, A. Guignard, I. W Kwee, D. Floreano, J.-L. Deneubourg, S. Nolfi, L. M. Gambardella, and M. Dorigo. Swarm-bot: A new distributed robotic concept. *Autonomous Robots*, 17(2-3):193–221, 2004.

[34] J.D. Bjerknes and A. FT Winfield. On fault tolerance and scalability of swarm robotic systems. In *Distributed Autonomous Robotic Systems*, pages 431–444. Springer, 2013.

[35] S. Herbrechtsmeier, U. Witkowski, and U. Rückert. Bebot: A modular mobile miniature robot platform supporting hardware reconfiguration and multi-standard communication. In *Progress in Robotics*, volume 44 of *Communications in Computer and Information Science*, pages 346–356. Springer Berlin Heidelberg, 2009.

[36] C. Aguero and M. Veloso. Transparent multi-robot communication exchange for executing robot behaviors. In *Highlights on Practical Applications of Agents and Multi-Agent Systems*, volume 156 of *Advances in Intelligent and Soft Computing*, pages 215–222. Springer Berlin Heidelberg, 2012.

[37] Wei Ren, Randal W Beard, and Ella M Atkins. Information consensus in multivehicle cooperative control. *Control Systems, IEEE*, 27(2):71–82, 2007.

[38] T. Yasuda, editor. *Multi-Robot Systems, Trends and Development.* InTech, 2011.

[39] M. Mesbahi and M. Egerstedt. *Graph Theoretic Methods in Multiagent Networks.* Princeton Series in Applied Mathematics. Princeton University Press, 2010.

[40] K.A. Luthy, E. Grant, and T.C. Henderson. Leveraging rssi for robotic repair of disconnected wireless sensor networks. In *IEEE International Conference on Robotics and Automation*, pages 3659 –3664, 2007.

[41] Z. Qu, C. Li, and F. Lewis. Cooperative control with distributed gain adaptation and connectivity estimation for directed networks. *International Journal of Robust and Nonlinear Control*, 2012.

[42] M. Di Rocco, S. Panzieri, and A. Priolo. Formation control through environment pattern recognition for a multi-robot architecture. In *4th European Conference on Mobile Robots*, September 2009.

[43] A. Gasparri, A. Priolo, and S. Panzieri. A fitness-sharing based genetic algorithm for collaborative multi robot localization. *Intelligent Service Robotics*, 3(2):137–149, 2010.

[44] A. Milano, A. Priolo, A. Gasparri, M. Di Rocco, and G. Ulivi. An experimental validation of a low-cost indoor relative position localizing system for mobile robotic networks. In *IEEE Mediterranean Conference on Control and Automation*, pages 169 – 174, June 2011.

[45] A. Gasparri, A. Priolo, D. Carboni, and G. Ulivi. Development of a framework for the remote guidance of a multi-robot system by a human operator: A preliminary analysis. In *Convegno della Società dei Docenti e Ricercatori Italiani in Automatica*, 2011.

[46] A. Gasparri, . Priolo, and G. Ulivi. A swarm aggregation algorithm for multi-robot systems based on local interaction. Technical Report RT-DIA-193-2012, Università degli Studi Roma Tre, Dipartimento di Informatica ed Automazione, 2012.

[47] A. Gasparri, A. Priolo, D. Carboni, and G. Ulivi. A swarm algorithm for human supervisory control based on local communication. In *IEEE Multi-Conference on Systems and Control*, October 2012.

[48] A. Gasparri, G. Oriolo, A. Priolo, and G. Ulivi. A swarm aggregation algorithm for multi-robot systems with input saturations based on local interaction. In *IEEE/RSJ International Conference on Intelligent Robots and Systems*, October 2012.

[49] G. Oliva, A. Priolo, S. Panzieri, and G. Ulivi. Adding and removing nodes in consensus. In *20th Mediterranean Conference on Control and Automation, Barcelona , Spain*, pages 1031 – 1036, 2012.

[50] M. Bibuli, A. Gasparri, A. Priolo, G. Bruzzone, and M. Caccia. Virtual target based path-following guidance system for cooperative usv swarms. In *9th IFAC Conference on Manoeuvring and Control of Marine Craft*, September 2012.

[51] A. Leccese, A. Gasparri, A. Priolo, G. Oriolo, and G. Ulivi. A swarm aggregation algorithm based on local interaction with actuator saturations and integrated obstacle avoidance. In *IEEE International Conference on Robotics and Automation*, May 2013. To Appear.

[52] A. Priolo, A. Gasparri, E. Montijano, and C. Sagüés. A decentralized algorithm for balancing a strongly connected weighted digraph. In *American Control Conference*, June 2013. To Appear.

[53] A. Priolo, A. Gasparri, E. Montijano, and C. Sagüés. A decentralized algorithm for the left eigenvector estimation on strongly connected weighted digraphs. *Automatica*, SUBMITTED.

[54] Craig W. Reynolds. Flocks, herds and schools: A distributed behavioral model. *SIGGRAPH Computer Graphhics*, 21(4):25–34, August 1987.

[55] J. H. Reif and Hongyan Wang. Social potential fields: A distributed behavioral control for autonomous robots. *Robotics and Autonomous Systems*, 27(3):171–194, 1999.

[56] G. Beni and Ping Liang. Pattern reconfiguration in swarms-convergence of a distributed asynchronous and bounded iterative algorithm. *IEEE Transactions on Robotics and Automation*, 12(3):485 –490, jun 1996.

[57] A. Martinoli, K. Easton, and W. Agassounon. Modeling swarm robotic systems: A case study in collaborative distributed manipulation. *The International Journal of Robotics Research*, 23(4-5):415–436, 2004.

[58] T. Schmickl, H. Hamann, H. Wörn, and K. Crailsheim. Two different approaches to a macroscopic model of a bio-inspired robotic swarm. *Robotics and Autonomous Systems*, 57(9):913–921, 2009.

[59] Kristina Lerman, Alcherio Martinoli, and Aram Galstyan. A review of probabilistic macroscopic models for swarm robotic systems. In *Swarm robotics*, pages 143–152. Springer, 2005.

[60] V. Gazi and K. M. Passino. Stability analysis of swarms. *IEEE Transactions on Automatic Control*, 48(4):692–697, 2003.

[61] T. Chu, L. Wang, and T. Chen. Self-organized motion in anisotropic swarms. *Journal of Control Theory and Applications*, 1:77–81, 2003.

[62] V. Gazi. Swarm aggregations using artificial potentials and sliding-mode control. *IEEE Transactions on Robotics*, 21(6):1208 – 1214, dec. 2005.

[63] W. Li and X. Wang. Adaptive velocity strategy for swarm aggregation. *Physical Review Letters E*, 75, Feb 2007.

[64] L. Barnes, M.A. Fields, and K. Valavanis. Unmanned ground vehicle swarm formation control using potential fields. In *IEEE Mediterranean Conference on Control & Automation*, pages 1–8, 2007.

[65] S. Nouyan, A. Campo, and M. Dorigo. Path formation in a robot swarm. *Swarm Intelligence*, 2(1):1–23, 2008.

[66] A.K. Ray, P. Benavidez, L. Behera, and M.M. Jamshidi. Decentralized motion coordination for a formation of rovers. *IEEE Systems Journal*, 3(3):369 –381, sept. 2009.

[67] W. Li. Stability analysis of swarms with general topology. *IEEE Transactions on Systems, Man, and Cybernetics, Part B: Cybernetics*, 38(4):1084 –1097, aug. 2008.

[68] DV Dimarogonas, MM Zavlanos, SG Loizou, and KJ Kyriakopoulos. Decentralized motion control of multiple holonomic agents under input constraints. In *IEEE Conference on Decision and Control*, volume 4, pages 3390–3395, 2003.

[69] J.R.T. Lawton, R.W. Beard, and B.J. Young. A decentralized approach to formation maneuvers. *IEEE Transactions on Robotics and Automation,*, 19(6):933 – 941, dec. 2003.

[70] Liu Bo and Yu Hai. Flocking in multi-agent systems with a bounded control input. In *International Workshop on Chaos-Fractals Theories and Applications*, pages 130 –134, nov. 2009.

[71] D. Kostic, S. Adinandra, J. Caarls, N. van de Wouw, and H. Nijmeijer. Saturated control of time-varying formations and trajectory tracking for unicycle multi-agent systems. In *IEEE Conference on Decision and Control*, pages 4054 –4059, dec. 2010.

[72] K. Pahlavan, Xinrong Li, and J.P. Makela. Indoor geolocation science and technology. *IEEE Communications Magazine*, 40(2):112–118, Feb 2002.

[73] P. Bahl and V. N. Padmanabhan. Radar: an in-building rf-based user location and tracking system. In *IEEE Conference on Computer Communications*, volume 2, pages 775–784, 2000.

[74] K. Kaemarungsi. Distribution of wlan received signal strength indication for indoor location determination. In *1st International Symposium on Wireless Pervasive Computing*, page 6 pp., Jan. 2006.

[75] K. Pahlavan, P. Krishnamurthy, and A. Beneat. Wideband radio propagation modeling for indoor geolocation applications. *IEEE Communications Magazine*, 36(4):60–65, Apr 1998.

[76] Yongguang Chen and H. Kobayashi. Signal strength based indoor geolocation. In *IEEE International Conference on Communications*, volume 1, pages 436–439, 2002.

[77] Jan Duha Peter Brida, Peter Cepel. Geometric algorithm for received signal strength based mobile positioning. *Radioengineering*, 14(1), April 2005.

[78] Wenbing Yao Harrison Yuan, Qiang Ni and Yonghua Song. Design of a novel indoor location sensing mechanism using ieee 802.11e wlans. In *The Seventh Annual PostGraduate Symposium in Telecommunications and Network System (PGNet)*, June 2006.

[79] A. Kemppainen, J. Haverinen, and J. Roning. An infrared location system for relative pose estimation of robots. In *16-th Syposium of Robot Design, Dynamics, and Control*, pages 379–386, June 2006.

[80] J. Pugh, X. Raemy, C. Favre, R. Falconi, and A. Martinoli. A fast onboard relative positioning module for multirobot systems. *IEEE/ASME Transactions on Mechatronics*, 14(2):151 –162, April 2009.

[81] Z. Qu, C. Li, and F. Lewis. Cooperative control based on distributed estimation of network connectivity. In *IEEE American Control Conference*, pages 3441 –3446, 2011.

[82] A. D. Dominguez-Garcia and C. N. Hadjicostis. Distributed strategies for average consensus in directed graphs. *IEEE Conference on*

Decision and Control and European Control Conference, pages 2124–2129, 2011.

[83] K. Cai and H. Ishii. Average consensus on arbitrary strongly connected digraphs with dynamic topologies. In *IEEE American Control Conference*, pages 14–19, 2012.

[84] K. Cai and H. Ishii. Average consensus on general strongly connected digraphs. *Automatica*, 48(11):2750 – 2761, 2012.

[85] H. Atrianfar and M. Haeri. Average consensus in networks of dynamic multi-agents with switching topology: Infinite matrix products. *ISA Transactions*, 51(4):522 – 530, 2012.

[86] S. Chen, L. Zhao, and Y. Han. Multi-agent aggregation behavior analysis: The dynamic communication topology. *Journal of Systems Science and Complexity*, 21:209–216, 2008.

[87] T. B. Curtin, J. G. Bellingham, J. Catipovic, and D. Webb. Autonomous oceanographic sampling networks. *Oceanography*, 6(3):86–94, 1993.

[88] E. Fiorelli, N. E. Leonard, P. Bhatta, D. A. Paley, R. Bachmayer, and D. M. Fratantoni. Multi-auv control and adaptive sampling in monterey bay. *IEEE Journal of Oceanic Engineering*, 31(4), 2006.

[89] M.R. Benjamin, J.A. Curcio, J.J. Leonard, and P.M. Newman. Navigation of Unmanned Marine Vehicles in accordance with the rules of the road. In *IEEE International Conference on Robotics and Automation*, pages 3581 –3587, Orlando (FL), USA, May 2006.

[90] M. Breivik. Formation control with Unmanned Surface Vehicles. Technical report, Centre for Ships and Ocean Structures; Norwegian University of Science and Technology, 2009.

[91] M. Breivik. *Topics in guided motion control of marine vehicles*. PhD thesis, Department of Engineering Cybernetics, Norwegian University of Science and Technology, 2010.

[92] M. Bibuli, M. Caccia, L. Lapierre, and G. Bruzzone. Guidance of unmanned surface vehicles: Experiments in vehicle following. *IEEE Robotics Automation Magazine*, 19(3):92 –102, sept. 2012.

[93] A. Aguiar, J. Almeida, M. Bayat, B. Cardeira, R. Cunha, A. Häusler, P. Maurya, A. Oliveira, A. Pascoal, A. Pereira, M. Rufino, L. Sebastião, C. Silvestre, and F. Vanni. Cooperative control of multiple marine vehicles: Theoretical challenges and practical issues. In 8^{th} *Conference on Manoeuvring and Control of Marine Craft*, pages 412–417, Guaruja (SP), Brazil, September 2009.

[94] M. Bibuli, G. Bruzzone, M. Caccia, and L. Lapierre. Path-following algorithms and experiments for an unmanned surface vehicle. *Journal of Field Robotics*, 26(8):669–688, 2009.

[95] J.C. Latombe. *Robot Motion Planning*. Kluwer Academic Publishers, 1991.

[96] C. D. Meyer, editor. *Matrix analysis and applied linear algebra*. Society for Industrial and Applied Mathematics, 2000.

[97] R. Aragues, E. Montijano, and C. Sagues. Consistent data association in multi-robot systems with limited communications. In *Robotics: Science and Systems*, pages 97–104, 2010.

[98] R. Aragues, G. Shi, D. V. Dimarogonas, C. Sagues, , and K. H. Johansson. Distributed algebraic connectivity estimation for adaptive event-triggered consensus. In *IEEE American Control Conference*, pages 32 –37, 2012.

[99] R. Olfati-Saber, J. A. Fax, and R. M. Murray. Consensus and cooperation in networked multi-agent systems. *Proceedings of the IEEE*, 95(1):215–233, 2007.

[100] F. Bullo, J. Cortés, and S. Martínez. *Distributed Control of Robotic Networks*. Applied Mathematics Series. Princeton University Press, 2009.

[101] R. Carli, F. Fagnani, A. Speranzon, and S. Zampieri. Communication constraints in the average consensus problem. *Automatica*, 44(3):671 – 684, 2008.

[102] M. Di Rocco, F. La Gala, and G. Ulivi. Seatta: A small and cheap mobile unit to test multirobot algorithms. *IEEE Robotics Automation Magazine*, PP(99):1, 2012.

[103] Paul Maxim, Suranga Hettiarachchi, W Spears, D Spears, J Hamman, Thomas Kunkel, and Caleb Speiser. Trilateration localization

for multi-robot teams. In *Proceedings of the Sixth International Conference on Informatics in Control, Automation and Robotics, Special Session on Multi-Agent Robotic Systems*, 2008.

[104] K. Pahlavan and P. Krishnamurthy. *Principles of Wireless Networks: A Unified Approach*. Prentice Hall PTR, 2001.

[105] S. Ali and P. Nobles. A novel indoor location sensing mechanism for ieee 802.11 b/g wireless lan. In *4th Workshop on Positioning, Navigation and Communication*, pages 9 –15, March 2007.

[106] J. D. Parsons. *The Mobile Radio Propagation Channel*. Wiley, 1992.

[107] J. Rencheng, W. Hongbin, P. Bo, and G. Ning. Research on rssi-based localization in wireless sensor networks. In *4th International Conference on Wireless Communications, Networking and Mobile Computing*, pages 1–4, Oct. 2008.

[108] I. Kelly and A. Martinoli. A scalable, on-board localisation and communication system for indoor multi-robot experiments. *Sensor Review*, 24(2):167–180, 2004.

[109] J. F. Roberts, T. S. Stirling, J-C. Zufferey, and D. Floreano. 2.5 d infrared range and bearing system for collective robotics. In *IEEE/RSJ International Conference on Intelligent Robots and Systems*, pages 3659–3664. IEEE, 2009.

[110] J. Weng, P. Cohen, and M. Herniou. Camera calibration with distortion models and accuracy evaluation. *IEEE Transactions on Pattern Analysis and Machine Intelligence*, 14(10):965 –980, October 1992.

[111] F. Chang, C. J. Chen, and C. J. Lu. A linear-time component-labeling algorithm using contour tracing technique. *Compututer Vision Image Understanding*, 93:206–220, February 2004.

[112] D. V. Dimarogonas and K. J. Kyriakopoulos. On the rendezvous problem for multiple nonholonomic agents. *IEEE Transactions on Automatic Control*, 52(5):916 –922, May 2007.

[113] S. Mitra and T. Acharya. Gesture recognition: A survey. *IEEE Transactions on Systems Man and Cybernetics Part C Applications and Reviews*, 37(3):311–324, 2007.